Location of wideband impulsive noise source

Huat, Peck Chye

Award date:
2002

Awarding institution:
University of Bath

Location of Wideband Impulsive Noise Source

Submitted by

Peck Chye Huat

for the degree of

Doctor of Philosophy in Electrical and Electronic Engineering

The University of Bath, UK

2002

ProQuest LLC
789 East Eisenhower Parkway
P.O. Box 1346
Ann Arbor, MI 48106-1346

The University of Bath, UK

Abstract

LOCATION OF WIDEBAND
IMPULSIVE NOISE SOURCE

by Peck Chye Huat

A thesis is presented which offers a solution for locating Wideband Impulsive Noise (WIN) sources. It is motivated by the need of the Radiocommunications Agency (UK) for an automatic method to locate such sources causing interference to other systems (especially analogue and digital TV). The rapid growth and use of communication equipment has increased the utilisation of the available frequency spectrum that has intensified the need to keep interferences to a minimum. Electrical discharges from faulty thermostats, heavy current switching, flickering fluorescent lamps etc., can all cause unacceptable levels of interference. Currently, experts in the field of noise location use handheld radio sets and engineering experience to locate such interference. In an endeavour to alleviate the heavy reliance on engineering judgement (which implies the use of many experienced operatives) to carry out the noise location task, a proto-type impulsive noise location system has been developed. The principles, construction, validation, deployment and performance of the system are all described in this thesis.

TABLE OF CONTENTS

ACKNOWLEDGMENTS

The author wishes to express his sincere appreciations to Dr. Philip J. Moore (Supervisor) and Dr. Ian A. Glover for their professional advices and assistances in the preparation of this manuscript. Also, special thanks to Omicron electronics, Austria, and Radiocommunications Agency, UK, for funding this project.

Thanks to Mr B. Taylor and Mr S. O'Connel, from the Radiocommunications Agency, for assisting the experiments in Whyteleaves laboratory, and Mr T. Adams and Mr C. Wallenkamp from Melksham substation, National Grid Company (NGC), for arranging the tests carried out in the substation.

Additionally, the author would like to thank the technicians, Mr M. Edwards and Mr D. Hatten from the Radio Systems and Radio Science Group of the University of Bath for assisting in many aspects of the practical experiments and Mr J. Sims and Mr D. Parker from the Electronic and Electrical Engineering department workshop for producing excellent customized design products. And also, thanks to Miss I. Portugues for assisting in certain aspects of the software developments.

Finally, I would also like to thank a very special friend, Miss P. Yu, for her support.

LIST OF JOURNAL PUBLICATIONS (OCT. 99 TO FEB. 02)

Peck C. H., Moore P. J., "Direction Finding of Wideband Impulsive Noise Source," *IEEE Transaction on Electromagnetic Compatibility (EMC)*, vol. 43, No. 2, pp. 149-154, May 2001.

Peck C. H., Moore P. J., "An Effective Front-end for VHF-UHF Monitoring Systems," Selected as one of the best papers in *IPEC 2001*, and to be published in the *Journal of Institution of Engineers (IES)*, Singapore.

Peck C. H., Moore P. J., " Location of Wideband Impulsive Noise Source," To be submitted to *IEEE Transaction on Electromagnetic Compatibility (EMC)*.

LIST OF CONFERENCE PUBLICATIONS (OCT. 99 to FEB. 02)

Peck C. H., Aggarwal R. K., "An Accurate Fault Location Technique in Distribution Systems Using Artificial Neural Network," *UPEC*, Belfast, UK, Sep. 2000.

Peck C. H., Moore P. J., "An Investigation into Spark Generated Electromagnetic Interference and Its Impact on Radio Frequency Reception," *UPEC*, Belfast, UK, Sep. 2000.

Peck C. H., Moore P. J., "Source Identification and Analysis of Wideband Electromagnetic Interference Generated by Switchgears in a High Voltage Substation," *EMC York*, University of York, UK, 2000.

Peck C. H., Moore P. J., "Switchgear Condition Monitoring using Radio Frequency Emission," *IPEC*, Singapore, May 2001.

Peck C. H., Hickery D., Moore P. J., "Detection of Reverse Corona due to Remnant Space Charge for AC Voltage Measurements," *International Symposium on High Voltage Engineering (ISH)*, Bangalore, India, Aug. 2001.

MAJOR DEMONSTRATION

Live demonstration of the impulsive noise locator system at the *CISPR Summer meeting 2001* in Bristol (UK).

LIST OF FIGURES

Chapter ***Page No.***

Chapter 4

Chapter 5

Chapter 6

Chapter 7

Chapter 8

LIST OF TABLES

Chapter ***Page No.***

LIST OF ABBREVIATIONS

2D – Two dimensional

3D – Three dimensional

AC – Alternating Current

AD – Analogue-to-Digital

AM – Amplitude Modulation

AOA – Angle Of Arrival

ATDC – Adaptive Time Delay estimation based on Cumulants

CBM – Condition Based Monitoring

CW – Continuous Wave

DC – Direct Current

DCC – Direct Cross-Correlation

DF – Direction Finding

DOA – Direction Of Arrival

DWCC – Direct-Wave Cross-Correlation

EI – Electrical Interference

EMC – Electromagnetic Compatibility

EMI – Eeletromagnetic Interference

ESD – Electrostatic Discharge

FFT – Fast Fourier Transform

FIR – Finite Impulse Response

FM – Frequency Modulation

FT – Fourier Transform

GPS – Global Positioning System

HT – Hannan and Thomson processor

HW – Hanning Window

IF – Intermediate Frequency

LO – Local Oscillator

PD – Partial Discharge

PL – Position Location

RF – Radio Frequency

RF – Radio Frequency

RFI – Radio Frequency Interference

RM – Resolution Map

SCOT – Smoothed Coherence Transform

SNR – Signal to Noise Ratio

SSB – Single Side Band

TDE – Time Delay Estimation

TDOA – Time Difference Of Arrival

TOA – Time Of Arrival

TSOA – Time Sum Of Arrival

TV – Television

UHF – Ultra High Frequency

VHF – Very High Frequency

WIN – Wideband Impulsive Noise

Introduction

LOCATION OF WIDEBAND IMPULSIVE NOISE SOURCE

0.1 Overview of the problem

A radio communication system may experience several kinds of noise. Most noises, such as thermal, atmospheric, or galactic noise, can be accurately approximated by a Gaussian model. Gaussian (normal) distribution plays a predominant role in the realm of signal processing. Its simple justification by the central limit theorem, attractive properties, and ability to lead to simple solutions, have established it as one of the most important statistical distribution in almost every aspect of signal processing, as well as in many other areas of engineering science. These result in a wide range of very well established filtering techniques to treat the Gaussian noise problems.

However, man-made noises appear in the urban environment, created by electrical activities such as car ignition, partial discharges from power lines, heavy current switching of a substation switchgear, arc welding, fluorescent lighting, etc., can be very different and varies with situation and condition. Such a noise is difficult to characterise or model mathematically. Some common characteristics in these noises, however, can be noted by experience. It usually consists of a series of electromagnetic pulses bursting at relatively short time duration compare to a normal radio transmission. And, it is often of intermittent nature with frequencies covering across a broad bandwidth depending on the nature of the source. For

these characteristics, it will be conveniently referred to as the Wideband Impulsive Noise (WIN) in the thesis.

Screening and filtering techniques for WIN and related interferences are complicated and difficult to be implemented digitally or in an analogue system. WIN is of non-deterministic nature and only by applying plausible assumptions and confining a design to a limited range of conditions may a screen or filter be realised. Even so, such precautionary measures can never be 100 percent fool-proofed when challenged by all kinds of possible interference offered by the dynamic modern world.

Wideband impulsive noise is by and large accountable for wideband disturbances to communications systems and is now a subject of considerable research. Due to the increasing utilisation of the broadcast radio spectrum, set off by the growth of mobile communications and wideband digital services, the Electromagnetic Compatibility (EMC) requirements for impulsive noise interference must be continually reviewed. An allied aspect to the progression of EMC in this area is the ability to locate the impulsive noise source in order that remedial action may be taken.

Another reason for the importance of WIN location lies in the fact that frequency-spreading techniques are increasingly used for wireless communications: this means that the noise spectral components can only be associated with a genuine noise source if the location is known.

Impulsive noise location is therefore an indispensable first step in electromagnetic interference detection as deciphering the contents of such emission is usually impracticable. Interested parties in locating impulsive noise source include managers of radio spectra, electricity supply operators and EMC specialists.

0.1.1 Consequences of "Noisy" Thermostats on TV and Radio Receptions

A thermostat commonly found in a domestic environment, if faulty, could generate electrical interference that disturbs the reception quality of radio and television. Such an event can happen on a fairly random basis depending on the use of the equipment.

Unlike other sources of interference, which will be discussed in Chapter 2, WIN can interfere with a wide range of communication equipment and it is difficult to detect since its existence is only in short bursts of intermittent impulse. The effects of noise interference created by a faulty thermostat on the UHF analogue TV signal can be seen in Figure 0.1.

Fig. 0. 1. (a) A frame of normal TV broadcast.
(b) A frame being interfered by noise generated by a faulty thermostat.

From the facts file of the Radiocommunications Agency, such a circumstance is mostly experienced by analogue TV users in the bandwidth of 500-850MHz. A similar phenomenon can be caught on FM radio at 88-108MHz. An audible noise of cracking nature can be heard from both reception device and typically lasts from a few seconds up to 20 seconds or longer. It repeats typically every 10 minutes but, in some cases, a faulty thermostat may arc several times per minute.

Switching operation of a thermostat in central heating systems, refrigerators, freezers, etc are all potential sources of interference problem.

0.1.2 Present Method of Dealing with Radio Interference from a Faulty Thermostat

An investigation to track down the noise source will typically start from a suspicious area, which is commonly deduced to be the home of the complainer. A test may begin by checking on the circuit breaker or fuse panel and de-energise each circuit in the house. If the noise is still noticeable, it can be certain that the noise source is not in the house under investigation. A process of elimination may be repeated to narrow down the scope of investigation.

When suspicions arise, a quick check for the effects of electrical interference, caused by faulty gas boiler thermostat, can be accomplished using a simple household device such as a portable battery-operated radio, preferably one that covers Amplitude Modulation (AM), Frequency Modulation (FM), and short-wave.

A problematic thermostat will generate interference that can be easily heard on the radio for about more than a second. It will sound similar to a series of cracking noise occurring on fairly random basis. The replacement for a new thermostat is likely, if for once the duration of the interference exceed the acceptable limit.

The thermostat mechanism works in a form abiding to the general characteristics of a hysteresis operation curve. When a thermostat in a boiler system is faulty, it looses its hysteresis characteristics and result in a series of random and almost unpredictable switching operations. In some cases, the contacts are old and worn out and begin to weld very slightly. This result in a very fast repetitive opening

and closing action of the current carry contacts, generating intermittent radio interference.

The majority of the radio interference assignments, about 90% of the total investigated by the Radiocommunications agency, were related to old gas boiler systems. One of the main reasons is the relatively harsh working environment of a gas boiler system as compare to other domestic thermostats.

The only effective cure is to suppress or replace the thermostat. This makes it necessary to trace and locate it, which can be time consuming particularly if interference is related to radio reception. The source may be a considerable distance from the affected equipment. Even in the case of television broadcast reception, when the source is likely to be more local, there may be a number of suspect premises near enough to be the cause.

Cases of interference have been reported with the source found at 90 metres away and five households being affected! Unless a locator system can be designed to carry out the task automatically, which is problematic with its intermittent nature, it can take a very long time for hunting process with no assurance of success.

0.2 A New Approach to the Problem

The patience of job and qualifications of an experienced operative are the prerequisites for locating and correcting consumer-created interference. Even if a staff of such qualifications and aptitude is on the job, the task of locating and correcting the noise source is long, tedious and easily compromised if odd situations arise. The ability to locate a Wideband Impulsive Noise (WIN) source becomes a valuable and inevitable first step in mitigating the problems of noise interference caused by thermostats all over the country (UK).

To advance the noise location process, an endeavour to design a WIN locator system, on hardware and software basis, was taken to detect and locate noisy thermostats quickly so that the average efficiency of carrying out such tasks can be improved.

0.3 Other Possible Applications of WIN Location

A research in this field will establish and open up new areas of possibilities and even develop the potential of locating similar kinds of impulsive noises. Some examples of noises belong to the same category are, the electrical noise generated by partial discharges from a defective high-voltage power line conductor, electrical interference from an old electric clock on the mantle, a flickering fluorescent light and so on.

0.3.1 Switchgear Condition Monitoring

Previous researches carried out at the University of Bath, over the past five years, has shown that high voltage switching generates transient RF emissions that can be received by a normal AM receiver over a distance of more than 10km. The results show good correlation between RF emissions and switching duration; this is an important aspect in determining the health of the switchgears.

In general, power systems are exposed to elements such as wind, rain, heat, frost, pollution etc., and within these influences, many parts of the equipment must operate instantaneously, after long periods of quiescence. The general state of the interruption medium, insulation medium and the contacts of a circuit breaker must be in optimum condition.

Taking these points into consideration, it can be seen to be beneficial that switchgear is frequently examined or monitored on-line. Monitoring system health and predicting imminent failures on-line in critical power system components such as circuit breakers and isolators, however, cannot be easily done, especially in the old systems where the existing infrastructure may unable to support such activities. Regular maintenance plan are often required and usually very expensive. Sometimes, it is even disruptive, creating inconvenience such as putting the circuit breakers off-line for any work to carry out. A more flexible and economical regime would have a better understanding of the circuit breaker's health via on-line monitoring, and the monitoring system itself can easily be maintained or upgraded without compromising the integrity of the whole circuit-breaker system. In this way, it is hoped that an optimal resource allocation can be achieved.

A highly potent research on a new concept in switchgear condition monitoring, using the switching induced electromagnetic transient emission can be a very attractive approach. The ability to identify incipient faults and make accurate predictions well in advance of system failure is the key technical challenge addressed by condition monitoring researchers. It is postulated that advanced analysis of the spatial characteristics of the switching induced EMI may infer to some very important conditions of the switchgear, such as the inter-pole switching time, that otherwise could only be measured by a clamp-on evaluation system. Such a system will work without compromising the integrity and good track record of an old system switchgear monitoring via non-contact sensors with minimum installation requirement. An investigation to verify the hypothesis was carried out by incorporating the proto-type Wideband Impulsive Noise Location System and the results are reported in the thesis.

0.4 Outline of the Thesis

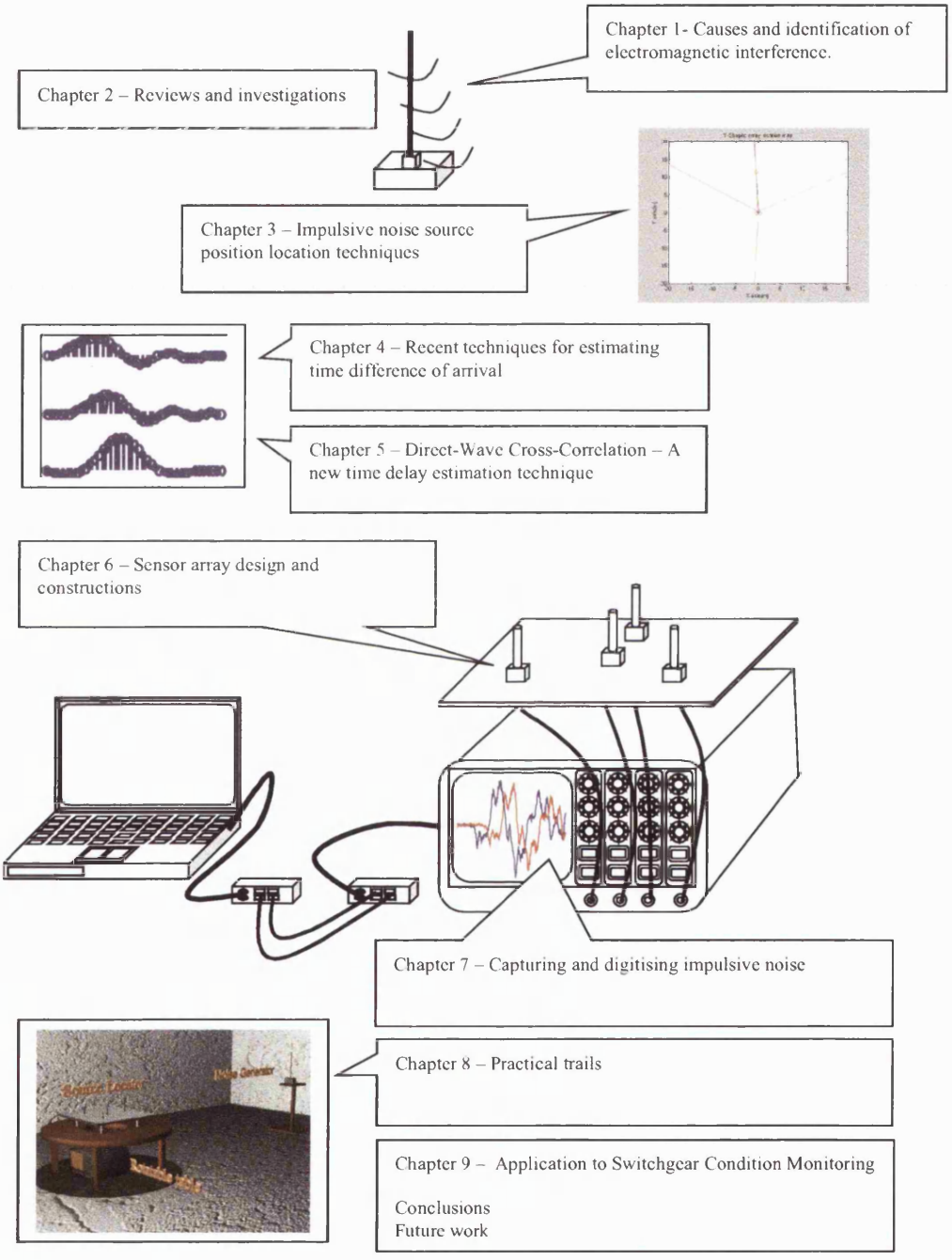

Fig. 0. 2. Outline of the thesis.

Chapter 1

CAUSES AND IDENTIFICATION OF ELECTROMAGNETIC INTERFERENCES

Introduction

There can be a few reasons as to why radio communications equipment receives interferences. For instances, the common types of interference to televisions are caused by communication equipment, high voltage switching etc. One main reason of interference is the distance between the transmitting source and the system's reception aerial. Interference is at least an occasional problem with most types of radio equipment, including wireless microphones. The effects of interference range from being a minor annoyance to serious consequences of making the wireless system completely unusable. Serious interference is not as common as is sometimes assumed, especially when some simple precautions are taken. However, when it does occur, it can be highly frustrating.

1.1. Types of Electromagnetic Interference

"Interference" is defined as a confusion of received radio signals due to stray and undesired signals. It is also defined as something that causes the confusion. Interference to radio signals occurs whenever an undesired voltage, signal, or disturbance is present in sufficient strength to be heard in the presence of the desired signal. Apart from that, there are many types of electromagnetic interferences [Eas77,Har70,Kib99,Par77] and for discussion purposes, it is generalised into three basic types: Electrical Interference (EI), Radio Frequency Interference (RFI) and inter-modulation. Computers and digital equipment, heavy

electrical equipment, lighting systems, faulty electrical devices such as thermostat, etc., causes EI. RFI is caused by radio and TV transmitters, communications equipment, cable television systems and other types of equipment that generate radio frequency energy as part of their operation. Inter-modulation is a type of interference caused by the internal combination of strong radio signals in wireless receivers.

A basic understanding of the symptoms and causes of the three types of interference is the key to deal with such problems effectively.

1.1.1 Electrical Interference (EI)

A typical environment includes many sources of electrical noise, for example, hand-held two-way radios, arc welders [Bar99], switching of large inductive loads, high fault currents, and high-energy fast transients associated with switching at the generator or transmission voltage levels [Her79]. The increasing use of advanced analogue and microprocessor based systems in electrical substation, reactor protection and other safety-related plant systems has introduced concerns with respect to the creation of additional noise sources and the susceptibility of this equipment to the electrical noise already present in the electrical substation, arc furnaces of an iron and steel factory and nuclear power plant environment [Mar85].

Electrical interference does not benefit anyone and is almost never intentional. With few exceptions, the equipment causing electrical interference problems was never intended to be a source of RF energy. Often, the interference is the result of a defect, failure or maintenance problem that can be readily corrected. Some types of electronic equipment simply tend to generate interference in the normal course of operation.

Generally, manufacturers are required to design and manufacture their products so that they do not cause harmful interference. In many cases, this is a legal requirement because the government has imposed regulations that place strict limits on the unintentional generation of RF interference. Manufacturers do their best to comply with these regulations because there can be severe penalties for the sale of devices not meeting the standards. Refer to Appendix B for EMI/EMC standards for commercial and non-military only.

However, these regulations are in the development stage and are not extensive enough to cover all types of equipment, such as lighting equipment and industrial electrical gear. In addition, electronic equipment that does conform to government requirements can still interfere with wireless systems if certain precautions are not taken. Age, wear and inadequate maintenance can also take their toll on equipment and cause it to eventually become a source of interference. In some instances, equipment was manufactured before the government regulations were in place, and there may have been no effort made to reduce interference.

1.1.2 Different Types of Electrical Interference (EI)

Noise from electrical equipment, noise generated by electronic devices such as computers, interference from natural sources such as lightning, etc are examples of several types of electrical interference. Perhaps surprisingly, all forms of electrical interference of power system origin are relatively rare and account for only a small percentage of all wireless interference problems. To a large extent this is because reduction of harmful interference has become a priority of both government and industry in recent years. Improvements in the design of wireless equipment have also contributed.

Electrical machinery and lighting systems are sources of electrical interference too. In most cases, the interferences are resulted from sparking, arcing or electrical discharges. In other instances, interferences may be caused by electrical control devices such as motor speed controls, temperature controllers, lighting dimmers, etc. High-voltage equipment, especially neon signs, is also a known source of electrical interference.

Sparking is common in electric motors with brushes, particularly older motors, certain kinds of large industrial motors and those with speed controls. Many home appliances and small tools such as vacuum cleaners, blenders and hand drills also use motors with brushes. Filters [Tur88] can be added to this type of motor to greatly reduce the interference caused by sparking. However, this was not a common practice in the past, and filters may be left out of present-day motors to reduce cost. In most cases, older and poorly maintained motors are more likely to cause interference than new units.

Arcing does not just cause interference [Bar99,Sin95], it is often presents a serious fire and safety risk. Aside from arc welding, they are usually caused by defective wirings and equipments, loose connections and failed insulators. Although high-voltage circuits are more prone to arcing, it often occurs in lower-voltage circuits when loose wires rub against each other or close to an earth plain. Loose electrical contacts can also arc when disturbed by vibration or shock. Arcing frequently tends to be intermittent, since a continuous arc soon burns away the conductors, or triggers a shutdown or complete failure. Intermittent occurrences make finding the exact source of the problem difficult.

Neon signs are particularly prone to arcing, because of the very high voltages present. This generally occurs near the tube supports or at connection points. Often, wires in neon systems are merely twisted together rather than being

soldered. This does not usually greatly affect the operation of the tube, but can create serious interference problems for wireless systems. Tubes can induce high voltages into metal objects close to them, causing secondary arcs in mounting frames and supports.

Electrical controllers, especially lamp dimmers and motor speed controllers, can be significant interference sources. Older theatrical lighting controllers are particularly prone to causing interference, especially those used with neon systems. Where dimmed fluorescent lights are used, both the dimmers and the lamps themselves are potential interference sources. Modern dimmers and controllers are much less likely to cause interference problems and it is still good practice to keep the wireless receiving antennas away from such devices.

In those cases where electrical interference does become a problem, the most commonly encountered type is RF noise generated by computers, digital equipment or a faulty thermostat. The interference can usually be identified by its characteristic of raspy whining or buzzing sound. Sometimes, a particular device will cause interference when actively processing, but not when idle.

Digital delays, digital effects processors and other equipment containing DSPs (digital signal processors) are more likely to cause wireless interference than computers [Tsl87]. This is because such devices are often mounted in the same cabinet or equipment rack as the wireless receivers. Generally, this type of interference is only a problem when the receiver is close to the digital device.

A digital device can generate interference that travels back through the AC power wiring or audio cables, eventually reaching the wireless receiver. At higher frequencies, the interference can sometimes travel on the outside of cables to the receiver. Physically separating both the devices and their power and audio cables

will usually minimize the problem. In a few instances, using a separate power source for the digital device or installing a line filter might prove necessary.

Manufacturers of computers and digital equipment are required to control the amount of interference they generate and to obtain government approval of each model or type that they sell. However, under the rules, digital devices are still allowed to leak a very small amount of interference, sometimes enough to disturb a sensitive wireless receiver mounted next to the device. Loose or missing case screws can also greatly increase the amount of interference leaking from an approved digital device. In addition, older equipment might not have been designed to minimize interference because in the past the regulations sometimes were not taken very seriously.

Natural sources, mostly lightning [Gab87,Uma82], account for only a very small percentage of electrical interference problems. Improved designs have made receivers less vulnerable to RF noise bursts from lightning. However, noise bursts on the incoming AC power line can still cause problems with wireless receivers and other sensitive audio gear, especially when lightning strikes power lines. In areas where lightning is common, surge protectors with high-performance AC line filters can be a wise investment.

1.1.3 Radio Frequency Interference (RFI)

This type of interference is caused by radio frequency (RF) signals on or near the frequency of the affected wireless receiver [Har70]. The interfering signals might have been transmitted intentionally, or unintentionally as the result of some defect or undesired characteristic of the source. It is not necessary that the interfering signal be exactly on the same frequency as the wireless system to be troublesome.

Strong RF signals that are near the wireless frequency can affect the operation of the wireless receiver, causing audio and reception problems.

Other wireless microphone transmitters are a frequent source of RF interference problems. In some instances, a wireless system includes both a body-pack and a handheld transmitter. Unless considerable care is taken, it is not unusual to accidentally turn on both transmitters at the same time. In this situation, the receiver will produce an extremely loud audio tone and the system will be completely unusable.

Similarly, if two wireless systems happen to use the same frequency, only one transmitter can be used at a time. Having two systems on the same frequency occurs more often than expected, especially in situations where wireless users come and go with their own systems. Synthesized equipment can also be troublesome in this regard, since a given model usually shares a particular small set of frequencies. If the frequency of a transmitter is changed, the chances are relatively high that there will be a conflict with another system of the same type.

Another source of interference is harmonics from FM radio stations and communications transmitters. Powerful FM station transmitters usually have a small amount of output at twice their operating frequency (the "second harmonic"), and this can be a source of interference to wireless systems operating in the VHF TV band. Unless the FM transmitter power is high and the transmitter nearby, interference from this source is rare. However, it is best to avoid wireless frequencies that are near harmonics of local FM radio stations.

Communications transmitters also have harmonic outputs that can potentially interfere with wireless systems. Protection of TV broadcasting is a government priority, so frequency assignments and technical requirements for

communications transmitters are such that the likelihood of problems is small. Generally, in the rare instances when interference from communications transmitters is experienced, it is a result of inter-modulation or defective equipment. Misadjusted or poorly maintained communications transmitters can have excessive harmonic or spurious output.

Spurious outputs from various kinds of RF equipment are occasional sources of interference. Cable television systems, communications receivers, cordless phones, remote garage door openers and even home TV and FM receivers can cause interference in rare instances. When the obvious sources of interference have been eliminated, it is always wise to suspect any electronic device capable of transmitting or receiving an RF signal, or which uses RF in its operation.

AM radio stations are sometimes a source of interference. However, in the vast majority of cases, this problem is not due to direct interference by the AM station. Wireless systems operate at frequencies far above that of AM transmitters and it is extremely unlikely that a transmitter harmonic or spurious output will affect a wireless receiver. AM radio transmitters sometimes interfere with many types of audio equipment, including mixers, power amplifiers, processors and other non-RF devices.

Normally, interference by AM radio stations is only a problem when the transmitter is close by. The high RF energy levels present directly affect sensitive audio circuitry, usually introducing the AM signals into the audio system. In general, the interference is picked up by audio cables or comes in through the power lines, and may still be present even when the wireless receiver is turned off. The solutions to this problem involve filtering and shielding of audio and power cables - quite different from the techniques required to eliminate direct RF interference. Solving RF interference problems almost always involves either

eliminating the source of the interfering signal or changing the frequency of the wireless system. Many interference problems of this type can be avoided entirely by simply selecting frequencies other than those already in use by local TV stations and other nearby wireless systems.

1.1.4 Interference cause by Inter-modulation

Inter-modulation is a type of interference sometimes encountered in radio communication systems such as wireless microphone systems [Kib99]. Inter-modulation differs from other forms of interference in that it is created in the wireless system itself, not directly by some external source. Other types of interference are caused by other transmitters on the wireless operating frequency, TV station carriers, the harmonic output of transmitters at lower frequencies, spurious emissions from various kinds of electronic equipment, and similar external sources. In each case, the interfering signal is on a frequency very near that of the wireless system.

Interference due to inter-modulation is caused by strong signals that are generally different from the wireless frequency. Instead, these strong signals overload some circuit in the wireless receiver, causing the circuit to internally generate harmonics of the strong signals. These harmonics then combine, or mix, in the receiver to create a new frequency that was not present at the receiver input. The newly created frequency, called an "inter-modulation product", then interferes with the wireless system in much the same way as other sources of interference.

Signals from nearby wireless transmitters are often stronger than the signals from local TV stations and frequently cause their own set of inter-modulation problems. The third and fourth harmonics of strong input signals can also mix in various combinations to create additional types of inter-modulation products, as

can combinations of three input signals. Collectively, these various troublesome combinations are commonly referred to as "intermod". Reliable and trouble-free wireless operation depends upon avoiding frequencies that are vulnerable to intermod.

The quality of the RF filtering in the receiver also has a major effect, since reducing the level of an interfering signal by even a small amount will lower the level of any inter-modulation products generated by a much greater amount. Thus, relatively small improvements in a receiver's overload capabilities and filtering can greatly enhance its inter-modulation performance. This is one of the reasons that higher quality equipment is less likely to have interference problems than cheaply made ones.

RF preamplifiers or active splitters can also be sources of inter-modulation problems [Zar74]. Once an inter-modulation product has been generated by one of these devices, the damage is done and no receiver will be able to reject the interference. For this reason, it is important to keep wireless transmitters well away from the receiving antennas to avoid overloading the RF preamplifiers. This is also the reason that it is best to avoid RF preamplifiers and active splitters when possible by using high-performance antennas and low-loss coaxial cables.

1.2. Understanding and Preventing Radio Frequency Interference

Radio-based devices such as walkie-talkies and pagers have been in use for many years but only until recently, there have been an increased number of radio frequency equipment in our daily life. This combined with the greater clock speed of our microprocessor-based systems and increased use of digital communication systems complicates the electromagnetic environment in our facilities.

The instrumentation systems must be able to function in the presence of high-frequency interference, which is commonly referred to as radio frequency interference (RFI). It is also sometimes referred to as electromagnetic interference (EMI), though this is somewhat of a misnomer as EMI covers a wider range of frequencies.

RFI can be defined as objectionable high-frequency electromagnetic radiation where the source is further away than the radiation's wavelength. Shorter than this distance is called the near field and electric or magnetic fields will dominate the interference coupling mechanism. The effectiveness of coupling RFI into a system is a function of the radiating source, its strength, the characteristics of the transmission path, the distance involved, and the sensitivity of the receiver.

Four basic methods can minimize RFI effects:

- Eliminate the radiating source.
- Shield either the source or the receiver.
- Separate the source and the receiver by a distance.
- Improve circuit design.

The most effective method for getting rid of an interference problem is to remove the radiating mechanism. Conversion of electromechanical contacts, for example, to solid state would remove the arc-generated RFI. Electrostatic discharge (ESD) generated RFI could be reduced by removing the charge generating mechanism or by providing a method to bleed off the charge.

Shielding is probably the most common means used to reduce the effects of RFI [Bro00]. Shielding can work both to prevent RFI from radiating out and preventing RFI from getting in. The effectiveness of a shield is a function of the

material, the frequency, the angle of incidence, coverage, and the thickness of the material. Metal is commonly used to shield RFI. Plastic materials used as shields are coated or impregnated with reflective and adsorptive materials or have embedded screens.

Often it is the enclosure openings, seams, and joints that are the limiting factors of the shield's effectiveness. Reduction in opening dimensions, screens, coatings, and special gasketing [Ada92] are some of the methods used to prevent RFI from getting into or out of enclosures. Cables in metal conduit are generally protected against RFI, but cables in a cable tray may open up windows of exposure. The effectiveness of cable shields such as aluminium foil, braided, and coaxial is a function of the material, frequency, thickness, and the shield coverage.

Distance can be used to provide separation between RFI generating equipment and the sensitive equipment by reducing the field strength of the RFI at the receiver. Administrative controls can also be used to prohibit RFI sources from being operated near sensitive equipment.

Circuit design can also help. Some common techniques used to minimize the effects of RFI include component location, conductor lengths, and component selection as well as the use of differential inputs, twisted pair cabling, common mode chokes, and ferrite beads. Some referred standards can be found in Appendix B.

Prevention and cure can generally sum up the approaches of tackling these problems. In curing, a very important parameter in the problem solving equation is the ability to identify and locate the position of an interfering source. One reason interference problems can be frustrating is that it is often difficult to know where to start tackling the problems. Sometimes it seems that everything affects

the problem, but nothing solves it. Simply knowing which type of interference is present and its physical location helps avoid wasting time on unproductive approaches and greatly simplifies the process of finding the real source of the problem. Only when a problem is identified and located can it be dealt with accordingly.

It was decided, after a well-investigated feasibility studies conducted via comprehensive literature survey and realistic practical experiments, that the project, described in the thesis, was undertaken in October 1999 to endeavour the location of wideband electromagnetic interference using an antenna array system via powerful signal processing algorithms. Chapter 2 presents the details of the feasibility studies.

1.3. References

[Ada92] Adams J. W., "Electromagnetic shielding of RF gaskets," *IEEE International Symp. EMC*, pp. 154-157, Anaheim, CA, United States, Aug. 1992.

[And82] Anderson P. M., Timko K. J., "A probabilistic model of power system disturbances," *IEEE Trans. on Circuits & Systems*, Vol. CAS-29, No. 11, pp. 789-96, USA, Nov. 1982.

[And92] Andria G., Salvatore L., Savino M., Trotta A., "Techniques for identification of harmonics in industrial power systems," *IMTC '92. IEEE Instrumentation and Measurement Technology Conference (Cat. No. 92CH3151-8) IEEE*, pp. 114-19, New York, NY, USA, 1992.

[Bar99] Bartlett E. J., Moore P. J., "Experimental investigation into VHF electromagnetic radiation from power system arcs," *Eleventh International Symposium on High Voltage Engineering (Conf. Publ. No.467). IEE.* Part Vol.1, pp. 295-8, London, UK, 1999.

[Bro00] Brown P., "EMC and interference suppression in power systems," *Electronic Engineering*, Vol. 72, No. 881, pp. 39-42, Publisher: Miller Freeman, UK, Jun. 2000.

[Eas77] Easton K. J., "Television interference from (overhead) power lines," *IEEE Trans. on Cable Television*, Vol. CATV-2, No. 4, pp.162-8, USA, Oct. 1977.

[Gab87] Gabrielson J. C., "The Aerospace Engineer Handbook of Lightning Protection," *Gainsville*, VA: Interference Control Technologies, 1987.

[Har70] Harvey J. L. W., "Radio frequency interference from electric power systems," *Proceedings of the Institution of Radio & Electronics Engineers, Australia*, Vol. 31, No. 8, pp. 269-75, Australia, Aug. 1970.

[Her79] Herman J. R., "Electromagnetic Ambients and Man-made Noise," *Gainsville*, VA: Interference Control Technologies, 1979.

[Kal97] Kaluza P., "Stochastic analysis of harmonic interference in power systems," *E&I Elektrotechnik und Informationstechnik*, Vol. 114, No. 6, pp. 298-303, Publisher: Springer-Verlag, Austria, 1997.

[Kib99] Kibria M., Zhang M., "Mobile inter-modulation interference (MIM) in cellular band-A due to CDMA transmissions in cellular band-B," *1999 IEEE 49th Vehicular Technology Conference (Cat. No.99CH36363). IEEE.* Part Vol. 3, pp. 2313-17, Piscataway, NJ, USA, 1999.

[Lof97] Loftness M. O., "Power line RF interference-sounds, patterns, and myths," *IEEE Trans. on Power Delivery*, Vol. 12, No. 2, pp. 934-40, Apr. 1997.

[Mar83] Mardiguian M., "How to Control Electrical Noise, *Gainsville*, VA: Interference Control Technologies, 1983.

[Par77] Parrish E. A., McDonald W. E., Aylor J. H., Gritton C. W. K., " Electromagnetic interference source identification through fuzzy clustering," *Proceedings of the 1977 IEEE Conference on Decision and Control. IEEE.* Part II, pp. 1419-23, New York, NY, USA, 1977.

[Shi00] Shih C. H., Keri A. J. F., Feero W. E., Maruvade P. S., Jutras P., Plante M., "Discussion of "An investigation to identify possible sources of electromagnetic field transients

responsible for exposures reported in recent epidemiological studies" Closure to discussion," *IEEE Trans. on Power Delivery*, Vol. 15, No. 4, pp. 1342-3, Oct. 2000.

[Sin95] Singh N., "Arcing generated electromagnetic fields associated with a high-voltage power system of the space station," *Proceedings IEEE Southeastcon '95. Visualize the Future (Cat. No.95CH35793). IEEE*, pp. 337-40, New York, NY, USA, 1995.

[Tsl87] Tsliovich A., "Statistical EMC – a new dimension in electromagnetic compatibility of digital electronic system," *Proc. IEEE International Symp. EMC*, pp. 469-474, 1987.

[Tur88] Turin L. S., "Designing of interference suppressing filters for switching transistor converters," *Ninth International Wroclaw Symposium and Exhibition on EMC*, pp. 639-642, Poland, June 1988.

[Uma82] Uman M. A. and Krider E. P., "A review of natural lightning – experimental data and modelling," *IEEE Tans. On EMC*, Vol. 24, pp. 79-112, May 1982.

[Zar74] Zarkiewicz R. S., "Deformations of the cross- and inter-modulation in HF resonance amplifiers." *Elektronika*, Vol. 15, No. 3, pp. 132-4, Poland, 1974.

Chapter 2

FEASIBILITY STUDIES

Introduction

The objective of this chapter is to evaluate, through realistic experimental investigation, the possibility of Direction Finding (DF) an impulsive noise source. It is used to aid a later work of fixing the location of an impulsive noise source. Experiments were conducted using a spark generator as the source. The waveforms were captured using a two-antenna array sampling at 1 GS/s. Digital signal processing technique, based on correlation, were employed to allow the assessment of the time delay between the antennas. Results in a non-ideal radio propagation environment show that the bearing can be estimated with an accuracy of 20°. Detailed information about the direction finding techniques is included.

2.1 Background of Direction Finding Theory

While radio DF for navigation purposes (cooperative DF) is losing its importance due to the availability of satellite navigation systems, the requirement for determining the location of emitters increases with the mobility of the communication equipment. Radio monitoring follows in line with ITU guidelines to search for interference sources and localization of non-authorized transmitters as deciphering the contents of such emissions is usually impossible.

The localization of emitters is often a multi-stage process and nothing straightforward. In general, the basic principle behind these algorithms is based on the assumption that the velocity of the electromagnetic wave is measurable

and it is traveling at a constant speed of light in vacuum i.e. $3\times10^{8} m/s$. This also justified the ability to measure the distance traveled by an electromagnetic wave over a measured period of time. Exact details of these algorithms are often a lot more complicated and will be introduced in chapter 3.

Consider an emitting source at a point producing an electromagnetic wave that propagates outwards in all direction. If two receivers are setup in two unique spaces, the wavefront will reach the receiver which is closer to the emitting source and then follow by the second receiver. This order, however, may change if the two receiver remains in the same position with the source replace to some other different positions. A more refine way of representing the change is by measuring the time difference of the wavefront reaching the receivers. With simple mathematics, the general direction of the emitting source can be determined since a unique time different will correspond to a unique angle if the source is bounded within 180 degrees. If another pair of receivers is being setup to perform the same task at another two unique locations, the intersection between the two directions, given by the two systems, will indicate the position of the emitting source. A better illustration, again, can be found in chapter 3.

If this is so, the dominating factors, that dictate the performance of a location system, will be based upon:

- how accurately can a waveform be measured. Since electromagnetic wave travels at a speed of light, a small time difference would cover a very huge distance in space.

- the ability of current technology to support such a measurement to the required precision. To process a waveform digitally with good resolution, a

relatively high sampling rate is required. This has to conform to the availability of off-the-shelf products with such specifications.

- other factors such as sensor choice, array design, etc may contribute to the accuracy of a measurement.

Most experiences and knowledge can be gained by taking a safe approach, before investing commitments into the project. This was achieved by conducting simplified experiments that focus only on a single parameter required in a location algorithm, which is the time delay estimate. This parameter can be easily converted to indicate the general direction of the source for performance assessment. An estimation of the approach's feasibility can, therefore, be concluded. Other assessment methods may be viable, however it was decided that taking the direction finding approach has the best combination in all aspects of the work. The feasibility studies has led to:

- a better understanding of the University's ability to support such a project with the current available equipment and resources.

- knowledge and information enrichment, as very little references were reported on this area of work.

- a decision on the value of pursuing the project further.

- knowledge assistance in the design of a proto-type system.

The studies and experiments have provided an indispensable first step in radio frequency detection and location. Practical results combined with theoretical findings are used in the justifications of the feasibility studies.

2.1.1 Historical Development

DF techniques have existed for as long as electromagnetic waves have been known. It was Heinrich Hertz who in 1888 found out about the directivity of antennas when he made his investigations in the decimetric wave range. An application of this for determining the direction of incidence of electromagnetic waves was proposed in 1906 in a patent of Scheller on a homing DF method. The initial DF units were polarization direction finders. They consisted of a rotatable electric or magnetic dipole whose axis is brought to coincidence with the direction of the electric or magnetic field. The knowledge about the polarization direction then led to the direction of incidence. The rotating-loop direction finder is one of the best-known direction finders of this type.

In 1907 Bellini and Tosi discovered the DF principle that was named after them: a combination of two crossed directional antennas (e.g. loop antennas) with a rotatable coil goniometer for determining the direction Despite this invention, rotating-loop direction finders were mostly used in the First World War.

The invention of Adcock meant a great step in the improvement of the DF accuracy of sky waves in the short-wave range. The pharmacist by profession realized, in 1917, that with the aid of vertical linear antennas (rod antennas or dipoles) directional characteristics can be generated corresponding to that of loop antennas but do not pick up any interfering horizontally polarized field components (In 1972 G. Eckard proved that this does not hold true without any restrictions). It was not until 1931 that Adcock antennas were first employed in practical applications in Great Britain and Germany.

Sir Watson-Watt made in the years 1925/26 the step from the mechanically moved goniometer direction finder to the electronic visual direction finder. As

from 1943 British naval vessels were equipped with crossed loops and three-channel Watson-Watt direction finders for the short-wave range ("huff-duff" for detecting German submarines). As from 1931 camouflaged direction finders were available for use in vehicles and as portable direction finders for detecting spies.

The first short-wave direction finder operating on the Doppler principle was built in 1941. The rapid progress in the development of radar in Great Britain made it necessary to cover higher frequency ranges: in 1943 the first direction finders for "radar observation" at around 3000 MHz were delivered. As from 1943 wide aperture circular array direction finders (Wullenweber) were built for use as remote direction finders. Since the 1950s, airports all over the world have been equipped with VHF/HF Doppler DF systems for air-traffic control.

In the early 1970s, digital technique made its way into DF and radiolocation; digital bearing evaluation and digital remote control are the main outcomes of this development.

As from 1980 digital signal processing has been increasingly used in DF. It permits the implementation of the interferometer direction finder and initial approaches towards the realization of multiwave direction finders (super resolution technique).

The first theoretical considerations were made much earlier. Another important impulse for the development came from the requirement for DF of frequency-agile emissions such as frequency- hopping and spread spectrum signals. The main result of this development was the broadband direction finder, which is able to simultaneously carry out the search and DF process on the basis of digital filter banks (usually with the aid of Fast Fourier Transform).

These days, radio direction finding techniques are used in many discipline such as mobile telecommunications, navigations and so on. However, direction finding of wideband noise is a new discipline on its own and, so far, similar attempts have been made recently without much success [Tun00].

2.2 Direction Finding of Wideband Impulsive Noise Sources

A common source of wideband interference is caused by a spark and can be easily generated by equipments, devices or events such as car ignition coil, fluorescent blast, static discharge, switching, thermostat, insulation break down in a supply line or faulty equipments and so on. Other sources of impulsive disturbances include electrical switchgear of all voltage levels, from 765 kV circuit breakers to power system fault arcs, caused predominantly by atmospheric disturbances to overhead lines, corona discharges on high voltage plant and so on.

Impulsive noise caused mainly by electrical discharges can either be complete or partial in nature. They cause frequency reception equipments to fail or deteriorate in reception quality for a very short period of time. However, users of frequency sensitive equipments are constantly irritated by such events and perceive them as failures or inferior production standards of the equipments. These demand the need to expand on the quality and quantitative data on this area of research and look into the possibility of categorising, and locating them.

2.2.1 Difficulties in Direction Finding of Impulsive Noise Sources

Radio frequency (DF) is now very well established in many areas including mobile communication [Ali99,Fea99] and sonar and radar systems [Car73a,Car73b,Car81,Ham74,Han73,Rot71]. DF signal processing utilises the records of multiple sensors to locate one or more sources of coherent energy. It is

usually assumed that the signal wavefront is plain and emitted from a point source.

The task of a radio direction finder is to estimate the direction of an emitter by measuring and evaluating electromagnetic field parameters. Usually the azimuth is sufficient to determine the direction; measurement of the elevation interest for emitters located in high platforms.

Only in the case of undisturbed wave propagation is the direction of the emitter identical with the direction of incidence of the radio waves. Usually there are a large number of partial waves arriving from different directions making a scattered field. The direction finder takes spatial and temporal samples from this wavefront and supplies, in the ideal case, the estimated values for the most probable direction of the emitter observed. The bearing can be referred to the following reference directions:

- True north (true radio bearing)
- Magnetic north
- Vehicle axis or relative radio bearing

The major difficulty in DF of signals generated by impulse transients is the prior knowledge of the source to be located in a known frequency band. Impulse transients are wideband and, due to their electrical discharge origins, often occur non-deterministically. In addition, the characteristics of the impulse transients vary more with the electrical source circuit and local conditions of the discharge, rather than the nature of the discharge itself.

For these reasons, DF of impulsive noise can be problematic with unknown variation from one situation to another, and little literature is available in this area.

2.2.2 Approach to Impulsive Noise Direction Finding

Direction finding (DF) of the impulsive sources relies upon the estimation of time delay of signals received from two spatially separated antennas. The bearing of the source can then be calculated from the time delay and the antenna positions. DF is fundamental to locating impulsive noise sources, since time delay estimates from multiple antenna pairs can be processed to reveal the impulsive origin.

Recent work describing the location of partial discharges from defective insulation [Tun00] utilised a 4-antenna array and conventional delay estimation calculations. The delay estimation error reported is almost an order of magnitude greater than results described here - an improvement made possible by more efficient signal processing techniques.

The finite time duration of impulsive transients and the wideband nature of their frequency components make them difficult to DF, if not expensive for such a system to be realized. Electromagnetic transients generated by high voltage switching is about $20\mu s$ [Pec00] and spark discharge can be as short as $1\mu s$ – refer to Figure 4. Generally a high sampling rate and multiple observations are required to achieve a statistically significant estimation of the pulse characteristics.

To DF the source of impulsive noise, a non-intrusive interference location technique based on electromagnetic wave propagation is robust and attractive if only its accuracy is within a reasonable tolerance. The accuracy of such technique is therefore directly proportional to the variance of the DF technique and the projection method employed. The next few sections will explain the DF algorithms for non-coherent electromagnetic transients generated by spark discharge.

2.2.3 Spark Generator as Impulsive Noise Source

Sparks can be ignited in many ways and in different conditions by different things or equipments. They are often discharges that occur with very short duration of time. A thermostat of an electric heater may cause sparks that last typically about 0.01sec or a domestic switching could have just about the same duration.

Often these sparks are impulsive and causes a wide spread of energy in the frequency domain. Consequently, it is very difficult to design screens that could effectively shield out such interferences and the impact on frequency sensitive equipment can reach to an unacceptable level. Therefore, a spark generator was built to generate a series of impulsive noise train as the interference source for the investigations.

2.2.4 Signal Model

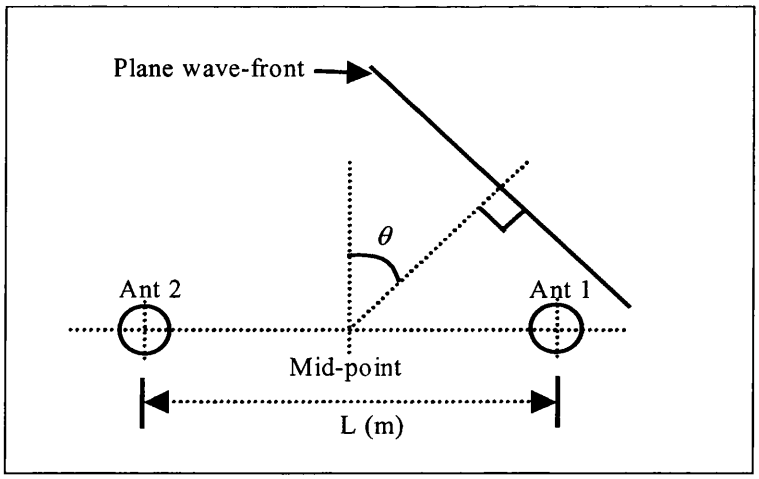

Fig. 2. 1. Determine bearing from time-delay.

DF relies upon reception of a target signal, $s(t)$, at two spatially separated receivers. If the source of the target signal is nearer to one receiver than the other,

then a time delay, D, between the receptions of $s(t)$ at the two receivers will be apparent. The time delay, being a function of receiver separation and the velocity of propagation of $s(t)$, can be used to calculate the bearing of target source from the receivers. In this context the target is the radiated component of an impulsive noise source that is received by two antennas, as shown in Figure 2.1. Assuming that the antennas are not responsive to static fields, all antenna signals may be considered to be zero mean.

The bearing, θ, of the noise source from the antenna baseline can be calculated from an estimation of D by:

$$\theta = \sin^{-1}\left(\frac{D}{D_{\max}}\right) \quad , \quad D_{\max} = \frac{L}{c} \tag{2. 1}$$

where $D_{\max}$ is the maximum possible time delay between the two antennas spatially separated by L metres and c is the speed of light assumed to be constant at $3x10^8 m/s$.

2.2.5 Experiment Setup

The source of the impulsive noise was generated using a simple spark gap. Constant streams of discharges were generated at intervals regulated by a pulse generator. This form of noise is representative of vehicle ignition systems, or the momentary breakdown of a power system insulation gap before, and sometimes during, the establishment of a stable conducting arc [Tex82]. The experimental spark generator is based on the well known automotive inductive discharge principle. The equipment allows a discharge length of up to 1cm to be drawn with momentary flash of visible light accompanied by a sharp audible noise.

To capture the radiated electromagnetic transient, a two-channel digital real-time Tektronix oscilloscope, having a sampling resolution of 1GS/s, was placed 25 metres from the spark generator. The oscilloscope was connected to two helically wound receiving antennas, spatially separated by 15cm. The antenna array was rotatable between 0°, where the antennas were equidistant from the spark generator, through to 90°, where one antenna was 15 cm nearer the generator than the other; this latter position gave the maximum time lag between the antenna signals (see Figure 2.2).

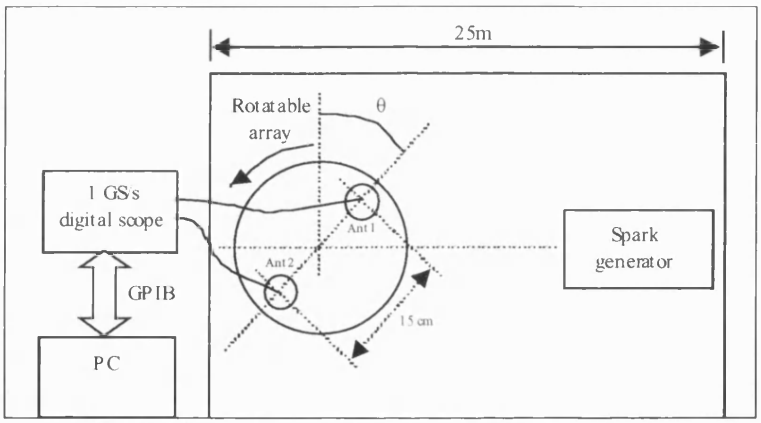

Fig. 2. 2. Impulsive noise generator and acquisition system.

The scope was amplitude triggered and recorded 2,500 data points, which were transferred directly to a computer hard disk. During the experimental procedure, the antenna array was rotated between 0° and 90° at 10° intervals; at every array position, 5 separate data recordings were made. The tests were made in a University building that was deliberately chosen to provide a realistic environment for the objectives of the work. Therefore, the tests benefited from neither a screened, nor anechoic environment.

The maximum time delay, corresponding to the two antennas and the spark generator being co-linear (i.e. $\theta = 90°$ in Figure 2.2), is $0.5ns$ assuming that the

signal propagates at $3x10^8 m/s$. Since the sampling interval is $1ns$, it is necessary to interpolate between sampling points to find the cross-correlation peak.

2.2.6 Results

The one-shot event of a discharge can be observed in Figure 2.3.

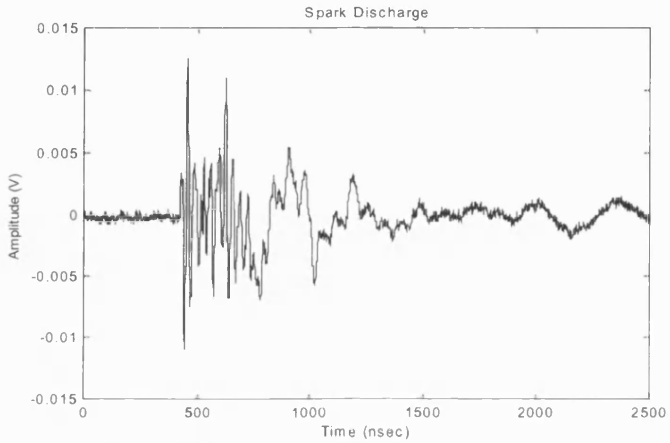

Fig. 2. 3. Time domain waveform of impulsive noise.

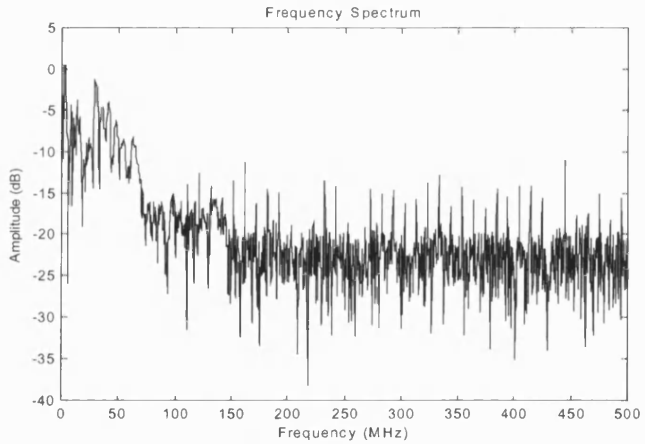

Fig. 2. 4. Filtered frequency spectrum.

The event exhibits an excursion of a typical transient with characteristics of damped sine waves decaying exponentially with time. Two dominant frequency components are apparent in Figure 2.3. The spectrum of the discharge, measured independently using a 2.5GHz spectrum analyser, showed that the majority of the signal power occurred in the region 0 – 100MHz. Although the antenna signals were sampled at 1 GS/s, the oscilloscope inputs are bandlimited to 100MHz; the antenna signals are effectively 5 times oversampled. An FFT plot of Figure 2.3 is shown in Figure 2.4.

The method of calculating the time delay experienced between the array elements is described in detail in chapter 4. The relevant results are shown here. An example of the magnitude squared coherence function (MSC) is shown in Figure 2.5. The MSC is bounded within the range of 0 and 1 as described in details in chapter 4. Ideally, the desirable characteristic for the MSC would be unity for all frequencies. However, in view of the 100MHz bandwidth of the oscilloscope, the MSC demonstrates a high level of coherence within this spectral region.

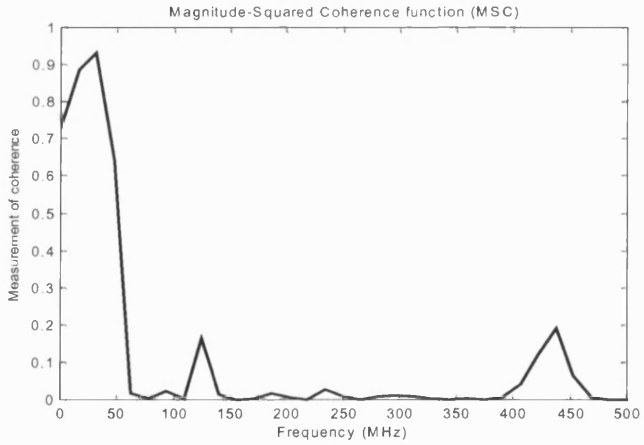

Fig. 2. 5. Magnitude-Squared Coherence.

From the MSC and the cross spectrum, a weighting function is found and applied as described in chapter 4, in the frequency domain, to the modified cross-correlation expression, which is then evaluated using the Inverse Fast Fourier Transform (IFFT). An example of the cross-correlation estimation is shown in Figure 2.6.

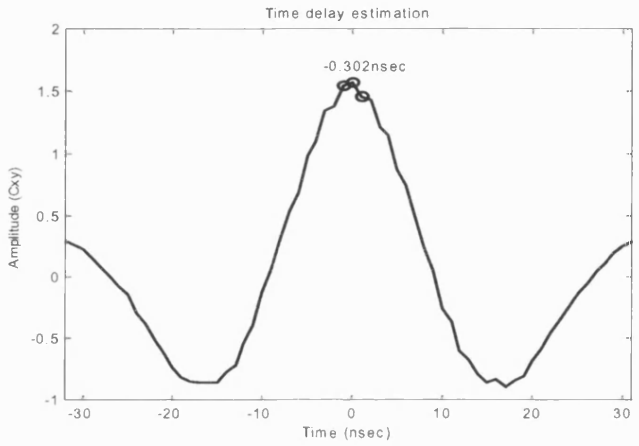

Fig. 2. 6. Time delay estimation.

In principle, the delay is estimated from Figure 2.6 by measuring from the peak of the main lobe to the time axis origin. In practice this measurement is complicated by the required delay ($0.5ns$ maximum) being less than the chosen sampling interval ($Ts = 1ns$). To overcome this difficulty, a 20^{th} order polynomial was fitted to the curve of the cross-correlation function which, due the periodogram based spectral estimation method, consists of 32 points. The position of the peak was found by differentiating the polynomial and searching for the zero crossing using a time-step of $1ps$. Polynomial curve fitting gave significantly improved results compared to a simple linear interpolation technique used initially.

The results for DCC and HT estimators, two different weighting functions, are presented in Figure 8 and 9 respectively. The delay estimates for each data recording are shown discretely together with the mean of the estimates for each array angle. Also shown on the Figures is the ideal delay curve calculated assuming plane wave propagation between the spark source and the antenna array. Since the spark generator was constructed compactly, it can be assumed to act as a point source in which case the wave propagates, more correctly, with a spherical wavefront. However, calculations show, for the experimental setup used, that the path length difference between plane or spherical wavefront propagation is negligible.

2.2.7 Discussion of Results

Considering the mean of the individual estimates, it is clear that the HT estimator, having a maximum bearing error of 20°, provides greater accuracy than the DCC approach, having a maximum error of 57°. It is interesting to note that both the DCC and HT mean curves deviate from the ideal characteristic at similar positions, e.g. overestimating the delay at 10°and underestimating at 60°. It is likely that the general shape of the curves is due to multipath effects since the room used for the tests is part of a steel framed building and reflections from unknown metallic structures buried in the walls could not be prevented. The existence of multipath effects is further highlighted by the shape of the example time delay estimation curve of Figure 2.6. Although this curve has a clearly defined peak, it is not smooth, implying that it represents the aggregate of several local maxima. Considering the individual estimates, rather than the mean, it is clear that the HT yields a lower variance of estimates compared to the DCC approach using the 5 measurements taken for each angle.

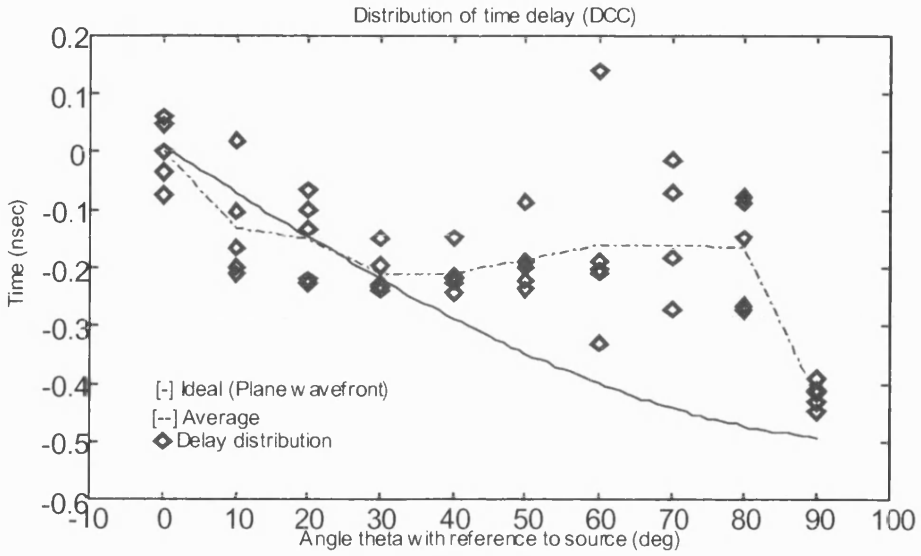

Fig. 2. 7. Results of direct cross-correlation.

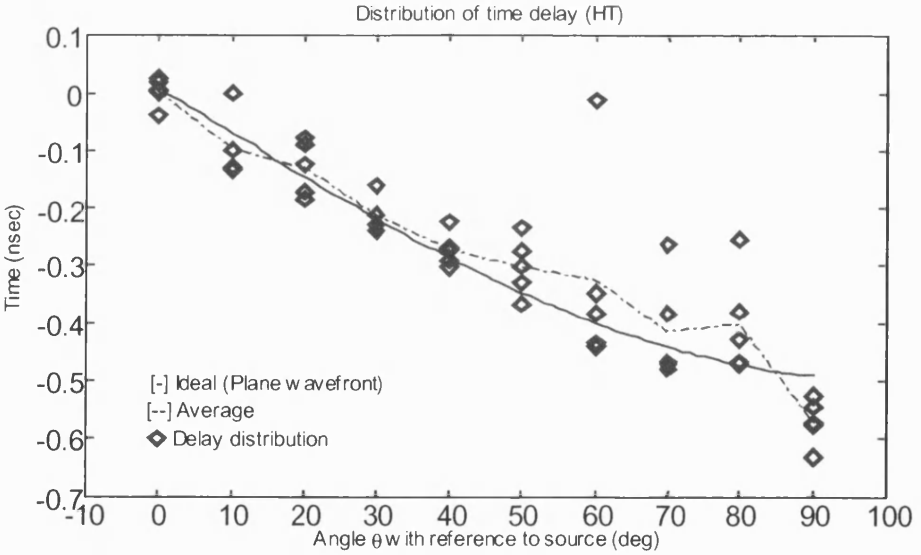

Fig. 2. 8. Results of Hannan and Thomson processor.

2.3 Discussions

A DF technique applicable to wide-band impulsive noise sources has been investigated using digital sampling equipment connected to two spatially separated antennas recording signals generated by a spark gap noise source. A digital signal processing technique based on the Hannan-Thomson delay estimation processor has shown to give a direction bearing accuracy of 20° using an average of 5 estimates. This technique has shown a significant increase in accuracy compared to the direct cross-correlation approach.

The results for this work were taken in a realistic working environment that was free from neither external noise nor multipath effects. Although the bandwidth of the receiving equipment is 100 MHz, and uses time samples that are large in comparison to the antenna spacing, the reported delay accuracy was estimated by a combination of 5 times oversampling and polynomial curve fitting of the correlation peak.

Finally, the investigation has shown the possibility of developing a impulsive noise source locator system to determine the location of a wideband impulsive noise source with more research and application of advance Digital Signal Processing (DSP) techniques, since the basic principle for direction finding and locating a source is similar.

The next chapter look at how the location of an impulsive noise source can be established.

2.4 References

[Ali99] Ali M., "The system applications of novel methods of location and tracking of cellular mobiles," *IEE Colloquium Novel Methods of Location and Tracking of Cellular Mobiles and their System Application*, pp. 6/1-4, May 1999.

[Bril83] Brillinger D. R., Krishnaiah P. R., "Handbook of statistics 3 – Time series in the frequency Domain," *Elsevier Science Publishers B. V.*, pp. 111-123, 1983.

[Car73a] Carter G. C., Knapp C. H. and Nuttall A. H., "Estimation of the magnitude-squared coherence function via overlapped fast Fourier transform processing," *IEEE Trans. Audio Electroacoustics*, vol. AU-21, no. 4, pp. 337-344, Aug. 1973.

[Car73b] Carter G. C., Nuttall A. H. and Cable P. G., "The smoothed coherence transform," *Proc. IEEE (Letter)*, vol. 61m, pp. 1497-1498, Oct. 1973.

[Car81] Carter G. C., "Time delay estimation for passive sonar signal processing," *IEEE Trans. Acoust, Speech, Signal Processing*, vol. ASSP-29, no. 3, Jun. 1981.

[Fea99] Featherstone W., Strangeways H. J., "Mobile transmitter AOA estimation under multipath conditions using an MLE based superresolution algorithm and comparison with weighted spectrum methods," *IEE Colloquium Novel Methods of Location and Tracking of Cellular Mobiles and their System Application*, pp. 4/1-5. May 1999.

[Ham74] Hamon B. V. and Hannan E. J., "Spectral estimation of time delay for dispersive and non-dispersive systems," *Appl. Statist.*, vol. 23, no. 2, pp. 134-142, 1974.

[Han73] Hannan E. J. and Thomson P. J., "Estimating group delay," *Biometrika*, vol. 60, pp. 241-253, Feb. 1973.

[Kna76] Knapp C. H. and Carter G. C., "The generalized correlation method for estimation of time delay," *IEEE Trans. Acoust., Speech, Signal Processing*, vol. ASSP-24, pp. 320-327, Aug. 1976.

[Neh94] Nehorai A. and Paldi E., "Vector-Sensor array processing for electromagnetic source localization," *IEEE Trans. Signal Processing*, vol. 42, no. 2, pp. 376-398, Feb. 1994.

[Pec00] Peck C. H. and Moore P. J., "Source identification and analysis of wideband electromagnetic interference generated by switchgears in a high voltage substation," *Proceedings of the EMC York 2000 Conference*, Jul. 2000.

[Pec01] Peck C. H. and Moore P. J., "A Direction-Finding Technique for Wide-Band Impulsive Noise Source," *IEEE Trans. EMC*, vol. 43, no. 2, pp. 149-154, May 2001.

[Rot71] Roth P. R., "Effective measurements using digital signal analysis," *IEEE Spectrum*, vol. 8, pp. 62-70, Apr. 1971.

[San99] Sanchez M. G., Haro L. D., Ramon M. C., Mansilla A., Ortega C. M., and Oliver D., "Impulsive noise measurements and characterization in a UHF digital TV channel," *IEEE Trans. Electromagn. Compat.*, vol. 41, no. 2, May 1999.

[Sar96] Sarmadi M., "Radio and television interference caused by corona discharges from high-voltage transmission lines: fast changing parameters influencing RN generation," *Proc. of the American Power Conference 58th Annual Meeting*, vol.2, pp.1601-6, 1996.

[Sch86] Schmit R. O., "Multiple emitter location and signal parameter estimation," *IEEE Trans. Antennas and Propagation*, Vol. AP-34, No. 3, pp. 276-280, Mar. 1986.

[Tex82] Texas A & M Research Foundation, "Detection of arcing faults on distribution feeders", Electric Power Research Institute, Final Report EL-2757, 1982.

[Tun00] Tungkanawanich A., Abe J., Kawasaki Z. I. and Matsuura K., "Location of partial discharge source on distribution line by measuring emitted pulse-train electromagnetic waves," *Proceedings of IEEE Power Engineering Society Winter Meeting 2000*, IEEE catalogue 00CH37077C, CDROM 0-7803-5938-0.

Chapter 3

IMPULSIVE NOISE SOURCE POSITION LOCATION TECHNIQUES

Introduction

Position Location (PL) is a complex process and usually consists of a hybrid of mathematical methods to achieve the whole algorithm. Each of these methods, if not considered carefully, can have serious deterioration to the overall performance of a locator. Impulsive noise position location is accomplished in two stages. The first stage involves estimation of the Time-Difference-Of-Arrival (TDOA) between the sensors. The second stage utilises an efficient algorithm to produce an unambiguous estimate to fix the location of the source. In a search for the most effective and efficient algorithm, mathematics from navigation science has been investigated. Other problems such as inherent mathematically correct solutions that contradict with the true practical solution are carefully considered and discussed in detail in this chapter.

3.1 Overview of Different Position Location Techniques

Position Location (PL) systems can be classified by the number of measurements used such as multilateration or trilateration; and by the type of measurement used such as phase, time or frequency. Multilateration PL systems are systems that utilize measurements from four or more sensors to estimate the three-dimensional (3D) location of the source. Trilateration PL systems are those that utilize measurements from three sensors to estimate the two-dimensional (2D) location of the source. The next few sections will briefly describe the few viable techniques for estimating position location of an impulsive noise source and also to assess the inherent limitations in the physics of position location.

3.1.1 Direction Finding Position Location Systems

Direction Finding (DF) PL systems estimate the PL of a source via measuring the Direction-Of-Arrival (DOA) of the source. This is also referred to as the Angle-Of-Arrival (AOA) of the source. The DOA measurement restricts the location of the source along a line in the estimated DOA. Multiple DOA measurements from multiple sensors are used in a triangulation configuration to estimate the location of the source that lies on the intersection of these lines. Consequently, DF PL systems are also known as DOA or AOA PL systems. Figure 3.1 illustrates a two dimensional (2D) PL solution for DF systems.

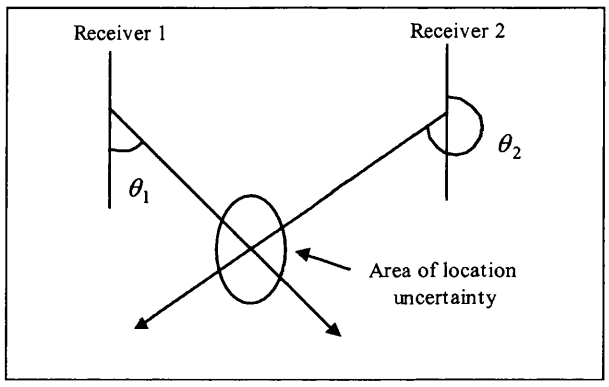

Fig. 3. 1. Direction Finding Based Position Location.

While only two DOA estimates are required to approximate the PL of a source, multiple DOA estimates are commonly used to improve the estimation accuracy. DOA estimation is performed by signal parameter estimation algorithms which exploit the phase differences or other signal characteristics between closely spaced sensor elements of a sensor array and employ phase-alignment methods such as beam/null steering [Tsa96]. The spacing of sensor elements within the sensor array is typically less than half wavelength of all received signals. This alignment is required to produce phase differences on the order of π radians or less to avoid

ambiguities in the DOA estimate. The resolution of DOA estimators improves as the baseline distances between the sensors increase. However, this improvement is at the expense of ambiguities. As a result, DOA estimation methods are often used with short baselines to reduce or eliminate the ambiguities and long baselines to improve resolution.

3.1.2 Range-based Position Location Systems

Range-based PL systems [Abe89] can be categorized as ranging, range sum, or range difference PL system. The type of measurement used in each of these systems defines a unique geometry, or configuration, of the PL solution. Ranging PL systems locate a source by measuring the absolute distances between the source and the sensors. A range measurement is determined by estimating the Time-Of-Arrival (TOA) of the signal propagating between the source and the sensor. The TOA estimate defines a sphere of constant range around each sensor. The intersections of multiple spheres produced by multiple range measurements from multiple sensors provide the PL estimates of the source. Consequently, ranging systems are also known as TOA or spherical PL systems.

Range sum PL systems measure the relative sum of ranges between a source and the receiving sensors respectively. These systems measure the Time-Sum-Of-Arrival (TSOA) of the propagating signal between two sensors to produce a range sum measurement. The range sum estimate defines an ellipsoid around the sensors, and when multiple range sum measurements are obtained, the PL estimate of the source is at the intersection of the ellipsoids. As a result, range sum PL systems are also known as TSOA or elliptical PL systems.

Range difference PL systems measure the relative difference in ranges between the source and sensors respectively. These systems measure the Time-Difference-

Of-Arrival (TDOA) of the propagating signal between two sensors to produce a range difference measurement. The range difference measurement defines a hyperboloid of constant range difference with a sensor at the foci. When multiple range difference measurements are obtained, producing multiple hyperboloids, the PL estimate of the source is at the intersection of the hyperboloids. Consequently, range difference PL systems are also known as TDOA or hyperbolic PL systems. Throughout the thesis, systems of this class will be referred to as hyperbolic PL systems.

3.1.3 Ranging or Spherical Position Location Systems

Ranging PL systems measure the absolute distance between a source and a set of sensors through the use of TOA measurements. The TOA measurements are related to range estimates that define a sphere around each sensor. When measurements are made from multiple sensors with known locations, the spheres described by the range measurements intersect at a unique point indicating the PL estimate of the source. If the spheres described by the range measurements intersect at more than one point, an ambiguous solution to the PL estimate results. Redundant range measurements, resulting in a multilateration ranging PL estimation, are commonly made to reduce or eliminate PL ambiguities. To clarify the ranging PL concept, consider a 2D ranging PL system using N sensors. The TOA of a signal at each sensor is estimated and related to the range measurement by the relationship:

$$R_i = cD_i \tag{3.1}$$

where R_i is the range measurement, c is the constant speed of light propagating at $3.0\times10^8 m/s$ and D_i is the TOA estimate at the ith sensor. The mathematical

relationship between range measurements, for the known coordinates of N sensors, and the coordinates of the source is:

$$R_i = \sqrt{(x-x_i)^2 + (y-y_i)^2} \quad , \quad i = 1,2,\ldots,N \tag{3.2}$$

where (x_i, y_i) is the known coordinate of the ith sensor, R_i is the ith range estimate to the source at an estimated coordinate of (x, y). Equation (3.2) defines a set of non-linear equations whose solution (x, y) is the location coordinates of the source. In a practical application, where errors may exist in the measurement, the system can become inconsistent and a unique solution may or may not exist. This generally requires an error criterion to be selected and iterative techniques to be employed to produce a solution. A least squares fit is commonly used to simultaneously solve these equations for both the PL and error coefficients. Accurate time or phase measurements in ranging PL systems require strict clock synchronization between the source and the sensors.

A disadvantage of the ranging PL technique is that accuracy is very dependent on system geometry. Highest accuracy is attained when all ranging spheres intersect at 90 degrees. Degradation in performance is experienced as the intersections deviate from this angle.

3.1.4 Range Sum or Elliptical Position Location Systems

Elliptical PL systems locate a source by the intersection of ellipsoids describing the range sum measurements between multiple sensors. The range sum is determined from the sum of signal TOA's at multiple sensors. The relationship between range sum R_{ij}^s, and the TOA between sensors is given by:

$$R_{ij}^{s} = cS_{ij} = R_i + R_j \tag{3.3}$$

where c is the signal propagation speed and S_{ij} is the sum of TOA of sensors i and j. The range sum measurement restricts the possible source location to an ellipsoid. The ellipsoids that describe the range sum between sensors is given by:

$$R_{ij}^{s} = \sqrt{(x-x_i)^2 + (y-y_i)^2} + \sqrt{(x-x_j)^2 + (y-y_i)^2} \tag{3.4}$$

where (x_i, y_i) and (x_j, y_j) denote the locations of sensors i and j, and (x, y) is the PL estimate of the source. A source location can be uniquely determined by the intersection of three or more ellipsoids. Redundant range sum measurements can be made to improve the accuracy and resolve location solution ambiguities. While there are existences of some systems that are using this method, it appears to offer no performance advantage over the spherical or hyperbolic configurations.

3.1.5 Range Difference or Hyperbolic Position Location Systems

Hyperbolic PL systems estimate the location of a source by the intersection of hyperboloids describing range difference measurements between three or more sensors. The range difference between two sensors is determined by measuring the difference in time of arrival of a signal between them. The relationship between range difference R_{ij} and the TDOA between sensors is given by:

$$R_{ij} = cD_{ij} = R_i - R_j \tag{3.5}$$

where c is the speed of light propagating at a constant speed of $3.0\times10^{8} m/s$ and D_{ij} is the TDOA between the sensors i and j. The TDOA estimate, in the absence of noise and interference, restricts the possible source location to a hyperboloid of revolution with the sensors as the foci. In a 2D system, the hyperboloids that describe the range difference R_{ij}, between the sensors are given by:

$$R_{ij} = \sqrt{(x-x_i)^2+(y-y_i)^2} - \sqrt{(x-x_j)^2+(y-y_j)^2} \tag{3.6}$$

where (x_i, y_i) and (x_j, y_j) denote the locations of sensors i and j respectively, R_{ij} is the range difference measurement between sensor i and j, and (x, y) is the unknown coordinate of the source. If the source and sensors are coplanar, two-dimensional (2D) source location can be estimated from the intersection of two or more hyperboloids produced from three or more TDOA measurements, resulting in a hyperbolic trilateration solution. Three-dimensional 3D source location estimation is produced by the intersection of three or more independently generated hyperboloids generated from four or more TDOA measurements, resulting in a hyperbolic multilateration solution.

If the hyperbola determined from multiple sensors intersects at more than one point, then ambiguity in the estimated position exists. This location ambiguity may be resolved by using prior information about the source location, bearing measurements at one or more of the sensors, or redundant range difference measurements at additional sensor to generate additional hyperbolas. A major advantage of this TDOA method is that it does not require the knowledge of emission time from the source, as in a TOA method. Consequently, strict clock synchronization between the source and sensor is not required making PL of impulsive noise of arbitrary emission timing possible. Furthermore, the hyperbolic

PL method is able to reduce or eliminate common errors experienced on different channels. Conversely, precise clock synchronization is required for all sensors used for the PL estimate.

3.2 Discussion on Different Position Location Techniques

The two PL techniques considered, for locating impulsive noise source, are DF and hyperbolic methods. While DF systems exploit the relative phase differences between closely spaced sensor elements and employ phase-alignment methods for beam/null steering [Tsa96] to estimate the DOA of an electromagnetic waveform, hyperbolic methods exploit the relative time differences of the waveforms arriving at different sensors.

The need for high resolution arises primarily when closely spaced sources, give rise to multiple received waveforms, is unable to be separated by processing methods for the PL estimate to be made. For instance, when cross-correlating TDOA of multiple waveforms that are not separated by more than the widths of their cross-correlation peaks, the peak cross correlation of the waveforms usually cannot be resolved with conventional TDOA-based methods. To minimize this problem, the distance between platforms is typically made as large as possible to minimize overlap of adjacent peaks. This presents a fundamental resolution-limit problem for TDOA estimation of two closely spaced sources.

The best performing array-based DF methods attempt to resolve the resolution problem in locating multiple sources by simultaneously estimating multiple DOA rather than estimating the DOA of each waveform as is commonly done by conventional beamformers and TDOA-based techniques. Although DF techniques offer greater spatial resolution and the ability to simultaneously locate a number of waveforms, their complexity is typically much higher than that of

TDOA techniques and may not be feasible in the case of locating impulsive noise source, which is non-deterministic in nature.

3.3 Hyperbolic Position Location Systems

An interference source can be located using an array of sensors utilizing TDOA estimations between the sensors. Figure 3.2 is a locus plot of the possible source locations for a two-sensors system given a TDOA estimate D_{12} where:

$$cD_{12} = R_1 - R_2 \tag{3.7}$$

and c is the speed of light propagating at a constant speed of $3.0\times10^8 m/s$. The locus satisfies a general hyperbolic relationship described by:

$$\frac{x^2}{a} - \frac{y^2}{b} = 1 \tag{3.8}$$

$$a = (2g - (R_1 - R_2))/2 = (2g - cD_{12})/2 \tag{3.9}$$

$$b = \sqrt{g^2 - a^2} \tag{3.10}$$

The constants in equations (3.8) to (3.10) are defined in Figure 3.2.

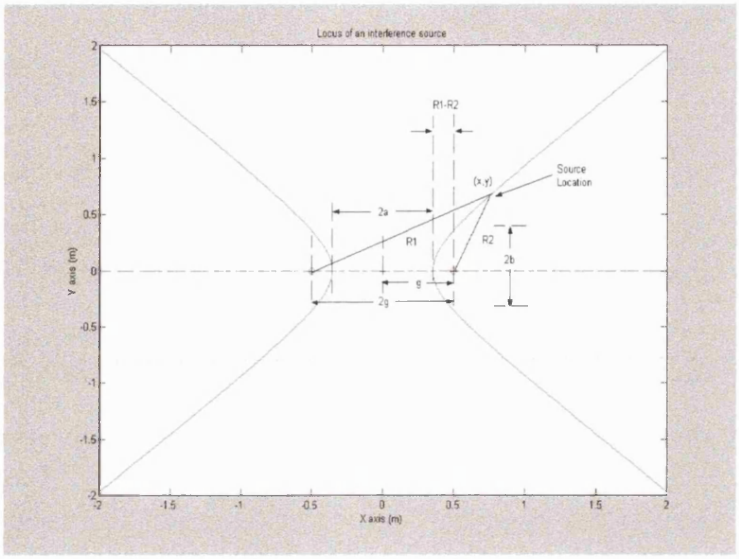

Fig. 3. 2. Locus plot of a two-sensors system of all possible interference locations.

3.4 Solutions for Hyperbolic Position Fixes

A fast solution to simultaneous hyperbolic equations with exact solution is of great importance in navigation science [Cha94,Foy76]. The main idea is to overcome the need for iteration algorithms typically used for solving simultaneous hyperbolic equations. They can be computationally intensive and typically require a relatively longer processing time and larger power requirement. Time can be a very critical factor in designing a spontaneous system where an instantaneous estimation is required on request. Minimising the power requirement is often needed for standalone systems or handheld such as a personal Global Positioning System (GPS) to ensure long battery life. Surprisingly, there is no reference to be found on applying such algorithms into the realm of RF location systems. Typically, an indirect iterative of more computationally intensive methods, such as Newton Raphson's, is employed.

3.4.1 Three-Input Position Location Systems

For three arbitrarily placed sensors and a consistent system of equations, there exists a direct solution. Fang [Fan90] has derived an exact solution for solving the unknown source coordinates directly. He establishes a coordinate system so that the first sensor is located at (0,0,0), the second at $(x_2, y_2 = 0, z_2 = 0)$ and the third at $(x_3, y_3, z_3 = 0)$. Realizing that by setting the second sensor position $y_2 = 0, z_2 = 0$, and for the third $z_3 = 0$ without the loss of generality, the relationships between the equations are greatly simplified.

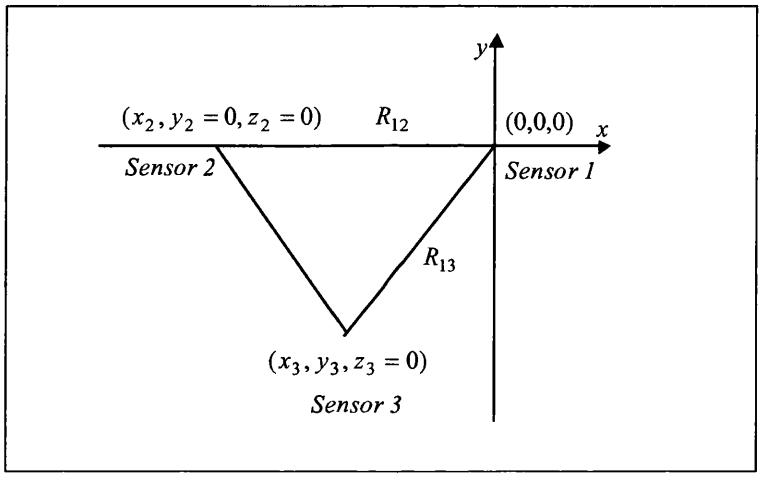

Fig. 3. 3. Position Location for three-sensors systems.

Figure 3.3 shows a source location relative to three sensors 1, 2, 3. A set of local right angle axes is chosen as shown. The origin is on one of the sensors, X-axis is along the sensor baseline, and Y-axis forms a right angle to the baseline. Let c be the constant speed of light propagating at $3.0\times10^8 m/s$, $D_{12} = D_1 - D_2$ and $D_{13} = D_1 - D_3$ be the differences in the TOA's, $cD_{12} = R_1 - R_2$ and $cD_{13} = R_1 - R_3$ are the distances between sensors 1, 2 and 1, 3 respectively. It can be easily derived, from Figure 3.3, that:

$$\sqrt{x^2+y^2+z^2}-\sqrt{(x-x_2)^2+y^2+z^2}=cD_{12}=R_{12} \tag{3.11}$$

$$\sqrt{x^2+y^2+z^2}-\sqrt{(x-x_3)^2+(y-y_3)^2+z^2}=cD_{13}=R_{13} \tag{3.12}$$

where x, y and z is the 3D coordinate of the source location. R_{12} and R_{13} are the range differences from the source location to the sensors – a function of the measured time difference of arrival. Rearrange the first term to the right hand side of both equations follow by squaring and simplifying:

$$R_{12}^2-x_2^2+2x_2x=2R_{12}\sqrt{x^2+y^2+z^2} \tag{3.13}$$

$$R_{13}^2-L_3^2+2x_3x+2y_3y=2R_{13}\sqrt{x^2+y^2+z^2} \tag{3.14}$$

where $L_3=\sqrt{x_3^2+y_3^2}$ is the length of the sensors baseline. These two equations, when squared, represent two hyperboloids of revolution with foci at sensors 1, 2 and 1, 3, respectively.

Note that for measurements consisting of sums instead of differences of times of arrival, a set of equations similar to (3.11) and (3.12) with positive signs between the radicals will result. This is interpreted as range sums instead of range differences. Squaring these new equations will give an identical result as in (3.13) and (3.14), although now they are representing ellipsoids of revolution rather than hyperboloids. Thus the derivations are applicable to range sum measurements as well as range difference measurements. Then y is obtained by equating (3.13) and (3.14) to produce:

$$y=ux+v \tag{3.15}$$

where

$$u = \frac{R_{13}(x_2 / R_{12}) - x_3}{y_3} \tag{3.16}$$

$$v = \frac{L_3^2 - R_{13}^2 + R_{13}R_{12}\left(1 - \left(\frac{x_2}{R_{12}}\right)^2\right)}{2y_3} \tag{3.17}$$

substituting (3.15) into (3.13) to obtain z:

$$z = \pm\sqrt{dx^2 + ex + f} \quad \text{or} \tag{3.18}$$

$$z^2 = dx^2 + ex + f \tag{3.19}$$

where

$$d = -[1 - (x_2 / R_{12})^2 + u^2] \tag{3.20}$$

$$e = x_2[1 - (x_2 / R_{12})^2] - 2uv \tag{3.21}$$

$$f = (R_{12}^2 / 4)[1 - (x_2 / R_{12})^2]^2 - v^2 \tag{3.22}$$

The curve produced by these equations is either an ellipse or a hyperbola depending on whether $x_2 < 0$ *or* $x_2 > 0$. Finally, the source location can be written as a vector depending on a single unknown parameter x:

$$\vec{R} = x\vec{i} + (ux + v)\vec{j} \pm \sqrt{dx^2 + ex + f}\,\vec{k} \tag{3.23}$$

To fix the source position on the ellipse or hyperbola, additional information is required. By restricting the problem to coplanar so that $z=0$, x is now obtainable as a solution of (3.19), i.e.,

$$d\cdot x^2+e\cdot x+f=0 \tag{3.24}$$

Solving the quadratic equation produces two admissible solutions corresponding to the two roots of (3.24). This two-fold ambiguity can be resolved by some knowledge of the general location of the source.

3.4.2 Four-Input Position Location Systems

Similarly for a four-sensors system an exact solution can be derived. Details of which can be found in [Buc00]. The following are extracts of the main details required to solve the problem of locating impulsive noise source using a four-sensors system:

$$cD_1 = R_1 = \sqrt{(x-x_1)^2+(y-y_1)^2+(z-z_1)^2} \tag{3.25}$$

$$cD_2 = R_2 = \sqrt{(x-x_2)^2+(y-y_2)^2+(z-z_2)^2} \tag{3.26}$$

$$cD_3 = R_3 = \sqrt{(x-x_3)^2+(y-y_3)^2+(z-z_3)^2} \tag{3.27}$$

$$cD_4 = R_4 = \sqrt{(x-x_4)^2+(y-y_4)^2+(z-z_4)^2} \tag{3.28}$$

For equation simplification, $R_{ij}=R_i-R_j$ and $x_{ij}=x_i-x_j$, where $i,j=1,2,3$. Solving the above four equations for the three unknowns of the source location coordinate, x, y and z, results in the following set of equations:

$$x = Gz + H \tag{3.29}$$

$$y = Iz + J \tag{3.30}$$

$$z = \frac{N}{2M} \pm \sqrt{\left(\frac{N}{2M}\right)^2 - \frac{O}{M}} \tag{3.31}$$

where

$$M = 4R_{13}^2(G^2 + I^2 + 1) - L^2 \tag{3.32}$$

$$N = 8R_{13}^2[G(x_1 - H) + I(y_1 - J) + z_1] + 2LK \tag{3.33}$$

$$O = 4R_{13}^2[(x_1 - H)^2 + (y_1 - J)^2 + z_1^2] - K^2 \tag{3.34}$$

$$G = \frac{E - B}{A - D} \tag{3.35}$$

$$H = \frac{F - C}{A - D} \tag{3.36}$$

$$I = AG + B \tag{3.37}$$

$$J = AH + C \tag{3.38}$$

$$K = R_{13}^2 + x_1^2 - x_3^2 + y_1^2 - y_3^2 + z_1^2 - z_3^2 + 2x_{31}H + 2y_{31}J \tag{3.39}$$

$$L = 2(x_{31}G + y_{31}I + 2z_{31}) \tag{3.40}$$

$$A = \left(\frac{R_{13}x_{21} - R_{12}x_{31}}{R_{12}y_{31} - R_{13}y_{21}}\right) \tag{3.41}$$

$$B = \left(\frac{R_{13}z_{21} - R_{12}z_{31}}{R_{12}y_{31} - R_{13}y_{21}}\right) \tag{3.42}$$

$$C = \frac{[R_{13}(R_{12}^2 + x_1^2 - x_2^2 + y_1^2 - y_2^2 + z_1^2 - z_2^2) - R_{12}(R_{13}^2 + x_1^2 - x_3^2 + y_1^2 - y_3^2 + z_1^2 - z_3^2)]}{2(R_{12}y_{31} - R_{13}y_{21})} \tag{3.43}$$

$$D = \left(\frac{R_{34}x_{23} - R_{32}x_{43}}{R_{32}y_{43} - R_{34}y_{23}} \right) \tag{3.44}$$

$$E = \left(\frac{R_{34}z_{23} - R_{32}z_{43}}{R_{32}y_{43} - R_{34}y_{23}} \right) \tag{3.45}$$

$$F = \frac{[R_{34}(R_{32}^2 + x_3^2 - x_2^2 + y_3^2 - y_2^2 + z_3^2 - z_2^2) - R_{32}(R_{34}^2 + x_3^2 - x_4^2 + y_3^2 - y_4^2 + z_3^2 - z_4^2)]}{2(R_{32}y_{43} - R_{34}y_{23})} \tag{3.46}$$

There are only two references, [Fan90,Buc00], found pertaining to this area of work – exact solution for hyperbolic and related position fixes. They proved to be invaluable to the area of work described in the thesis.

3.5 Simulation of a Hyperbolic Position Location System

A simulation of the Hyperbolic Position Location System has been made in order to establish its ability to locate a source at any position without any ambiguity. Given the required TDOA estimates a visual display of the location loci, represented by hyperbola curves, is provided for error checking. Only two pairs of these curves are required to produce an intersection which fixes the position of the source.

The redundant curves are for visual detection of abnormalities. A set of coherent hyperbolic curves, closing up at one intersection point to indicate the location of the source, is usually the result if the system is functioning properly. However, if the system is uncertain, it may still produce a location estimate but the result can be very misleading. With this visual aid, such an adverse effect is easily detectable. Figure 3.4 and 3.5 show the simulation results for Y-Shaped array and Square array Hyperbolic Position Location Systems respectively.

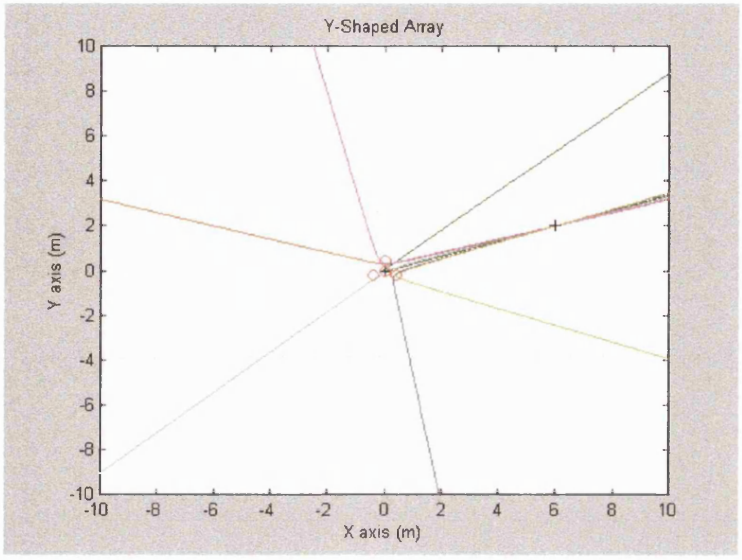

Fig. 3. 4. Example 1: Source Location x=6m, y=2m. Sensor spacing = 0.79m.

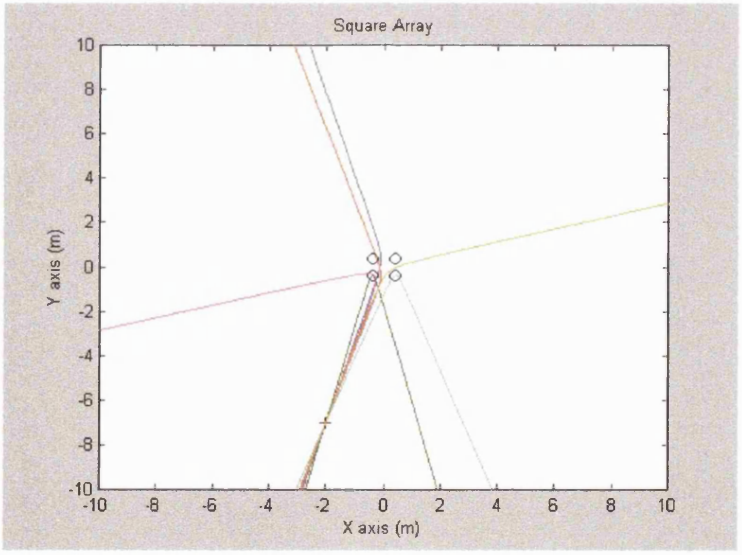

Fig. 3. 5. Example 2: Source Location x=-2m, y=-7m. Sensor spacing = 0.79m.

3.6 Inherent Difficulties in estimating Position Location using TDOA.

The performance of the Hyperbolic PL algorithm is closely related and dependent on the accuracy of TDOA estimates [Fri87]. The hyperbolic position location estimate is constructed by two or more hyperboloids intersect together to pin point the location of a noise emitter. Therefore, the performance of a locator system is mutual to the performance of the TDOA algorithm it employs. For a system to locate a source that is proportionally far away with relative to its sensors spacing, the error of the TDOA estimation has to be very small before the computed location becomes worthless. The following mathematical derivations can give an insight into the difficulties of location estimation and the physical limits of a source location system. For clarity, it is better to begin with a three-point linear array as show in Figure 3.6 below:

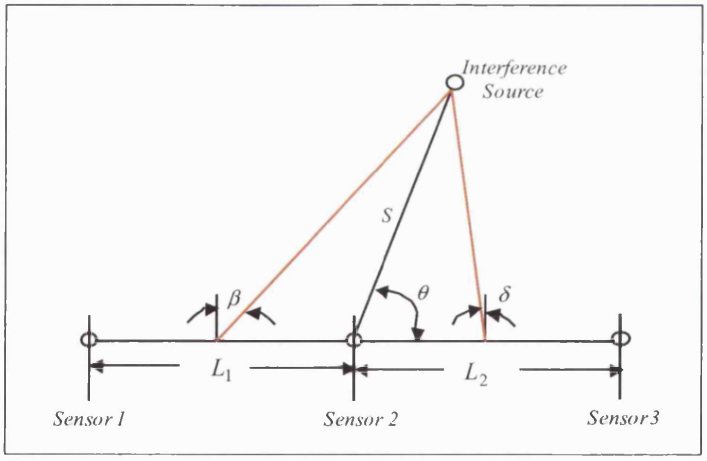

Fig. 3. 6. Three-sensors position location system with linear array.

By setting $\theta = 90^0$, a graph of location error versus source location and sensor spacing can be plotted as shown in Figure 3.7 below.

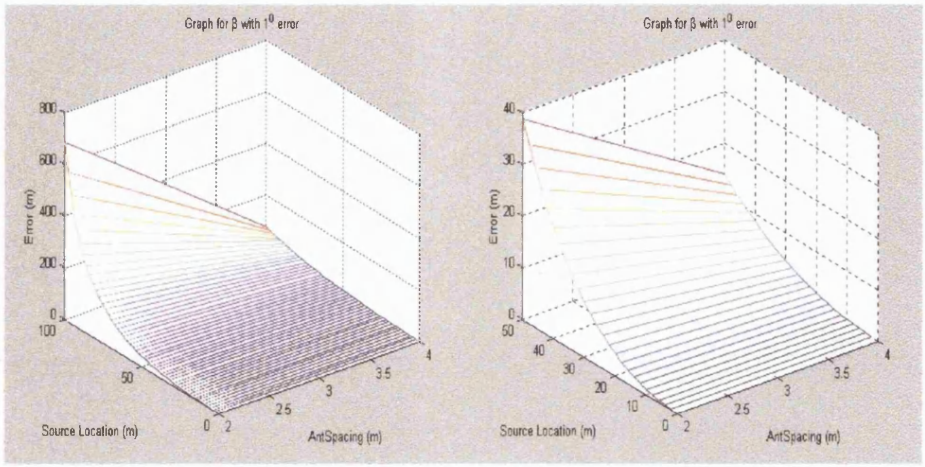

Fig. 3. 7. Graphs of location error versus source location and sensor spacing.

For a sensor array spacing of $L_1 = L_2 = 2$ metres, a source location of 100 metres away will produce an absolute error of over 600 metres if β has an error of +1 degree. This is equivalent to a TDOA estimation error of only $0.1163ns$. It can be observed from Figure 3.7, that in order to reduce such error and to reduce its sensitive towards the variance of the estimated source location, the sensor spacing has to be large enough, or the variance of the TDOA estimation has to be very small, or both. Signal processing becomes a vital part of the whole process in achieving an accurate and unambiguous result. The example uses an estimated TDOA between two sensors to relate to the AOA of a source by approximated relationships described by:

$$D_{21} \cong \frac{\sin(\beta)L_1}{c} \sec \tag{3. 47}$$

$$D_{32} \cong \frac{\sin(\delta)L_2}{c} \sec \tag{3. 48}$$

The relative TDOA between the sensors can be defined as:

$$D_{ij} = D_i - D_j \quad , \quad i, j = 1,2,3 \tag{3. 49}$$

The range R from the midpoint of the array to the source location can be expressed with an exact relationship in terms of D_{ij} and L_i as:

$$R = \frac{\left\{ L_1 \left[1 - \left(\frac{cD_{21}}{L_1} \right)^2 \right] + L_2 \left[1 - \left(\frac{cD_{32}}{L_2} \right)^2 \right] \right\}}{2\left(\frac{cD_{32}}{L_2} - \frac{cD_{21}}{L_1} \right)} \tag{3.50}$$

and bearing θ,

$$\theta = \cos^{-1}\left\{ \frac{[L_2^2 - 2RcD_{32} - (cD_{32})^2]}{2RL_2} \right\} \tag{3.51}$$

where L_i are the distances between the sensor pairs as shown in the Figure 3.6. For a large R, the middle term in the arccosine expression becomes dominant. If the spacing between the sensors is set equally i.e. $L = L_1 = L_2$, equation (3.50) can be reduced to:

$$R = \frac{2L^2 - (cD_{21})^2 - (cD_{32})^2}{2(cD_{32} - cD_{21})} \tag{3.52}$$

Consider a special case where the source location can only be on a vertical line that sits on the centre of the array i.e. $D = D_{32} = -D_{21}$, equation (3.52) can be further reduced to:

$$R = \frac{L^2 - (cD)^2}{2(cD)} \tag{3.53}$$

Substituting equation (3.53) into (3.51) gives:

$$\theta = \cos^{-1}(0) = 90^0 \tag{3.54}$$

The bearing stands for all values of $0 < cD \leq L^2$. This allows us to work out the effect of change in TDOA on the source location. Differentiating equation (3.53) in terms of delay:

$$-\frac{dR}{dD} = \frac{L^2}{2(cD)^2} + \frac{1}{2} \tag{3.55}$$

From equation (3.55), a small change in D, the TDOA estimate, causes a large change in R due to the term $(cD)^2$ and $c = 3\times10^8 m/s$. Thus, an accurate determination of the TDOA becomes a critical factor in achieving an accurate source location. Using equation (3.55), a series of graphs can be plotted to show the variation of the TDOA estimate and its effect on the source location with different sensor spacing L as shown in Figure 3.8 and 3.9.

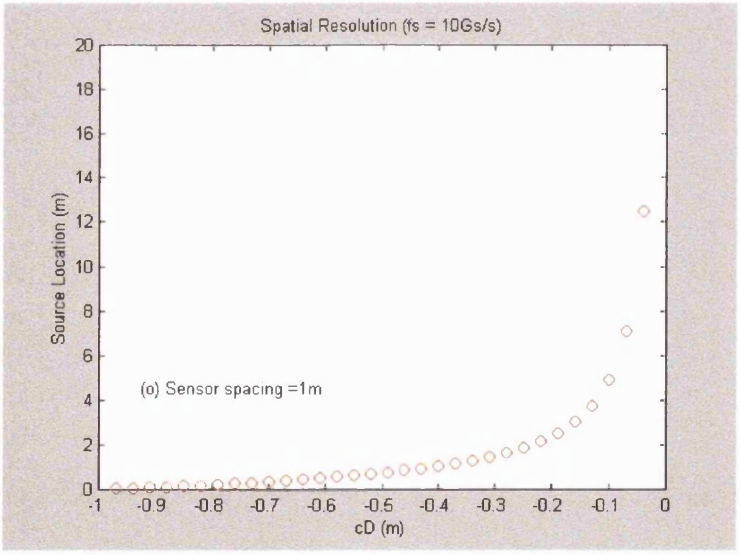

Fig. 3. 8. Graph of source location versus TDOA.

Notice that the curve in Figure 3.8 is plotted with circles to represent the discontinuity effect of spatial quantization due to a finite sampling rate, which is

10GS/s in this case. As the TDOA approaches zero, the gradient of the source location rises drastically causing the circles to stretch apart from each other. In space, this represents poor spatial resolution. Similarly, by increasing the sensor spacing to 2 metres instead of 1 metre, the curve pushes upwards, see Figure 3.9, to give a gentler slope. Now the source location is less sensitive to the TDOA estimate and with better spatial resolution as compare to the former case of 1 metre sensor spacing.

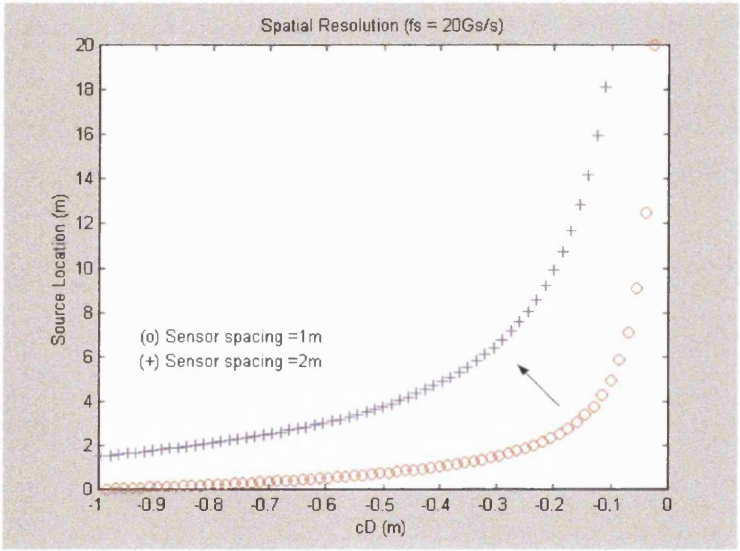

Fig. 3. 9. Graph of source location versus TDOA with two different sensor spacing.

Now, it can be clearly seen that the location error is dominated by the TDOA estimation alone since the rest of the parameters, i.e. L and c, are constants. These mathematical results help to develop a physical insight into the difficulties of position estimation of the source location. Inherent in the physics of the source location problem is the need to have large sensor array dimension, extremely accurate TDOA or close absolute range from the sensor array to the source – the three relationships are interlinked.

3.7 References

[Abe89] J. S. Abel and J. O. Smith, "Source Range and Depth Estimation from Multipath Range Difference Measurements," *IEEE Trans. on Acoustics, Speech, and Signal Processing*, vol. 37, no. 8, pp. 1157- 1165, August 1989.

[Buc00] Bucher R. and Misra D., "A Synthesizable Low Power VHDL Model of the Exact Solution of Three Dimensional Hyperbolic Positioning System," *New Jersey Center for Wireless and Telecommunication*, 2000.

[Cha94] Chan Y. T. and Ho. K.C., "A Simple and Efficient Estimator for Hyperbolic Location," *IEEE Trans. on Signal Processing*, vol. 42, no. 8, pp. 1905-1915, Aug. 1994.

[Fan90] Fang B. T., "Simple Solutions for Hyperbolic and Related Position Fixes," *IEEE Trans. on Aerospace and Electronic Systems*, vol. 26, no. 5, pp. 748-753, Sep. 1990.

[Foy76] Foy W. H., "Position-Location solutions by Taylor-series estimation," *IEEE Trans. on Aerospace and Electronic Systems*, vol. AES-12, pp. 187 -194, Mar. 1976.

[Fri87] Friedlander B., "A Passive Localization Algorithm and Its Accuracy Analysis," *IEEE Journal of Oceanic Engineering*, vol. OE-12, no. 1, pp. 234 -244, Jan. 1987.

[Tsa96] Tsakalides P., Nikias C. L., "The Robust Covariation-Based MUSIC (ROC-MUSIC) Algorithm for Bearing Estimation in Impulsive Noise Environment," *IEEE Trans. on Signal Processing*, vol. 44. no. 7, Jul. 1996.

Chapter 4

RECENT TECHNIQUES FOR ESTIMATING TIME DIFFERENCE OF ARRIVAL (TDOA)

Introduction

The Time-Difference-Of-Arrival (TDOA) of a signal can be estimated by two general techniques: subtracting Time-Of-Arrival (TOA) measurements from two sensors to produce a relative TDOA, or through the use of cross-correlation techniques in which the received signal on one sensor is correlated with the received signal at another spatially separated sensor. To eliminate the need for knowledge of the source emission time, differencing of the arrival time at the sensors is commonly employed. While determining the TDOA from TOA estimates is not a feasible method for arbitrary impulsive noise source, cross-correlation techniques dominate the chapter on TDOA estimation techniques. As such, the discussion of TDOA estimation is limited to Time Delay Estimation (TDE) techniques based on the fundamental principle of cross-correlation and higher-order correlation. In the chapter, a general model for TDE estimation has been developed and the recent techniques for TDE estimation are presented.

4.1 Overview of Different Time Delay Estimation Techniques

The Time Delay Estimation (TDE) problem occurs in various applications, for example, in the determination of range and bearing in radar and sonar [Nik88,Car81,Kna76,Ham74]. It also has esoteric applications, such as the measurement of the temperature of a molten alloy by measuring the passage time

of a signal. Other applications include tracking and location of Radio Frequency (RF) sources [Tun00].

4.1.1 General Signal Model for Time Delay Estimation Techniques

The basic model, see Figure 4.1, consists of two sensors record of delayed replicas of a signal in the presence of noise. The signals, $x_1(t)$ and $x_2(t)$, received by a pair of sensors spatially separated by a distance of cD, can be modeled as:

$$x_1(t) = s(t) + n_1(t) \tag{4.1}$$

$$x_2(t) = \alpha s(t + D) + n_2(t) \tag{4.2}$$

where D is the required delay, α is the relative amplitude of the second signal and c is the constant speed of light in vacuum, $3\times10^8 m/s$, respectively. $n_1(t)$ and $n_2(t)$ are wide-sense stationary, mutually uncorrelated Gaussian noise processes. The impulsive "noise" signal of interest, $s(t)$, is also uncorrelated with $n_1(t)$ and $n_2(t)$ and, being of finite duration, may be measured and treated statistically. This representation assumes no prior knowledge of the signals' characteristics and thus suited for this application.

4.1.2 Cross-Correlation

Estimation of time delay D is conventionally achieved using the cross-correlation function $C_{x_i x_j}(\tau)$. This is a measure of the similarity of two functions x_i and x_j, as one is displaced through time τ relative to the other, and is expressed as:

$$C_{x_i x_j}(\tau) = E[x_i(t) x_j(t + \tau)] \quad , \quad i, j = 1,2 \tag{4.3}$$

The frequency spectrums of the signal and noise components are therefore,

$$X(f) = \mathrm{F}\{x_i(t)\} \tag{4. 4}$$

$$S(f) = \mathrm{F}\{s(t)\} \tag{4. 5}$$

$$N(f) = \mathrm{F}\{n_i(t)\} \tag{4. 6}$$

where F denotes the Fourier transform. Section 4.6 describes how consistent frequency domain estimates of stationary signals can be obtained. The power spectral density can be expressed as:

$$P_{x_i x_j}(f) = \mathrm{F}\{C_{x_i x_j}(\tau)\} \tag{4. 7}$$

which, according to the Wiener-Khinchine theorem, is also equivalent to:

$$P_{x_i x_j}(f) = X_i(f) X_j{}^*(f) \tag{4. 8}$$

Making substitutions from equation (4.3) into (4.7):

$$P_{x_1 x_2}(f) = [S(f) + N_1(f)][\alpha S(f) e^{-j\omega D} + N_2(f)]^* \tag{4. 9}$$

Since it is assumed that the signal and noise are uncorrelated, the cross-spectral density works can be simplified to:

$$P_{x_1 x_2}(f) = \alpha P_{ss}(f) e^{-j\omega D} + P_{n_1 n_2}(f) \tag{4. 10}$$

Since $n_1(t)$ and $n_2(t)$ are zero mean, Gaussian and spatially uncorrelated, $P_{n_1 n_2}(f)$ is negligible. Equation (4.10) is reduced to:

$$P_{x_1x_2}(f) = \alpha P_{ss}(f)e^{-j\omega D} \tag{4. 11}$$

Equation (4.11) can be expressed in time domain as:

$$C_{x_1x_2}(\tau) = \alpha C_{ss}(\tau) * \delta(\tau - D) \tag{4. 12}$$

where * denotes convolution. Equation (4.12) shows that the correlation peak of $C_{ss}(\tau)$ is displaced through the required time delay of D seconds which may be readily estimated. Given the foregoing assumptions, $C_{ss}(\tau)$ is effectively the autocorrelation of the target signal $s(t)$. Note that $C_{x_1x_2}(\tau)$ can be estimated from a finite number of observations of the antenna signals $x_1(t)$ and $x_2(t)$.

4.1.3 Frequency Domain Weighting Function

In practice, the non-ideal signal propagation environment can make estimation of D problematic. This can be modelled by modification of equation (4.12) in the frequency domain:

$$C_{x_1x_2}(\tau) = \int \psi(f)P_{x_1x_2}(f)\exp(j2\pi f\tau)df \tag{4. 13}$$

where $\psi(f)$ is frequency weighting function given by $H_1(f)H^*_2(f)$. $H_1(f)$ and $H_2(f)$ are the frequency responses of the transmission paths between the impulsive noise source and the receiving antennas as shown in Figure 4.1.

Note that in the direct cross-correlation calculation there is no weighting function introduced to compensate for the effects of $H_1(f)$ and $H_2(f)$ i.e. $\psi(f)=1$. Consequently, the correlation will be poor when the Signal-to-Noise Ratio (SNR) is low.

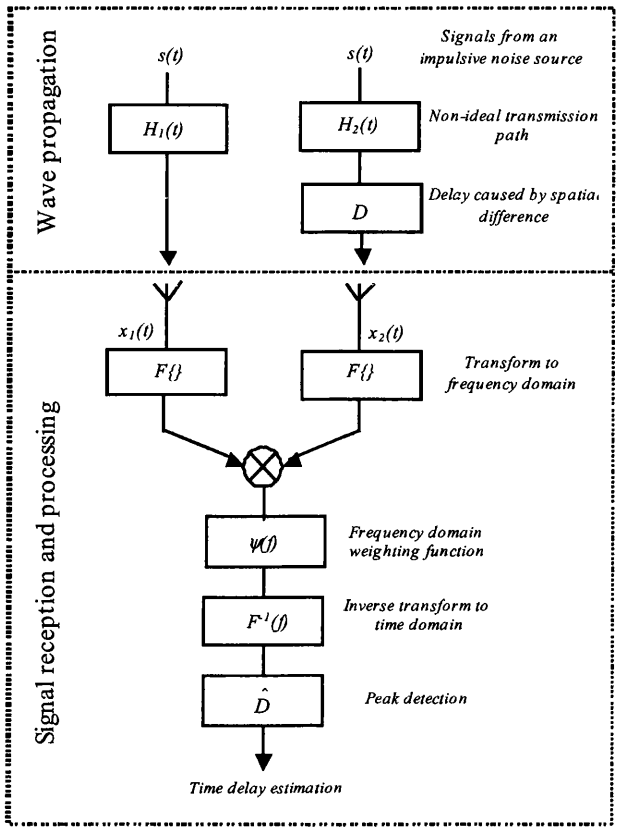

Fig 4. 1. Model of impulsive noise propagation and time delay estimation.

To improve the situation, the weighting function can be estimated and many approaches have been developed including the Roth processor [Rot71], the Smoothed Coherence Transform (SCOT) [Car73b], the Eckart filter [Kna76] and the Hannan and Thomson (HT) processor [Han73]. Their main characteristics and differences can be summaries in table 4.1.

Among the processors, two of them where of particular interest; namely the SCOT [Car73b] and the HT [Han73]. They have been applied to the area of impulsive noise source direction finding and location respectively [Pec01,Tun00] and will be discussed with further details.

Processor Name	Frequency Domain Weighting Function
Cross-correlation	*1*
Roth	$1/P_{x_1x_1}(f)$ *or* $1/P_{x_2x_2}(f)$
SCOT	$\frac{1}{\sqrt{P_{x_1x_1}(f)\cdot P_{x_2x_2}(f)}}$
Eckart	$\frac{P_{ss}}{[P_{n_1n_1}(f)P_{n_2n_2}(f)]}$
HT	$\frac{\lvert\gamma_{x_1x_2}(f)\rvert^2}{\lvert P_{x_1x_2}(f)\rvert\cdot\left[1-\lvert\gamma_{x_1x_2}(f)\rvert^2\right]}$

Table 4. 1. Table of different processors that employ frequency domain weighting functions to improve correlation peak.

4.1.4 The Smoothed Coherence Transform (SCOT)

The SCOT was developed as an *ad hoc* technique and is defined as a Fourier transform of the weighted coherence:

$$C_{x_1x_2}(\tau) = \int W(f)\gamma_{x_1x_2}(f)e^{jw\tau}df \tag{4. 14}$$

where

$$\gamma_{x_1x_2}(f) = \frac{P_{x_1x_2}(f)}{\sqrt{P_{x_1x_1}(f)P_{x_2x_2}(f)}} \tag{4. 15}$$

and $W(f)$ is a smooth windowing function such as Hanning window.

The SCOT is designed to accentuate the peak of a cross-correlation by introducing a weighting function specifically to determine time delay under the influence of weak correlated noise. The problem is best described by Figure 4.2:

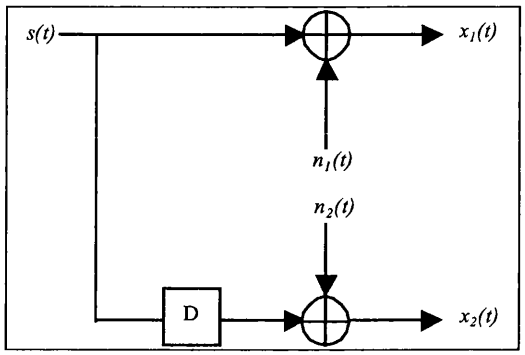

Fig 4. 2. Simplified time delay estimation model.

Consider a case where the three sources $s(t)$, $n_1(t)$ and $n_2(t)$ are uncorrelated. Both $x_1(t)$ and $x_2(t)$ contain the signal components of $s(t)$ with $x_2(t)$ being spatially delayed by time D. If the total power of the uncorrelated components, $n_1(t)$ and $n_2(t)$ is larger than $s(t)$, the true correlation peak indicating the time delay may be buried. The noise components however cannot be simply filtered away using a filter as $s(t)$ may contain both broadband and narrowband components. The complex coherence of $x_1(t)$ and $x_2(t)$ may be written as:

$$\gamma_{x_1x_2} = \frac{P_{ss}(f)\cdot e^{j\omega D}}{[P_{ss}(f)+P_{n_1n_1}(f)]^{1/2}[P_{ss}(f)+P_{n_2n_2}(f)]^{1/2}} \tag{4. 16}$$

If spectrum of $P_{n_1n_1}(f)$ or $P_{n_2n_2}(f)$ is much larger than $P_{ss}(f)$ at only a few frequencies, then $|\gamma_{x_1x_2}(f)| << 1$ only at these frequencies. If $P_{ss}(f)$ is highly correlated and its spectrum is much larger than $P_{n_1n_1}(f)$ and $P_{n_2n_2}(f)$ for the rest of the frequencies, then $|\gamma_{x_1x_2}(f)| \cong e^{j\omega D}$. Thus the SCOT, in this case, gives an approximation of the time delay estimation by a narrow pulse at $-D$.

Although the total power of $n_1(t)$ and $n_2(t)$ may be larger than the actual signal $s(t)$, the SCOT will enhance the true correlation peak by suppressing the overwhelming uncorrelated cross spectrum of the noises accordingly. The coherence function, which is used in the automatic frequency weighting adjustment scheme, needs to be estimated – see section 4.1.6.

4.1.5 Hannan and Thomson Processor (HT)

A detailed assessment of the major techniques available [Kna76] has concluded that the Hannan and Thomson (HT) processor [Hah73] provides the optimum likelihood weighting function, defined by:

$$\psi_{HT} = \frac{1}{\left|P_{x_1x_2}(f)\right|} \cdot \frac{\left|\gamma_{x_1x_2}(f)\right|^2}{\left[1-\left|\gamma_{x_1x_2}(f)\right|^2\right]} \tag{4.17}$$

The first right hand term is used to achieve good resolution and the second term adjusts itself to weight according to the phase coherence of the two signals. Derivation equation (4.17) is based on the assumption that the phases of the received signals are differentiable and have smooth derivatives. In estimating spectra and cross spectra for a pair of stationary signals, the estimation of the phase may be replaced by an estimation of the group delay.

To evaluate the second right hand term of equation (4.17), it is necessary to find values for the complex coherence function. This function measures the smoothness of the phase and, for two zero-mean stationary random processes $x_1(t)$ and $x_2(t)$, is defined [Car73b] as the normalized cross-spectral density i.e.:

$$\gamma_{x_1x_2}(f) = \frac{P_{x_1x_2}(f)}{\sqrt{P_{x_1x_1}(f)P_{x_2x_2}(f)}} \tag{4. 18}$$

By squaring the coherence function, a measure called the Magnitude-Squared Coherence (MSC) function is defined by [Car73a].

$$\left|\gamma_{x_1x_2}(f)\right|^2 = \frac{\left|P_{x_1x_2}(f)\right|^2}{P_{x_1x_1}(f)P_{x_2x_2}(f)}, \quad 0 \le \left|\gamma_{x_1x_2}(f)\right|^2 \le 1, \quad \forall f \tag{4. 19}$$

The terms in the equation are unknowns and need to be estimated.

4.1.6 Spectral Estimation

To evaluate equation (4.19), consistent estimates of $\left|\gamma_{x_1x_2}(f)\right|^2$ and $\left|P_{x_1x_2}(f)\right|$ are required. This can be achieved using the 50% overlapping strategy suggested in [Car73a], which is essentially similar to the more familiar Welch's averaging modified periodograms technique used here. A long sequence of data series $x(n)$, for the purpose of spectral analysis, is conventionally performed by dividing the data into L short sections of M size. Frequencies that are not integer multiples of the frequency resolution (ΔF) will leak out throughout the entire frequency axis. To improve the situation, the samples of each section are multiplied by a window function. The window function is applied to the data section to control leakage, which otherwise causes a bias in the estimate.

The Fourier transform of the L-modified sequences are then obtained using the Fast F
$$W_i(f_k) = \frac{1}{M}\sum_{n=0}^{M-1} x_i(n)a(n)\exp(-j2\pi nk/M)$$ollows:

$$W_i(f_k) = \frac{1}{M}\sum_{n=0}^{M-1} x_i(n)a(n)\exp(-j2\pi nk/M) \tag{4. 20}$$

where i is the section (time) index and k is the frequency index. The data window $a(n)$ is selected to achieve desired specification requirements, and $W_i(f_k)$ is the frequency spectrum of the modified input sequences. The L-modified periodograms are:

$$J_i(f_k) = \frac{M}{U}|W_i(f_k)|^2 \tag{4. 21}$$

where

$$U = \frac{1}{M}\sum_{n=0}^{M-1} a^2(n) \tag{4. 22}$$

and the FFT bin frequencies are:

$$f_k = k\frac{F_s}{M} = k\Delta F \tag{4. 23}$$

where F_s is the sampling frequency. The spectral estimate is finally obtained by averaging these modified periodograms:

$$P_x(f_k) = \frac{1}{L}\sum_{i=1}^{K} J_i(f_k) \tag{4. 24}$$

The Hanning window was chosen for the investigation. This function has side-lobe levels more than 70dB down, and a main-lobe with single-sided bandwidths of approximately four FFT bins. To keep the required FFT bin width alias free, it is necessary to increase the sampling frequency by a minimum factor of approximately four.

4.2 Adaptive Time Delay estimation based on Cumulants (ATDC)

Cross-correlation based methods assume that the sensor noises are uncorrelated. If the noise processes are correlated, it may not be possible to detect the peak of $C_{ss}(\tau)$ since it may be obscured by $C_{n_1n_2}(\tau)$, since $P_{n_1n_2}(f)$ can no longer be assumed to be negligible - refer to equation (4.10). If the signals are non-Gaussian, and the noise processes are Gaussian, third-order cumulants can be used even if the noise processes are correlated.

This is one of the main motivation of using cumulants of order $k > 2$ since the higher-order cumulants of a non-Gaussian signal can be recovered even in the presence of colored Gaussian noise [Nik93a,Nik93b,Men91,Swa91]. Chiang and Nikias [Chi90,Nik88] saw the advantage of using higher order statistics and developed a technique for estimating the difference in arrival time between signals corrupted by spatially correlated Gaussian noise source of unknown correlation.

4.2.1 Brief Introduction to Higher-Order Statistics (HOSA)

This section provides a brief introduction to the characterization of random processes using higher-order moments. The field is currently an area of intense research and new results are constantly being reported. The known results in higher order moments can easily fill a volume on their own.

The intent here is only to give a general description of the methods to aid the explanation of the techniques related to higher-order moments, and to give some references to the literature where more information about the topic can be found. The next few sections are general theoretical materials about higher-order moments and related functions.

4.2.2 Moments and Cumulants

The moments for a stationary random process is defined by:

$$M_{x_i} = E[x_i(t)] \tag{4.25}$$

$$M_{x_i x_j}(\tau) = E[x_i^*(t)x_j(t+\tau)] \tag{4.26}$$

$$M_{x_i x_j x_k}(\tau,\rho) = E[x_i^*(t)x_j(t+\tau)x_k(t+\rho)] \tag{4.27}$$

$$M_{x_i x_j x_k x_l}(\tau,\rho,\alpha) = E[x_i^*(t)x_j^*(t+\tau)x_k(t+\rho)x_l(t+\alpha)] \tag{4.28}$$

where * is a complex conjugate operator and $E[\,]$ is taking the expectation. i, j, k are the signals' reference numbers. The first two moments, (4.25) and (4.26), are equal to the commonly use mean and correlation function respectively. The 3rd and 4th moments, as described in equation (4.27) and (4.28), is sometimes known as higher-order correlation functions. For a complex signal, the expression given in equation (4.27) and (4.28) are only one of the many ways to define the moments. There is no compelling reason as to associating the complex conjugate with one term or the other. In special cases, it is useful to define the complex moments differently for different problems [Nik93a].

Although the moments provide all of the needed information for higher-order analysis of a random process, it is usually preferable to work with related quantities called the cumulants. Their use is analogous to the use of covariance instead of the correlation function in second moment analysis to remove the effect of mean.

Cumulants can be defined as terms in the expression of a cumulant-generating function or via certain partitions of the set of random variables [Ros85]. Explicit expressions for the first four cumulants for the case of a zero-mean random process are:

$$C_{x_i} = E[x_i(t)] = 0 \tag{4. 29}$$

$$C_{x_i x_j}(\tau) = E[x_i^*(t)x_j(t+\tau)] \tag{4. 30}$$

$$C_{x_i x_j x_k}(\tau,\rho) = E[x_i^*(t)x_j(t+\tau)x_k(t+\rho)] \tag{4. 31}$$

$$\begin{aligned} C_{x_i x_j x_k x_l}(\tau,\rho,\alpha) = {} & E[x_i^*(t)x_j^*(t+\tau)x_k(t+\rho)x_l(t+\alpha)] \\ & - C_{x_i x_k}(\rho)C_{x_j x_l}(\alpha-\tau) - C_{x_i x_l}(\alpha)C_{x_j x_k}(\rho-\tau) \end{aligned} \tag{4. 32}$$

Equation (4.32) is for complex random process. For real random process the 4th order cumulant is defined as:

$$\begin{aligned} C_{x_i x_j x_k x_l}(\tau,\rho,\alpha) = {} & E[x_i(t)x_j(t+\tau)x_k(t+\rho)x_l(t+\alpha)] - C_{x_i x_j}(\tau)C_{x_k x_l}(\alpha-\rho) \\ & - C_{x_i x_k}(\rho)C_{x_j x_l}(\alpha-\tau) - C_{x_i x_l}(\alpha)C_{x_j x_k}(\rho-\tau) \end{aligned} \tag{4. 33}$$

The expression for the 4th order cumulant involves the subtraction of the 4th order moment for the Gaussian process, which can be expressed in terms of 2nd order cumulants. This is why the expression is more complicated. In addition, the expressions differ by one term for the real and complex cases. The cumulants for order three or four, referred to as higher-order cumulants, for a Gaussian random process are identically zero.

4.2.3 Polyspectra

The spectral quantities related to the cumulants are called cumulant spectra, higher-order spectra or polyspectra. The 2nd order spectrum is the ordinary power spectrum defined as:

$$P_{x_i x_j}(\omega_1) = \sum_{\tau=-\infty}^{\infty} C_{x_i x_j}(\tau)e^{-j\omega_1\tau} \tag{4. 34}$$

The 3rd and 4th order spectra are called the bispectrum and trispectrum respectively. These quantities are the Fourier transforms of the 3rd and 4th order cumulants:

$$P_{x_i x_j x_k}(\omega_1,\omega_2)\sum_{\tau=-\infty}^{\infty}\sum_{\rho=-\infty}^{\infty}C_{x_i x_j}(\tau,\rho)e^{-j(\omega_1\tau+\omega_2\rho)} \tag{4. 35}$$

$$P_{x_i x_j x_k}(\omega_1,\omega_2,\omega_3)\sum_{\tau=-\infty}^{\infty}\sum_{\rho=-\infty}^{\infty}\sum_{\alpha=-\infty}^{\infty}C_{x_i x_j x_k}(\tau,\rho,\alpha)e^{-j(\omega_1\tau+\omega_2\rho+\omega_3\alpha)} \tag{4. 36}$$

Note that these higher-order spectra are periodic in each of their arguments $(\omega_1,\omega_2,\omega_3)$ with period 2π. Since for a Gaussian random process the higher-order cumulants are zero, the bispectrum and trispectrum for a Gaussian process are identically zero.

The 3rd and 4th cumulants and corresponding spectral quantities have been used in a number of applications dealing with non-Gaussian processes. Cumulants and spectra of order higher than the fourth are difficult to compute reliably and so far have found limited practical use.

It should be noted that when the random process has a density that is symmetric about the mean, the 3rd order cumulant and the bispectrum are identically zero and it is necessary to consider fourth-order quantities to perform any higher-order statistical analysis.

4.2.4 Symmetry Properties of Third Moment Quantities

It is obvious from the definition that the third-order cumulant has the symmetry property:

$$C_{x_i x_j x_k}(\rho,\alpha) = C_{x_i x_k x_j}(\alpha,\rho) \tag{4. 37}$$

In addition, it can be shown from the definition that for real random process the 3rd order cumulant has the following additional symmetry properties:

$$\begin{aligned} C_{x_i x_j x_k}(\rho,\alpha) &= C_{x_k x_i x_j}(-\alpha,\rho-\alpha) = C_{x_j x_i x_k}(-\rho,\alpha-\rho) \\ &= C_{x_j x_k x_i}(\alpha-\rho,-\rho) = C_{x_k x_j x_i}(\rho-\alpha,-\alpha) \end{aligned} \tag{4. 38}$$

For complex cumulant, knowledge of $C_{x_i x_j x_k}(\rho,\alpha)$ in half plane is sufficient to specify all of its other values, while for the real cumulant, knowledge in the first octant is sufficient to define it in all of the remaining five regions. These save the computational requirement of algorithms implemented using HOSA.

4.2.5 Higher-Order Statistics (HOSA) in Time Delay Estimation

The adaptive time delay estimation technique [Chi90] based on cumulants can be described by Figure 4.3 below:

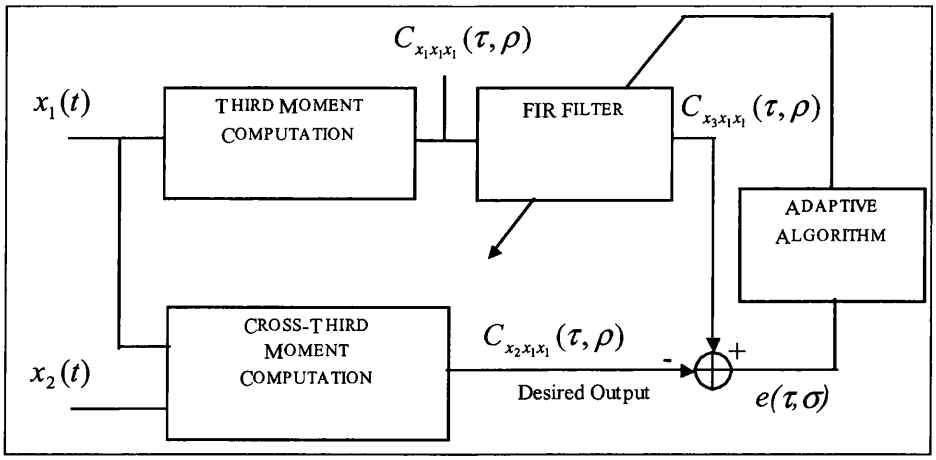

Fig 4. 3. Configuration of the adaptive time delay estimation method based on cumulants (ATDC).

For stationary case and assuming $\alpha = 1$ for simplicity, equations (4.1) and (4.2) may be rewritten as:

$$s(t+D) = x_1(t+D) - n_1(t+D) \tag{4. 39}$$

$$x_2(t) = x_1(t+D) - n_1(t+D) + n_2(t) \tag{4. 40}$$

This may be rewritten in a more general form suitable for practical purposes as:

$$x_2(t) = \sum_{i=-P}^{P} a_i x_1(t+i) - n_1(t+D) + n_2(t) \quad , \; P >> D \tag{4. 41}$$

To form a third order moment equation, both sides of equation (4.41) is multiplied by $x_1(t+\tau)x_1(t+\rho)$, followed by taking the expectations. This has worked out to be:

$$C_{x_2x_1x_1}(\tau,\rho) = \sum_{i=-P}^{P} a_i C_{x_1x_1x_1}(\tau - i, \rho - i) - C_{n_1x_1x_1}(\tau - D, \rho - D) + C_{n_2x_1x_1}(\tau,\rho) \tag{4. 42}$$

where

$$C_{x_1x_1x_1}(\tau,\rho) = E[x_1(t)x_1(t+\tau)x_1(t+\rho)] \tag{4. 43}$$

Equation (4.42) may be further reduced since the last two terms of the equation are identically zero due to the fact that the signal and noise are zero mean and the signal is independent from the noises which are assumed to be of Gaussian nature. Based on the parametric model described by (4.41), an adaptive version may be formed by:

$$C_{x_2x_1x_1}(n,\tau,\rho) = \sum_{i=-P}^{P} a_i(n) C_{x_1x_1x_1}(n,\tau+i,\rho+i) \tag{4. 44}$$

where n is the iteration (or time) index. The adjustment criteria, which determines the most suitable FIR filter coefficients $\{a_i\}$, is given by:

$$C_{x_3x_1x_1}(\tau,\rho) = \sum_{i=P}^{P} a_i C_{x_1x_1x_1}(\tau+i,\rho+i) \tag{4. 45}$$

The desired FIR filter coefficient will produce a minimum sum of the squared errors ξ between the desired output $C_{x_2x_1x_1}(\tau,\rho)$ and the actual output $C_{x_3x_1x_1}(\tau,\rho)$, where:

$$\xi \equiv \sum_{\tau}\sum_{\rho}[C_{x_3x_1x_1}(\tau,\rho) - C_{x_2x_1x_1}(\tau,\rho)]^2 \tag{4. 46}$$

This is better explained by Figure 4.3.

4.3 Simulations and Results

Four different techniques have been tested using simulated waveforms generated by MatLab routines. The signal-to-noise ratio (SNR) is defined as $20\log_{10}(\sigma_s/\sigma_n)$ where σ_s and σ_n are the standard deviation of the signal and noise respectively. The SNR in the simulation is set at 0dB having a time delay of 16 samples between the two signals as shown below in Figure 4.4.

The simulated waveforms were applied to four different processors: (i) Cross-Correlation, (ii) SCOT, (iii) HT processor and (iv) ATDC. The results show that all four processors were able to determine the exact time delay.

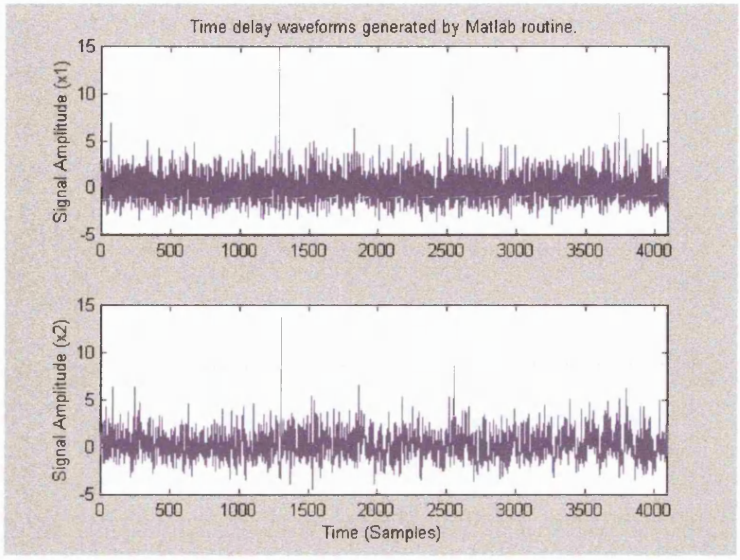

Fig 4. 4. Simulated signals for time delay estimations.

In special circumstance where correlated noise, i.e. coloured noise rather than simply with Gaussian noise, is present, the ATDC has shown to be more superior than the rest in suppressing the noise peak – see Figure 4.5. This is useful in preventing false delay estimation cause by overwhelming noise correlation peaks. The noise correlation peak can be observed in the Figure on each correlation. It has a broad base with lower correlation level and appears on the left of the true peak. This peak can severely degrade the delay estimate if the time delay is small. A small delay separation will cause the true peak to be overlapped by the noise peak and result in smearing of the true peak. Consequently, the true time delay is unable to be resolved. Usually, such circumstance many happened especially in a case where multi-path is present and this will be obvious in chapter 5 discussion.

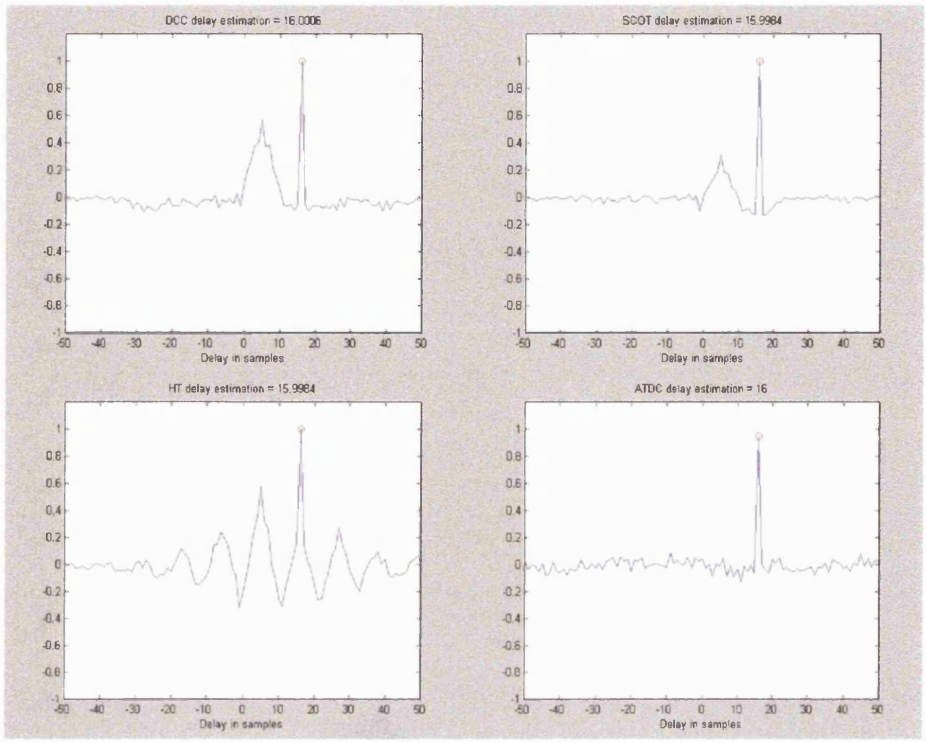

Fig 4. 5. Time delay estimation by four different techniques: 1. Cross-correlation, 2. SCOT, 3. HT processor and 4. ATDC.

4.4 Practical Tests

A practical test was carried out in a University classroom as described in Chapter 8. The basic elements of the test consist of two aerial type sensors separated spatially by 0.46 metres. The signals, Figure 4.6, were captured at a sampling rate of 2.5GS/s with 1GHz bandwidth. To improve the resolution of the estimates, the signals were interpolated by a factor of 10, which is equivalent sampling at 25GS/s. 50 pairs of signals were taken with the interference source place along the line of the sensor pair at a distance of 8 metres. They were applied to the four processors and the maximum variance σ^2 of the processors was computed to be about 0.1 of a sample over the 50 sets of data. A view of the performance for the four techniques can be seen on Figure 4.7.

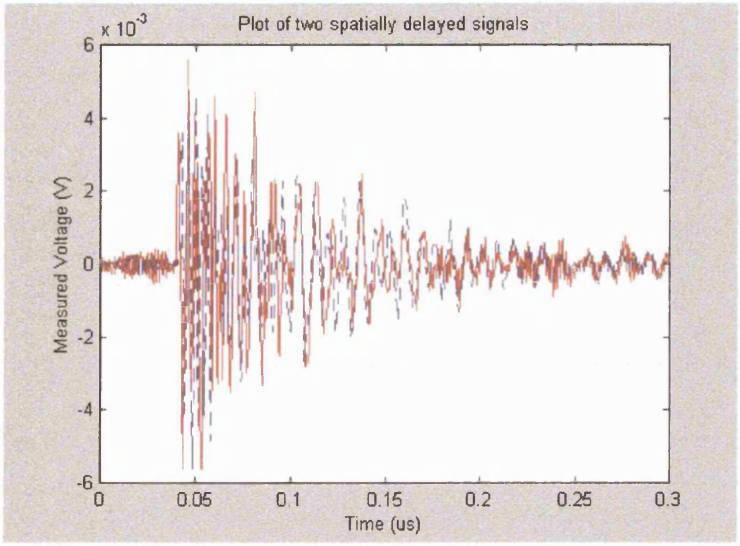

Fig 4. 6. Plot of two signals received at a spatial separation of 0.46 metre.

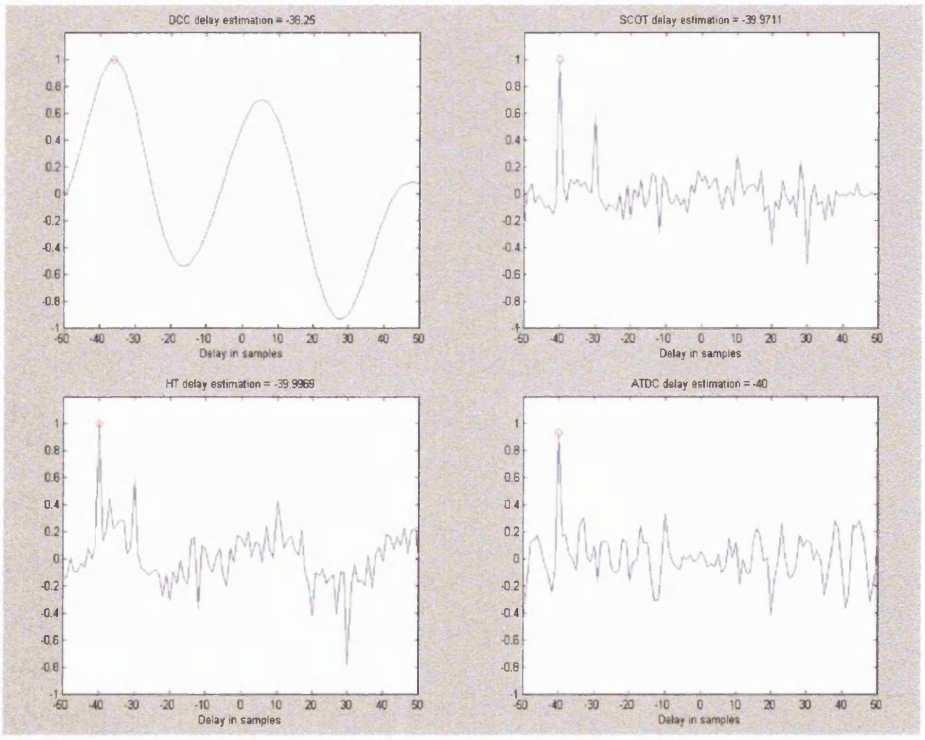

Fig 4. 7. Performance of different processors under a practical test.

Figure 4.7 shows that the normal cross-correlation gives the broadest peak showing the lowest time delay resolution when compared to the rest. It also shows that the ATDC is the most effective in suppressing correlated noise peaks that appear on the shoulder of the main peak. This result is therefore consistent with the theoretical simulations presented earlier.

Since the source is placed at a position giving maximum time delay between the sensor pairs, the anticipated time delay for the antenna separation of 0.46 metre is 38.3 samples. In this case, the best processors were the HT and SCOT. They were about 1.6 samples out from the actual result. However, this works out to be about 2.39 degrees. Although this was an improvement to an earlier work [Pec01] mainly by introducing a higher sampling rate, it is still far too large an error to construct a sensible locator system as illustrated in chapter 3. There are several reasons that may have caused a bias to the results:

1. The processing algorithms.
2. The effects of multipath.
3. Mutual coupling between the antennas.
4. Design and construction of the receiving front-end and array geometry.

4.5 Summary

To develop a locator based on closely spaced sensors, the accuracy of the time delay estimation has to be improved in order to make any sensible location estimation. A high accurate time delay estimation technique *ad hoc* to this application is required. This may be achieved by exploiting the available advantages and characteristics of processing impulsive noise source. By observing the signals characteristics closely, it is anticipated that an *ad hoc* time delay estimation technique may be derived on the basis of the following points:

1. The signals are typically of wide-band transient characteristics with sharp rising edge and good signal-to-noise ratio. A signal detection algorithm may not necessary and a simple triggering algorithm base on amplitude is deemed adequate for this purpose. This will reduce valuable processing time and the number of algorithm stages to minimise possible errors introduced during the long processing.

2. Better time delay estimation may be achieved by reducing the effects of multi-path and the effects of cross-talking between the receiving sensors. It is deemed that by employing advance Digital Signal Processing (DSP) techniques may help.

3. Overall performance may be improved by minimising possible distortion that could result in the front-end reception via antenna design and strategic geometrical arrangement of the sensors.

Based on these findings, a new processor for time delay estimation applied to impulsive noise source has been developed and presented in chapter 5.

4.6 References

[All77] Allen J. B., "Short-time spectral analysis, synthesis and modification by discrete Fourier transform," *IEEE Trans. Acoust., Speech, Signal Processing*, vol. 25, pp. 235-38, Jun. 1977.

[Bril81] Brillinger D. R., *Time Series: Data Analysis and Theory*, McGraw Hill, 1981.

[Bril83] Brillinger D. R., Krishnaiah P. R., "Handbook of statistics 3 – Time series in the frequency Domain," Elsevier Science Publishers B. V., pp. 111-123, 1983.

[Car73a] Carter G. C., Knapp C. H. and Nuttall A. H., "Estimation of the magnitude-squared coherence function via overlapped fast Fourier transform processing," *IEEE Trans. Audio Electroacoustics*, vol. AU-21, no. 4, pp. 337-344, Aug. 1973.

[Car73b] G. C. Carter, Nuttall A. H. and Cable P. G., "*The smoothed coherence transform*," *Proc. IEEE (Letter)*, vol. 61m, pp. 1497-1498, Oct. 1973.

[Car81] Carter G. C., "Time delay estimation for passive sonar signal processing," *IEEE Trans. Acoust., Speech, Signal Processing*, vol. ASSP-29, no. 3, Jun. 1981.

[Chi90] Chiang H. H. and Nikias C. L., "A New Method for Adaptive Time Delay Estimation for Non-Gaussian Signals," *IEEE Trans. Acoust., Speech, Signal Processing*, vol. 38, no. 2, Feb. 1990.

[Eck52] Eckart C. "Optimal rectifier systems for the detection of steady signals," *Univ. California, Scripps Inst. Oceanography, Marine Physical Lab.*, Rep SIO 12692, SIO Ref 51-11, 1952.

[Gab46] Gabor D., "Theory of communication," *J.i.e. E.*, Vol. 93, pp. 429-59, 1946.

[Ham74] Hamon B. V. and Hannan E. J., "Spectral estimation of time delay for dispersive and non-dispersive systems," *Appl. Statist.*, vol. 23, no. 2, pp. 134-142, 1974.

[Han73] Hannan E. J. and Thomson P. J., "Estimating group delay," *Biometrika*, vol. 60, pp. 241-253, Feb. 1973.

[Has79] Hassab J. C. and Boucher R. E., "Optimum Estimation of Time Delay by a Generalized Correlator," *IEEE Trans. Acoust., Speech, Signal Processing*, vol. ASSP-27, pp.373-380, Aug. 1979.

[Her85] Hero A. O. and Schwartz S. C., "A New Generalized Cross Correlator," *IEEE Trans. Acoust., Speech, Signal Processing*, vol. ASSP-33, no. 1, Feb. 1985.

[Joh82] Johnson D. H., "The application of spectrum estimation methods to bearing estimation problems," *Proc. IEEE*, vol. 70, pp. 975-89, 1982.

[Kna76] Knapp C. H. and Carter G. C., "The generalized correlation method for estimation of time delay," *IEEE Trans. Acoust., Speech, Signal Processing*, vol. ASSP-24, pp. 320-327, Aug. 1976.

[Men91] Mendel J. M., "Tutorial on higher-order statistics (spectra) in signal processing and system theory: Theoretical results and some applications," *Proc. IEEE*, vol. 79, pp. 278-305, 1991.

[Nik87] Nikias C. L. and Raghuveer M. R., "Bispectrum estimation: A digital signal processing framework," *Proc. IEEE*, vol. 75, pp. 869-91, Jul. 1987.

[Nik88] Nikias C. L. and Pan R., "Time delay estimation in unknown Gaussian spatially correlated noise," *IEEE Trans.*

Acoust., Speech, Signal Processing, vol. 36, pp. 1706-14, Nov. 1988.

[Nik93a] Nikias C. L. and Mendel J. M., "Signal processing with higher-order spectra," *IEEE Signal Processing Magazine*, vol. 10, no. 3, pp. 10-37, Jul. 1993.

[Nik93b] Nikias C. L. and Petropulu A., *Higher-Order Spectra Analysis: A Nonlinear Signal Processing Framework*, New Jersey: Prentice-Hall, 1993.

[Pec01] Peck C. H. and Moore P. J. "A Direction-Finding Technique for Wide-Band Impulsive Noise Source," *IEEE Trans. Electromag. Compat.* vol. 43, no. 2, May 2001.

[Rag85] Raghuveer M. R. and Nikias C. L., "Bispectrum Estimation: A Parametric Approach," *IEEE Trans. Acoust., Speech, Signal Processing*, vol. 33, pp. 1213-30, 1985.

[Ran91] Rangoussi M. and Giannakis G. B., "FIR modeling using log-bispectra: Weighted least-squares algorithms and performance analysis," *IEEE Trans. Cir. Sys.*, vol. 38, pp. 281-96, 1991.

[Rio91] Rioul O. and Vetterli M., "Wavelets and signal processing," *IEEE Signal Processing Magazine*, pp. 14-38, Oct. 1991.

[Ros85] Rosenblatt M., "Stationary Sequences and Random Fields," *Birkhäuser*, Cambridge, Massachusetts, 1985.

[Rot71] Roth P. R., "Effective measurements using digital signal analysis," *IEEE Spectrum*, vol. 8, pp. 62-70, Apr. 1971.

[Sub84] Subba Rao, T. and Gabr M., *An Introduction to Bispectral Analysis and Bilinear Time-Series Models*, pp. 42-43, New York: Springer-Verlag, 1984.

[Swa91] Swami A. and Mendel J. M., "Cumulant-based approach to the harmonic retrieval and related problems," *IEEE Trans. Acoust., Speech, Signal Processing*, vol. 39, pp. 1099-1109, May 1991.

[Tun00] Tungkanawanich A., Abe J., Kawasaki Z. I. and Matsuura K., "Location of partial discharge source on distribution line by measuring emitted pulse-train electromagnetic waves", *Proceedings of IEEE Power Engineering Society Winter Meeting 2000*, IEEE catalog 00CH37077C, CDROM 0-7803-5938-0.

Chapter 5

DIRECT-WAVE CROSS-CORRELATION (DWCC) – A NEW TIME DELAY ESTIMATION TECHNIQUE

Introduction

Existing time delay estimation techniques are inadequate for estimating very short time delay imposed by a receiving sensor array of relatively small physical dimension and the impulsive nature of the noise source to be located. A new time delay estimation technique called the Direct-Wave Cross-Correlation (DWCC) is proposed and presented in this chapter. The algorithm is implemented via visual inspections and observations of signal trends obtained from practical experiments. The performance of DWCC is realistic and well demonstrated with an accuracy of better than 40×10^{-12} *sec in practical conditions. It is specially design to estimate very short time delay from an impulsive noise source and therefore no claims for optimality in diverse situations are made.*

5.1 Signal Modelling in Multipath Environment

The modelling problem considered is the estimation of the time delay between a pair of synchronised sensors spatially separated at a sensor spacing L. In addition to the general model described in chapter 4, the effects of multipath will be taken into account. Consider only an idealized reflective surface with a flat geometry depicted in Figure 5.1. In this situation, diffuse multipath arising from surface irregularities is ignored.

The incident field received at the sensors will generally consists of two basic components:

1. *Free-space* components that propagate from the source to the receiving sensors along a direct path. These components are also referred to as the *direct-wave* components.
2. *Multipath* components that are resulted from surface reflections. They reach the receiving sensors along indirect paths that point to the images of the source.

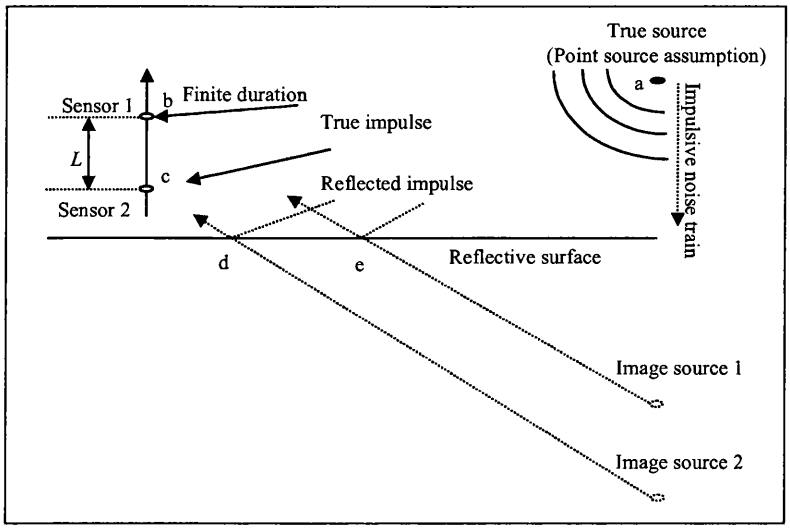

Fig. 5. 1. Effects of impulsive noise reception on a flat reflective surface.

Again, with reference to the Figure 5.1, the direct-wave component propagates from the source via a direct transmission path and reaches sensor 1 in the shortest time. The wavefront continues to propagate at a different angle towards the second sensor creating a time delay D_{cb} between the waveforms received by the two sensors. The delay can expressed by:

$$D_{cb} = D_{ab} - D_{ac} \tag{5. 1}$$

where D_{ab} and D_{ac} are time delays from the respective path as labelled in the Figure. Evaluating the delay is less complicated if the effects of multipath are negligible. On the other hand, if the effects of multipath are considerable, the problem of estimating the time delay can become difficult. An example of such a scenario will be in a domestic home where many highly reflective metal works exist.

In a case where a flat reflective surface is present, see Figure 5.1, number of image sources, equal to the number of sensors employed, are virtually created. This confuses a conventional time delay algorithm and adversely deteriorates its performance. In the worst case, the estimated time delay can be totally misleading. For modelling purposes, the signal $x_1(t)$ received by the sensor closest to the source can be written as:

$$x_1(t) = s(t) + n_1(t) + \sum_{v=1}^{M} \rho_v y_v(t + J_v(t)) \tag{5.2}$$

where $s(t)$ is a direct-wave transmitted from the source a of unknown characteristics and it is assumed to be zero-mean non-Gaussian stationary random process. $n_1(t)$ is zero-mean Gaussian noise statistically independent of $s(t)$. The last term equation (5.2) is a summation of multipath components reflected from M reflective surfaces and v is the index for the reflectors. $s(t)$, when reflected, is modified by a transfer function $h(t)$ to give $y(t) = s(t) * h(t)$. Since the reflected waves approach the sensor at a different time and space, they are shifted and weakens accordingly with a time delay $J(t)$ and a gain factor ρ. The reflected waves are assumed to be non-Gaussian and highly correlated with $s(t)$.

The signal $x_2(t)$ received by the second sensor is a delayed version of the first:

$$x_2(t) = \alpha s(t + D(t)) + n_2(t) + \sum_{w=1}^{N} \beta_w y_w(t + K_w(t)) \tag{5.3}$$

where α and β are gain factors and $D(t)$ and $K(t)$ are time delays for the direct-wave component and reflected wave components respectively. $n_2(t)$ is zero-mean Gaussian noise being added to the second sensor and it is statistically independent of $s(t)$. The last term of equation (5.3) represents the sum of reflected waves from N surfaces observed from the second sensor and may be a different number from the M surfaces observed from the first sensor.

The important point to note is that both the free-space and multipath components can be well defined in terms of the amplitude, phase difference, and direction. The geometry and propagation effects can be approximated. The reflection process is assumed to be ideal i.e. $h(f) = 1$ for the worst-case scenario. The source is assumed to be a point source in a stationary position and the radiated signals approach the sensors at a constant (speed of light) to give a respective time delay between the sensors, which is invariant with time. Under these conditions, the multipath model of Figure 5.1 may be viewed as *deterministic* and the equations above can be rewritten as:

$$x_1(t) = s(t) + n_1(t) + \sum_{v=1}^{M} \rho_v s(t + J_v) \tag{5.4}$$

$$x_2(t) = \alpha s(t + D) + n_2(t) + \sum_{w=1}^{N} \beta_w s(t + K_w) \tag{5.5}$$

Estimation of D is conventionally achieved using the cross-correlation function. This is a measure of the similarity of two functions x_1 and x_2 as one is displaced through time τ relative to the other, and is expressed as:

$$C_{x_1 x_2}(\tau) = E[x_1(t) x_2(t + \tau)] \tag{5.6}$$

Without considering the effects of multipath and assuming that $n_1(t)$ and $n_2(t)$ are zero mean, Gaussian and spatially uncorrelated, the cross-correlation was derived in chapter 4 to be:

$$C_{x_1x_2}(\tau) = \alpha C_{ss}(\tau) * \delta(\tau - D) \tag{5.7}$$

where * denotes convolution. However in the presence of multipath a more comprehensive equation of (5.7) becomes:

$$C_{x_1x_2}(\tau) = \alpha C_{ss}(\tau) * \delta(\tau - D) + \sum_{w=1}^{N} \beta_w C_{ss}(\tau) * \delta(\tau - K_w) + \sum_{v=1}^{M} \rho_v \alpha C_{ss}(\tau) * \delta(\tau - (D - J_v)) + \sum_{v=1}^{M}\sum_{w=1}^{N} \rho_v \beta_w C_{ss}(\tau) * \delta(\tau - (K_w - J_v)) \tag{5.8}$$

Assuming that there is only one flat reflective surface as depicted in Figure 5.1, i.e. $N = M = 1$, then the right hand terms of the equation represents the following:

Function	Equivalent cross-correlation *E[x,y]*
$\alpha C_{ss}(\tau) * \delta(\tau - D)$	x = Direct-wave (a-b), y = Direct-wave (a-c)
$\beta C_{ss}(\tau) * \delta(\tau - K)$	x = Direct-wave (a-b), y = Reflected wave (a-d-c)
$\rho\alpha C_{ss}(\tau) * \delta(\tau - (D - J))$	x = Reflected wave (a-e-b), y = Direct-wave (a-c)
$\rho\beta C_{ss}(\tau) * \delta(\tau - (K - J))$	x = Reflected wave (a-e-b), y = Reflected wave (a-d-c)

Table 5. 1. Description of terms.

Applying frequency weighting functions [Car73,Han73,Kna76] will not remove the multi-path components that will smear the true correlation peak, since most of them work according to the coherence of the signals and multipath components are highly correlative. Implementation of adaptive filters to minimise

the effects of multi-path components may be difficult as well. Therefore, a new and more accurate TDE method *ad hoc* to this application has to be implemented.

5.2 Direct-Wave Cross-Correlation

Previous research efforts [Car73,Han73,Kna76] were principally focused on frequency domain techniques and implementation of frequency weighting functions according to the coherence of the signals. The techniques were proved, in chapter 4, to be unsuitable for the application of wideband impulsive noise time delay estimation. A new approach to the problem, which will be described in the next few sections, utilises only the direct-wave components selected by time domain windowing functions for the cross-correlation. The results have shown to be far more superior.

5.2.1 Time Domain Windowing

In the case of an impulsive noise source, the impulses are of finite duration and when radiated, they travel towards the receiving sensors in a well-defined sequential order. The one with the shortest propagation path will be the first to reach the sensors. It can be easily deduced from Figure 5.1 that the time taken for the direct-waves to the sensors, D_{ab} and D_{ac}, are lesser than any of the reflected waves i.e.:

$$D_{ab} < D_{ad} + D_{dc} \tag{5.9}$$

$$D_{ac} < D_{ae} + D_{eb} \tag{5.10}$$

$$D_{ac} < D_{ad} + D_{dc} \tag{5.11}$$

$$D_{ab} < D_{ae} + D_{eb} \tag{5.12}$$

By fast sampling and with a suitable truncation or windowing technique, the multipath components in the signals can be taken out leaving mainly the direct-wave components to be analysed. This will minimise the error possibly introduced by the effects of multipath when estimating the time delay.

5.2.2 Method 1 - Signal Truncation by Rectangular Window

Figure 5.3 shows a pair of signals captured by two aerial type sensors at a spacing of 0.79m. Experimental details can be found in chapter 8. The waveforms exhibit an excursion of a typical transient with characteristics of a damped sinusoid decaying exponentially in the amplitude with time. At about 12*ns* the waveform patterns, from the two sensors, start to deviate from each other. The highly probable cause of this phenomenon is due to the effects of multipath since the test was done in a normal classroom with only rudimentary precautions to avoid multipath propagation. This is mainly to emulate the possible problems that may be encountered in a domestic environment when locating a noisy thermostat.

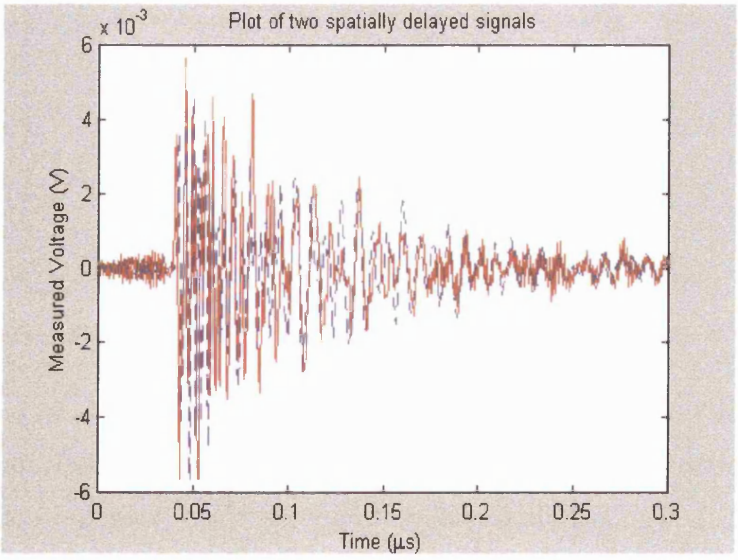

Fig. 5. 2. Impulsive noise received at a sensor spacing of 0.79m.

Applying the waveforms directly to existing time delay algorithms proved to be inadequate (see Chapter 4). From observing the waveforms in the Figure, it is deemed that a suitable signal pre-processing technique, such as truncation of the signal, will allow only on the direct-wave portion of the signal to be analyzed thus improving the overall time delay estimation. This implies a high sampling rate requirement in order to achieve a good signal resolution within the short time window when only the direct-wave is present in the waveform. Fortunately, fast sampling can be easily achieved by a current state of the art digital scope having a maximum sampling frequency f_s of 25GS/s. Increasing the sampling rate has the equivalent effect of zooming into the signal as shown in Figure 5.3. The details of waveform in the frontal portion can now be clearly seen.

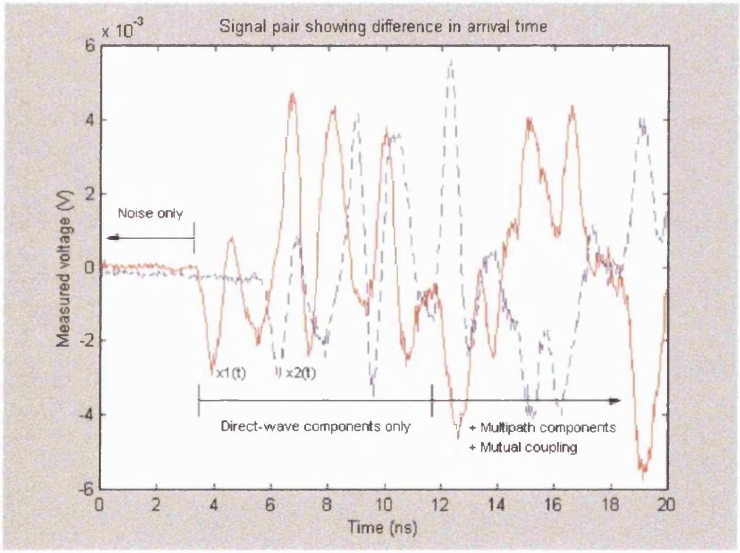

Fig. 5. 3. Signal pair showing difference in arrival time and various components of the signals.

Truncating the signal is similar to windowing, where only the direct-wave signal that is not affected by multipath components is taken. Signal truncation (or rectangular windowing) can be expressed mathematically by:

$$y_1(t) = x_1(t)W_1(t) = \left[s(t) + n_1(t) + \sum_{v=1}^{M} \rho_v s(t + J_v) \right] W_1(t) \tag{5. 13}$$

$$y_2(t) = x_2(t)W_1(t) = \left[\alpha s(t + D) + n_2(t) + \sum_{w=1}^{N} \beta_w s(t + K_w) \right] W_1(t) \tag{5. 14}$$

where the window function $W_1(t)$ and it is given by:

$$W_1(t) = \begin{cases} 0 & t < t_r \text{ , } t \geq t_w \\ 1 & t_r \leq t < t_w \end{cases} \tag{5. 15}$$

where t_r is the start time of the window function which is also equivalent to the triggering time of the reference signal. The symbols $t_w - t_r$ defines the time width of the window.

Results presented later are going to show that just by a simple signal truncation technique can improve the accuracy of the time delay estimation significantly. This shows that the multipath signal modelling is of good value. A more refine method is worthwhile considering to make further improvements to the technique.

5.2.3 Method 2 – Hanning Window (HW)

Rectangular windowing can result in discontinuities in the signal time-series, and are problematic in the context of the subsequent cross-correlation process. This can be addressed by adopting a window function that does not introduce such discontinuities. A good choice will be the Hanning Window (HW) defined by:

$$W_2(t) = \begin{cases} 0 & t < t_r \text{ , } t > t_w \\ 0.5\left(1 + \cos\left(2\pi \dfrac{t - t_r}{(t_w - t_r)}\right)\right) & t_r \leq t \leq t_w \end{cases} \tag{5. 16}$$

The optimum window width is determined via practical experimentation in a later section. The role of the window is to extract only the direct-wave section of the signal to be applied to a correlation algorithm leaving out the noise and multipath segments. The idea is best illustrated in Figure 5.4 as follows:

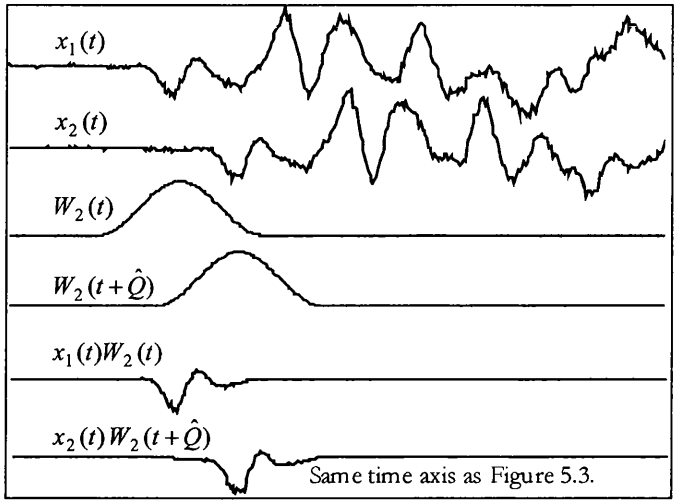

Fig. 5. 4. Illustration of DWCC method 2 pre-processing technique.

The time domain windowing functions are able to filter out the unwanted signal components in equations (5.4) and (5.5) i.e.:

$$\left[\sum_{v=1}^{M} \rho_v s(t+J_v)\right] W_2(t) \cong 0 \tag{5. 17}$$

$$\left[\sum_{w=1}^{N} \beta_w s(t+K_w)\right] W_2(t+\hat{Q}) \cong 0 \tag{5. 18}$$

$\hat{Q}$ is an unknown time shift of the window and has to be estimated. This leaves only the direct-wave components of the signals to be analyzed:

$$y_1(t) = x_1(t)W_2(t) = s(t)W_2(t) + n_1(t)W_2(t) \tag{5. 19}$$

$$y_2(t) = x_2(t)W_2(t+\hat{Q}) = \alpha s(t+D)W_2(t+\hat{Q}) + n_2(t)W_2(t+\hat{Q}) \tag{5. 20}$$

Equations (5.19) and (5.20) assume that the selection of the window time width $t_w - t_r$ is small such that:

$$t_w < t + J_v \tag{5.21}$$

$$t_w < t + K_w \tag{5.22}$$

Let $z(t) = s(t)W_2(t)$. When $\hat{Q} \cong D$, equations (5.19) and (5.20) become:

$$y_1(t) = z(t) + n_1(t)W_2(t) \tag{5.23}$$

$$y_2(t) = \alpha z(t - D) + n_2(t)W_2(t - D) \tag{5.24}$$

Since the noise components are uncorrelated, the cross-correlation of equations (5.23) and (5.24) gives:

$$C_{y_1 y_2}(\tau) = \alpha C_{zz}(\tau) * \delta(\tau - D) \tag{5.25}$$

This can be viewed as an auto-correlation function with its peak shifted to D from the centre indicating the required time delay.

5.2.4 Constructing the Hanning Window

The Direct Wave Cross-Correlation (DWCC) algorithm requires the window shift parameter $\hat{Q}$ and has to be estimated by shifting the window one sample-step at a time along the time series. A confidence value is calculated each time for establishing the optimum window location. The windowing function is designed to select a time-series segment in each signal that is most alike in all the channels and prepare them for the cross-correlation process. The measure of confidence level is equivalent to the correlation coefficient described by:

$$c\langle y_1, y_2 \rangle = \max\left\{ \frac{C_{y_1 y_2}(\tau)}{\sqrt{C_{y_1 y_1}(0) C_{y_2 y_2}(0)}} \right\} \quad , \quad c(y_1, y_2) < 1 \tag{5. 26}$$

It describes a normalized cross-correlation sequence such that the auto-correlation at zero lag has a maximum identical coefficient equals to 1.0. Search can now be performed by adjusting $\hat{Q}$ in step size equals to the sampling period $T_s = 1/f_s$, where f_s is the sampling frequency. To reduce the number of iterations required, an initial condition for $\hat{Q}$ may be derived from a simple cross-correlation described in method 1 and a limit condition may be specified. The adjustment of $\hat{Q}$ should be no more than the width of the window. The estimation of $\hat{Q}$ is more probable with a higher confidence level. As the confidence level approaches its highest possible point, the condition $\hat{Q} \cong D$ is assumed.

One may be tempted to use $\hat{Q}$ as the final estimate for the time delay D. However, in a digital system $\hat{Q}$ is quantized into the nearest sample and its error depends on the sampling frequency of the system. Since $\hat{Q}$ is only a single value result no further enhancement to the time delay resolution can be made. Therefore the correlation equation (5.25), where $\hat{Q}$ is a substituted variable, is preferred so that interpolation, polynomial and other curve-fitting techniques may be applied to improve the overall resolution of the estimate.

5.2.5 Extension to Multiple Sensor Inputs

For multiple signals $x_1, x_2, \ldots x_n$, a similar methodology as in the case of a two input system described earlier may be implemented. A simultaneous measure of confidence level for n signals can be made by:

$$\xi = \prod c_{ij}\left\langle y_i(t), y_j(t)\right\rangle, \ {}^{i=1,2,\ldots,n}_{j=1,2,\ldots,n,\ j\neq i} \tag{5. 27}$$

where $y = x(t)W(t)$. Only the unique delays are included in the calculation of equation. The number of unique delays P, assuming that a unique delay is calculated from two sensors from either direction, is a combination of 2 out of n input signals and can be defined as:

$$P = C_n^2 \tag{5. 28}$$

In this case, a sequential time-shift adjustment of each window, one at a time, is done with the confidence level calculated. The process is iterated until a highest possible confidence level or limit condition is met. This is very useful in the application of location source where two or more time delays are required to compute an estimated source position. Equation (5.27) also implies that the calculation of confidence level is improved as the number of sensor observations increases.

5.2.6 Limitations of the Algorithm

Selection of the window time width is a compromise between the variance of the cross-correlation estimation and the effects of multipath and mutual coupling. The windowing function has the effect of altering the phase of the signal. This effect is lessened with better approximation of the window time shift parameter $\hat{Q}$. To make the algorithm insensitive to the input variable $\hat{Q}$, the time width of the window used should be wide enough. A useful empirical rule is to set the width of the window to at least one cycle of the center frequency as defined by the receiving system.

5.2.7 Algorithm Flow Chart

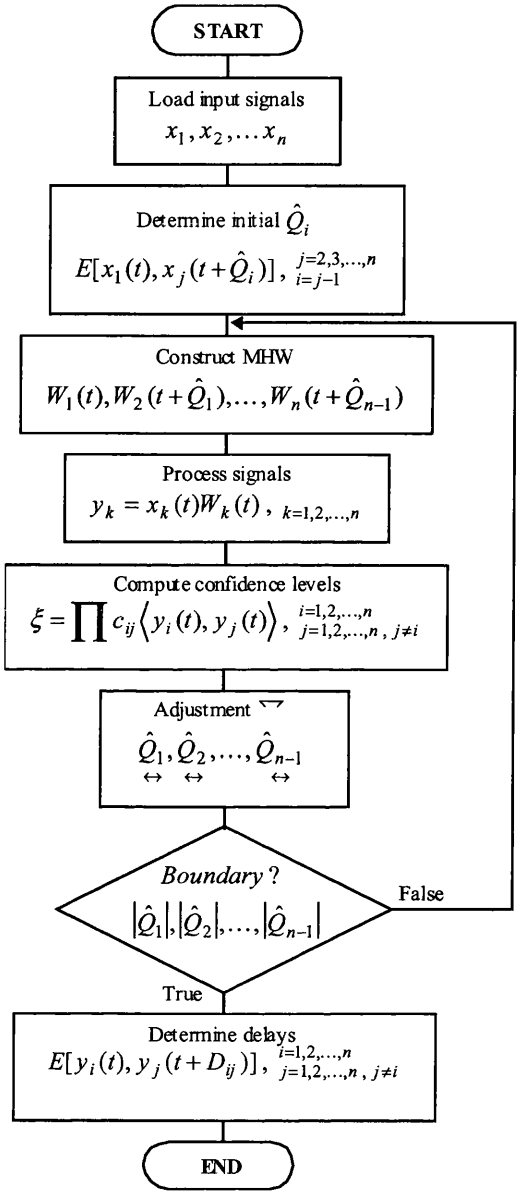

Fig. 5. 5. DWCC method 2 algorithm flowchart.

5.2.8 The Possibility of Applying a Weighting Function

It may seem reasonable that a frequency weighting function may be applied to sharpen the peak of the correlation. Such an approach is good for sharpening and distinguishing adjacent correlation peaks that smear into the true delay peak. In this case, however, the resolution of the algorithm is achieved in the expense of stability. This is because high-resolution techniques typically involve the estimation of spectral density from a finite observation. This is a big disadvantage in estimating time delays for fast impulsive noise transients since the pulse widths are typically $0.3\mu s$ and thus the spectrum cannot be estimated to any great degree of certainty. And also, the approach will increase the computational complexity and higher chance of introducing unwanted errors into the final estimate. Thus, a simple cross-correlation of the pre-processed data is deemed to be more suitable for this particular application since no adjacent correlation peak was observed when correlating the direct-wave only components.

5.3 Practical Tests and Results

The DWCC algorithm was tested in a practical environment described in detail in chapter 8.2.3. Only information required understanding of the graphical results are briefly introduced here. The sampling frequency employed f_s is 25GS/s. The duration of the signal records used is 500 samples or $20ns$ in equivalent as shown in Figure 5.3. A Y-Shaped array was used in the test and was setup as illustrated in Figure 5.6:

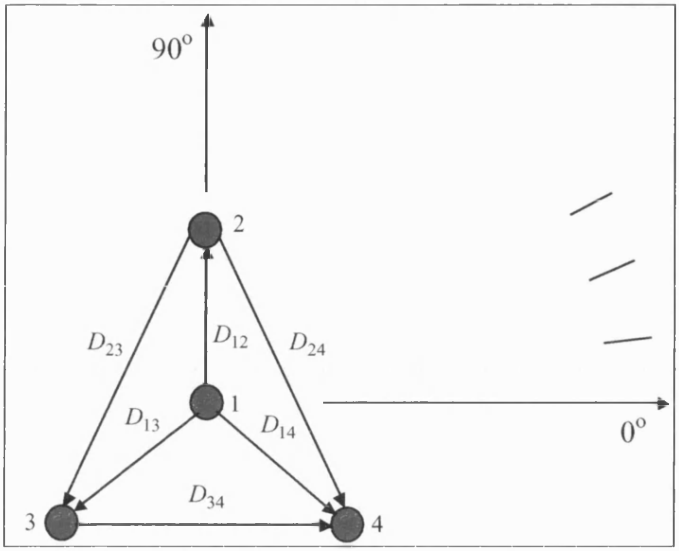

Fig. 5. 6. A Y-Shaped array configuration and delay labels.

At every 10 degrees, 30 records were taken. Before performing the DWCC, the width of the windowing function has to be set. By looking at the change of time delay over varying window size, near optimum window size may be selected. Figures 5.7, 5.8 and 5.9 show a typical example of the computed time delays over the application of different window width. The respective delays with reference to Figure 5.6 are D_{23}, D_{24} & D_{34}. The record is based on a noisy thermostat source triggering from a bearing of 90°, 10 metres from the array.

At window widths equal to 120 samples or above, the time delay estimation begins to deviate from the actual value significantly. This effect can be seen on all records, and in this case, the deviation has a peak of about 1 sample or 40×10^{-12} s. Other records have shown to have a peak deviation of about 3 samples or 120×10^{-12} s. Although this is only a very small figure, it has a significant impact on the accuracy of a source locator – see chapter 3. If the window width is too small, the variance of the delay estimations can become large. This is reflected in the Figures as saw-tooth features when the window width is set to 50 samples.

Therefore the window width worth considering is narrow down to the range from 50 to 100 samples.

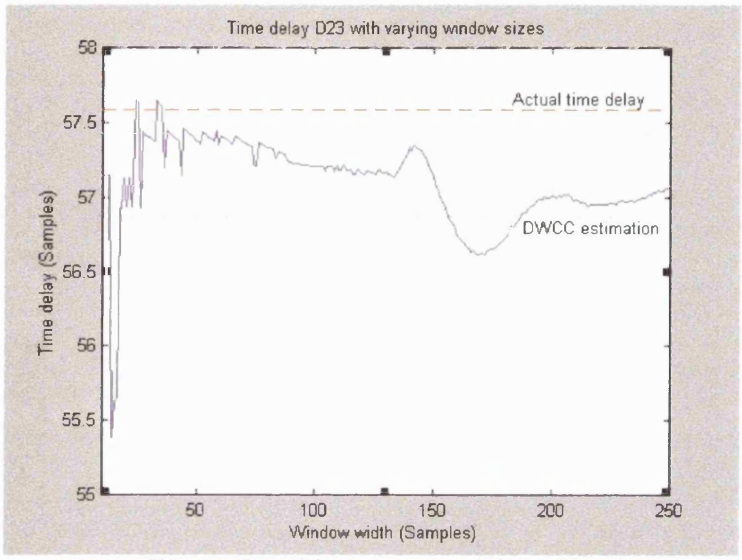

Fig. 5. 7. Time delay D_{23} versus window width.

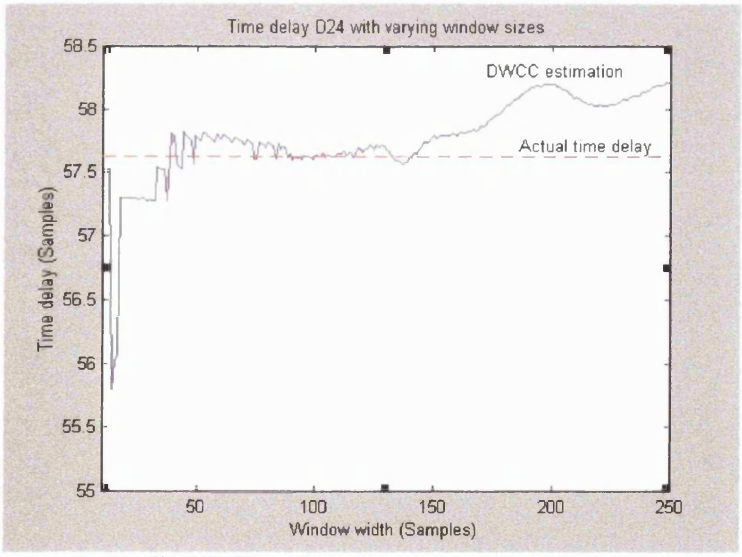

Fig. 5. 8. Time delay D_{24} versus window width.

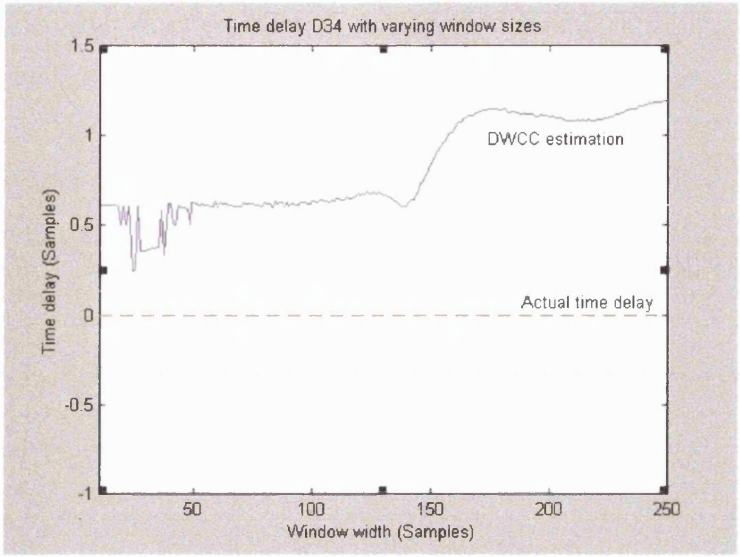

Fig. 5. 9. Time delay D_{34} versus window width.

Variances of time delay estimations for all six unique combinations of time delays, shown in Figure 5.6, were calculated using 30 signal records. Each at 10 degrees interval from 90 to 0 degrees, and for window width of 50, 70 and 90 samples. The results are shown in Figure 5.10, 5.11 and 5.12 respectively.

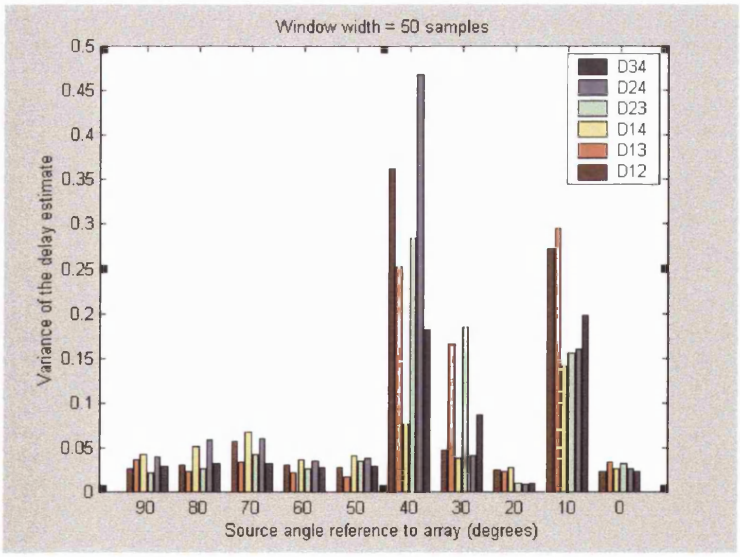

Fig. 5. 10. Variance of six time delays versus source angle for window width of 50 samples.

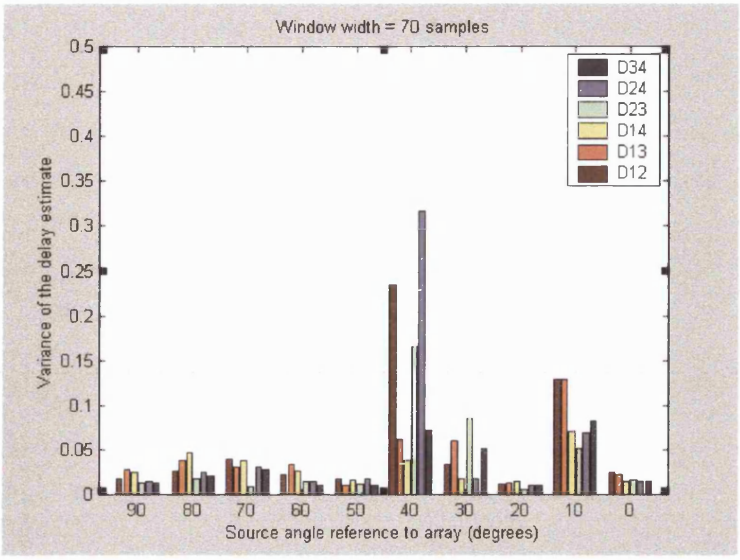

Fig. 5. 11. Variance of the six time delays versus source angle for window width of 70 samples.

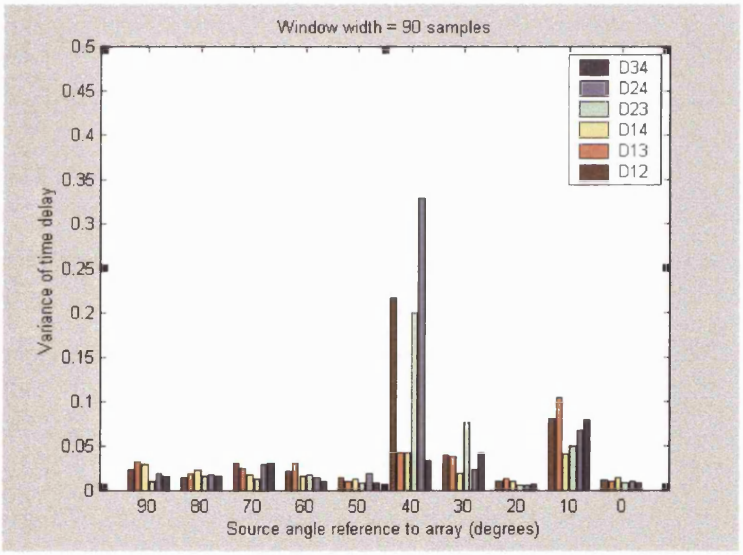

Fig. 5. 12. Variance of the six time delays versus source angle for window width of 90 samples.

The variance of the time delay estimation is largest when window width is 50 samples and smallest for 90 samples. The variance of the six delays seems to be fairly equal to each other. However, $D_{12}, D_{13} \& D_{14}$ will be discarded in the application of a source locator since the ratio of delay variance of maximum

possible delay is significantly larger than the $D_{23}, D_{24} \& D_{34}$. This is because the latter has a larger antenna spacing of 0.79m compared to 0.46m of the former. Finally the performance of the DWCC technique can be viewed vividly with a mean time delay plot over 30 estimates. The curves are compared with an ideal result, a pure sinusoidal, over a quadrant as shown in Figures 5.13, 5.14 & 5.15.

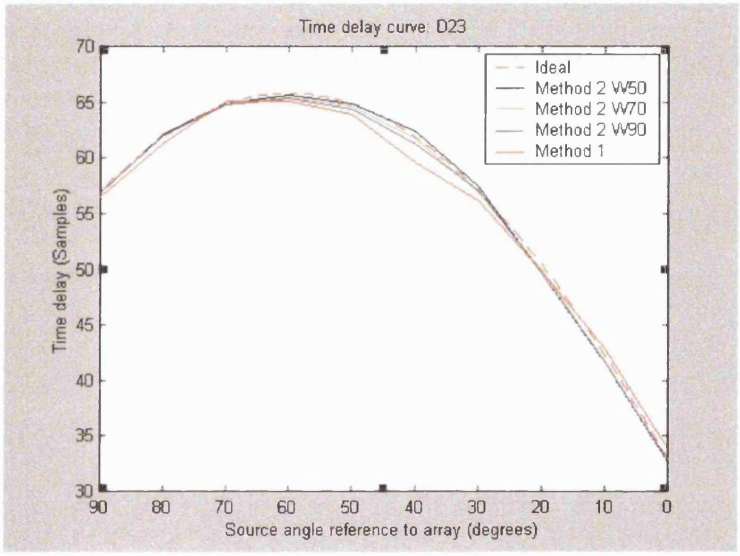

Fig. 5. 13. Time delay D_{23} versus source angle.

The best results were obtained from method 2 with a window width of 70 samples or $2.8ns$ in time. This stands for time delay curves $D_{23}, D_{24} \& D_{34}$. To build up a profile consisting of 30 different records takes only a fraction of a second. An interference signal generated by a faulty thermostat typically consist of a series of micro-pulses. Each of these pulses has duration of about $0.3us$. Using a feature available in the digital-scope called fast-frame, the average number of micro-pulses trigger by a faulty thermostat is established to be about 25000pulses/s.

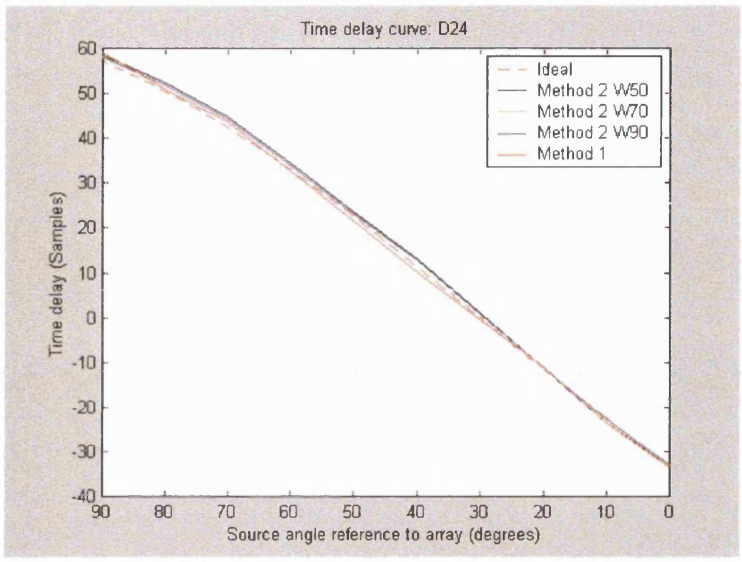

Fig. 5. 14. Time delay D_{24} versus source angle.

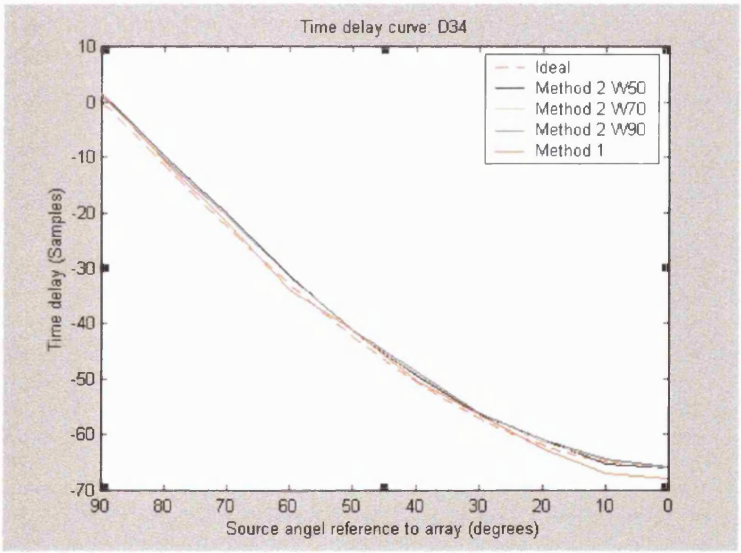

Fig. 5. 15. Time delay D_{34} versus source angle.

5.4 References

[Abe87] Abel J. S. and Smith J. O., "The spherical interpolation method for closed-form passive localization using range difference measurements," *Proc. ICASSP-87 (Dallas, TX)*, pp. 471-474, 1987.

[Car73b] G. C. Carter, Nuttall A. H. and Cable P. G., "*The smoothed coherence transform*," *Proc. IEEE (Letter)*, vol. 61m, pp. 1497-1498, Oct. 1973.

[Chi90] Chiang H. H. and Nikias C. L., "A New Method for Adaptive Time Delay Estimation for Non-Gaussian Signals," *IEEE Trans. Acoust., Speech, Signal Processing*, vol. 38, no. 2, Feb. 1990.

[Han73] Hannan E. J. and Thomson P. J., "Estimating group delay," *Biometrika*, vol. 60, pp. 241-253, Feb. 1973.

[Kna76] Knapp C. H. and Carter G. C., "The generalized correlation method for estimation of time delay," *IEEE Trans. Acoust., Speech, Signal Processing*, vol. ASSP-24, pp. 320-327, Aug. 1976.

[Pec01] Peck C. H. and Moore P. J. "A Direction-Finding Technique for Wide-Band Impulsive Noise Source," *IEEE Trans. Electromag. Compat.* vol. 43, no. 2, May 2001.

Chapter 6

SENSOR ARRAY DESIGN AND CONSTRUCTION

Introduction

The chapter discuss about source location resolution under the effects of digital quantisation and the possibility of minimising such phenomenon by strategic array design. A new performance assessment technique for choosing the most suitable area geometry is introduced. All discussions are focused on three and four-sensor array systems and assume the employment of hyperbolic based location algorithm. Experimental proofs are given to establish the effects of spatial quantisation. This will be introduced in last part of the chapter.

6.1 Array Geometry Assessment via Resolution Map

In a digital location system, received signals are converted into digital format for Digital Signal Processing (DSP). The sampling frequency f_s can impose a location limitation to the locator system even if the signals presented to the system are ideal, i.e. not corrupted by noise or modified by any transfer function. For example, the peak cross-correlation of two signals $x_1(t)$ and $x_2(t)$ received via a pair of spatially separated sensors at spacing L metres, see Figure 6.1, will give a corresponding time delay τ sec. The range of τ is therefore limited to $-L/c$ to L/c depending on the physical position of the source. The symbol $c = 3.0\times10^8 m/s$.

A resolution limit arises due to the finite sampling frequency of a practical system. Consequently, the estimated time delay τ also suffers from a limited resolution. This causes τ to change in discrete time steps of T_s rather than an ideally smooth and continuous form when it is varied within its range.

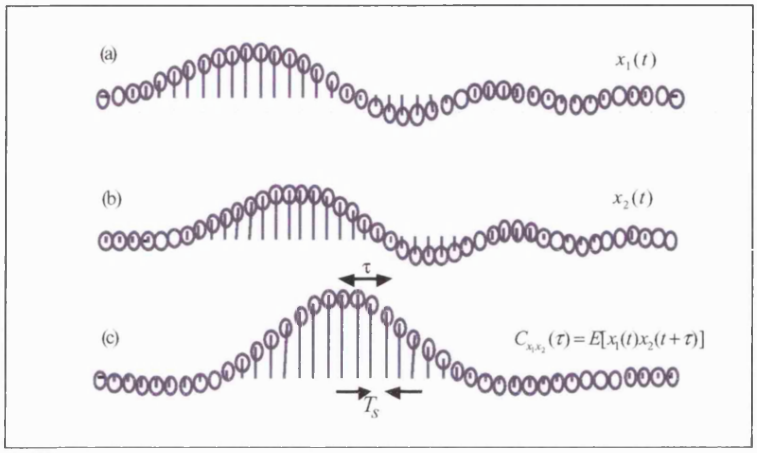

Fig. 6. 1. (a) and (b) are signals received by sensor 1 and 2 respectively. (c) is the resultant correlation of the two signals.

The number of time steps N_{T_s} for a given range of τ is therefore:

$$N_{T_s} = \frac{2L}{cT_s} = \frac{2f_sL}{c} \tag{6. 1}$$

Notice that N_{T_s} is directly proportional to the sampling frequency f_s and the spacing between the sensors L. This implies that by increasing f_s or L or both, N_{T_s} will increase accordingly. With more time steps to describe the fixed range of time delay τ, the time resolution of the system comparatively better off.

However, it is not possible to locate a source using a two sensor system except by restricting the source to a limited boundary defined by the line joining the two

sensors – see Figure 6.2. This line is often referred to as the baseline. Under such a boundary condition, the source location can be easily calculated given the exact time delay. For locator systems of finite sampling rate, the estimated source location can only be a value of the nearest spatial quantised step defined by:

$$\Delta S = \frac{L}{N_{T_s}} = \frac{c}{2f_s} \, metres \tag{6. 2}$$

For a time-delay τ, there is a hyperbolic curve representing the locus of all possible source locations corresponding to the delay – see chapter 3. A straightforward technique to access the spatial resolution of different array geometries can therefore be achieved by plotting the time delay hyperbolic curves in steps of ΔS over the sensor spacing L as shown in Figure 6.2 below.

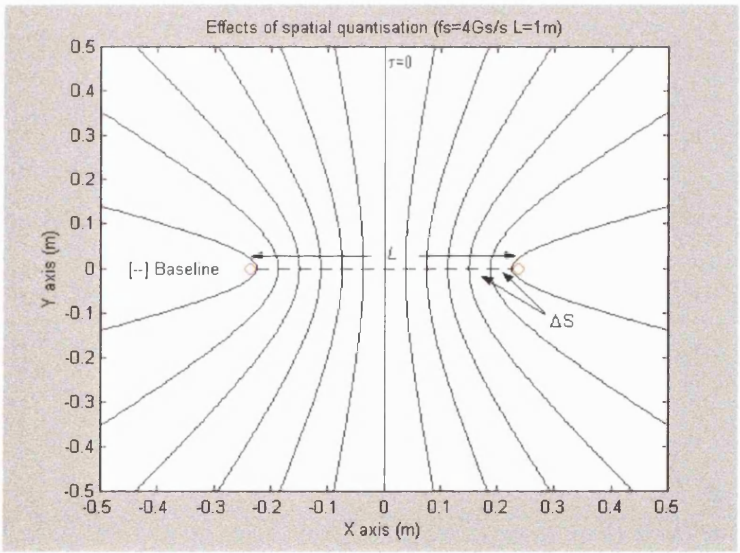

Fig. 6. 2. Hyperbolic curves in steps of ΔS.

Suitable adjustment and rotation of this set of result can be used to produce a new assessment tool called the Resolution Map (RM). It provides a visual display

of the location coverage for different array geometries. The word resolution in the name refers to the degree of which closely spaced source can be discriminated. The lines on a map reflect the possible locations of a source. A higher line density is interpreted as better resolution. In contrast, a large un-intersected region will expect to produce a larger location estimation error. It can be seen later that the choice of array geometry affects the performance of the system's ability to locate a noise source significantly, under the effects of digital quantisation.

6.2 Different Array Geometries

Choice of suitable array geometry can generally be influenced by a number of factors listed as follow:

- The number of input channels.
- The processing algorithm.
- Allowable physical dimension.
- The ability to enhance the performance of the locator system.

The most common array geometries are the uniformly spaced linear array, square array and Y-shaped array. Thus, these configurations are investigated here. Figure 6.3 shows the different types of array geometries.

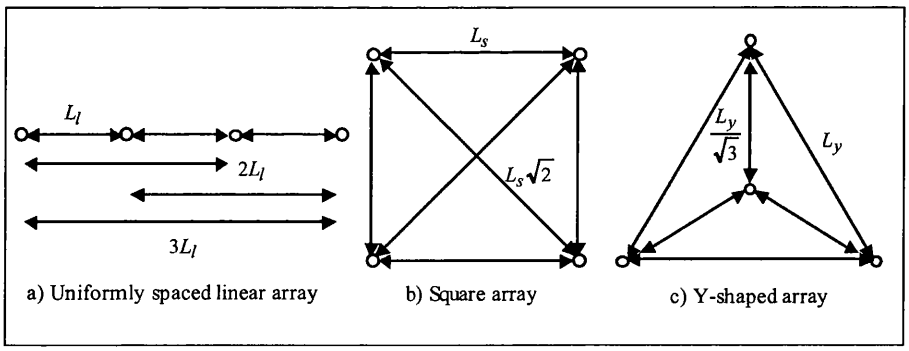

Fig. 6. 3. Sensor array of different geometries.

6.2.1 Assessment Criteria

Each of the arrays has sensor spacing of L_l, L_s and L_y for linear, square and Y-shaped array respectively. There are six unique pairs of delays for each configuration. Assuming that all the delays are utilised, the total baseline is defined as the total spacing between the sensors. For the linear array the total baseline is:

$$B_l = 10L_l \ metres \tag{6. 3}$$

Similarly the respective square and Y-shaped array total baselines are:

$$B_s = L_s(4+2\sqrt{2}) \ metres \tag{6. 4}$$

$$B_y = 3L_y(1+\frac{1}{\sqrt{3}}) \ metres \tag{6. 5}$$

An equal baseline, B = 10m, is set to assess the performance of different array geometries for a four-input system in the next few sections. The performance of the three array geometries, linear, square and Y-shape are reported.

6.2.2 Uniformly Spaced Linear Array

The simplest array geometry for a source locator is the linear array, which consists of antenna elements positioned in a straight line and separated at an equal distance say L_l - see Figure 6.2a. This configuration has been used to locate electric arcs generated in a substation [Sid97]. When assessing the array using the RM, it is found that such geometry performs best when the source is directly in front of the array. The general reasons for employing this geometry are mainly to reduce the complexity of DSP algorithms implementation and also the availability of well-established super-resolution algorithms [Sch86,Tsa96] for this shape.

Figure 6.4 show that regions adjacent to the array generally have poor location resolution. For a finite sampling rate, blind regions on either side of the array are created. These prevent the system from locating the source when it is positioned in these regions.

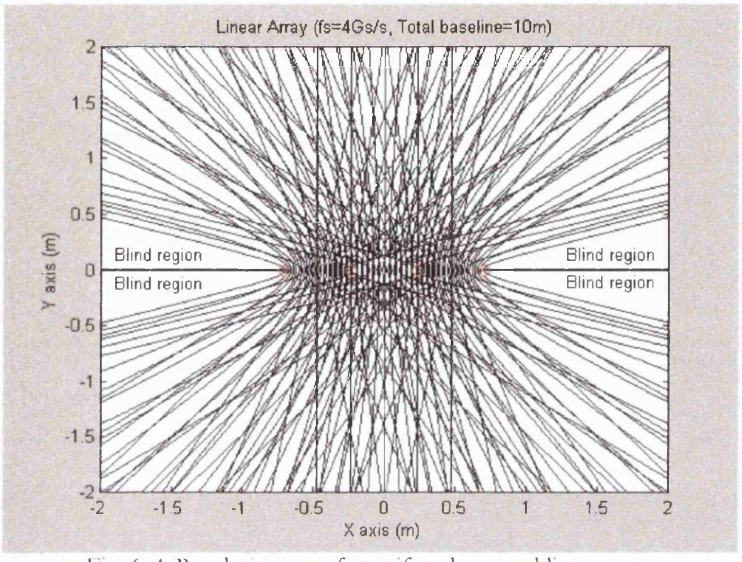

Fig. 6. 4. Resolution map for uniformly spaced linear array.

6.2.3 Square Array

To avoid the blind regions created by the linear array, a symmetrical geometry along the X and Y-axis, such as a square array, could be used. Figure 6.5 shows the resolution map for a square array. The mesh generally covers all the areas around the array avoid the creation of any blind region.

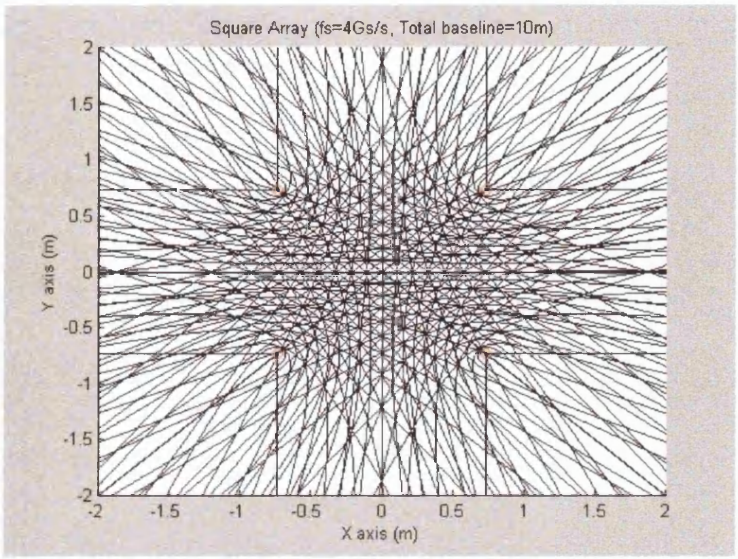

Fig. 6. 5. Resolution map for a square array.

It would be interesting to know if there is a better shape to achieve a finer mesh for the same given baseline. Finally, the design has advanced to the employment of an array geometry called the Y-Shaped array.

6.2.4 Y-Shaped Array

The Y-shaped array positions the sensors in such a way so that no baseline lies on the same angle as another. It is very important in improving the overall location capabilities of the system. It is shown in a later section, on practical experimental proof, that the time-delay variance is the smallest when the source lies on the centre axis perpendicular to the baseline. Thus, having baselines covering different angles will maximise the location coverage of the array.

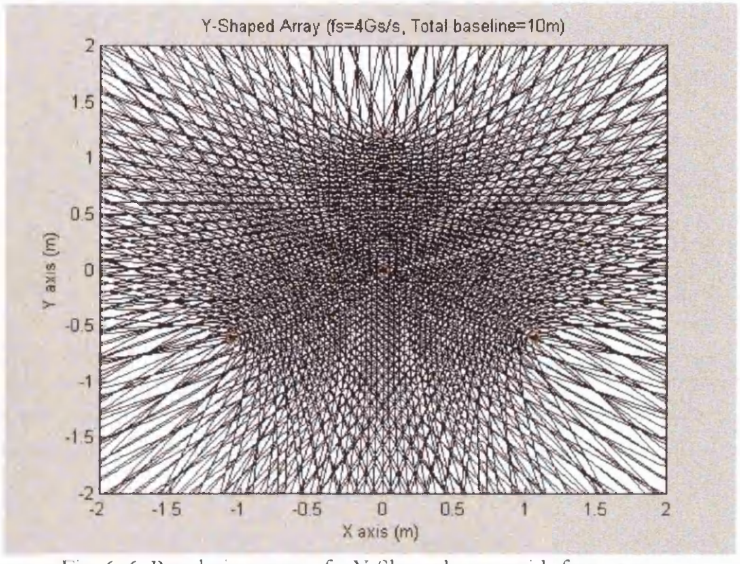

Fig. 6. 6. Resolution map of a Y-Shaped array with four sensors.

Apart from the advantages introduced earlier, it can be clearly observed from Figure 6.6 that the resolution map for the Y-Shaped array is the finest among the three choices.

If only three delays with the smallest variance are used, as recommended in chapter 5, the resolution map is as shown in Figure 6.7 below. Deterioration in the mesh is small, but the total baseline is decreased significantly to 6.34m. Another advantage of using only three delays is the availability of fast and accurate processing algorithms as introduced in chapter 3. Therefore, this is concluded as the best choice among the array geometries discussed here.

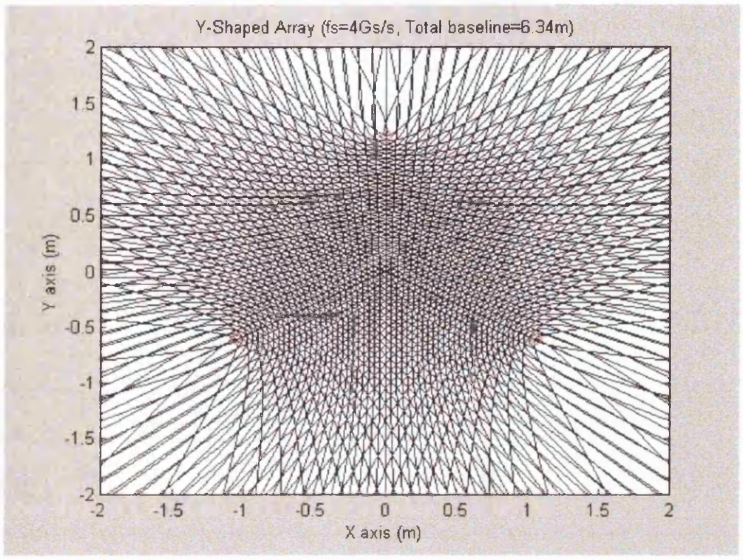

Fig. 6. 7. Resolution map for a Y-Shaped array with three sensors.

6.2.5 General Implications of a Resolution Map

Of all the three different array geometries investigated, the areas bounded by the sensors are finer than those outside the sensors. This implies that the best performance of a system may be achieved if the source to be located is positioned within the array. It can also be observed easily from the maps that the mesh are non-uniform, varies with angle and position, and therefore location of source from different angles and position will be of different accuracy.

The resolution maps have so far focused only on the aspects of digital quantisation effects and the exploitation of different array geometries to minimise such unwanted phenomenon so as to maximise the location resolution. It is based on the assumption that the received signals are not corrupted by noises of any type.

Therefore, it is important to know that the general performance of a source location system is also influenced by many other factors and not just the array geometry alone. The main factors can be listed here as follow:

- The performance of the sensors employed.
- The variance of the Time Delay Estimation (TDE) algorithm under the effects of noise and low Signal-to-Noise Ratio (SNR).
- The ability of the location algorithm to cope with non-ideal conditions stated above.

Under non-ideal conditions the resolution map is far more complex and only unique to the system under analysis as a whole.

6.3 Experimental Proof of Spatial Quantisation Effects

A practical experiment was formulated to show the effects of spatial quantisation by estimating the source location under some predefined distances. A time delay estimate will give a general bearing to the source and a predefined distance fixes the position of the source. The sensors, two identical helical antennas at 410MHz, were spaced at 0.32m apart and the interference source was moved around the sensors at fixed distances of 1m, 3m and 5m intersecting the dotted lines as shown in Figure 6.8. The dotted lines are the source locus at time delays equal to 0, 6, 12 and 15 samples and -6, -12 and -15 for the negative quadrant. Details of the time delay estimation technique can be found in chapter 5. Ten records, each consists of 500 samples and sampling at 25GS/s, were taken at each position and the estimated bearings are plotted on Figure 6.8 with blue crosses at the relevant distances.

A result obtained in such a formulation is purely influenced by only one parameter – the time delay estimate. Thus, the effects of quantised time delay estimation, as a direct consequence of digital quantisation, can be observed. As the time delay increases, the spread of the bearing results is seen to increase. E.g. at 0 degree delay all bearings are virtually identical, but at 15 samples, a range of approximately 10 degrees is observed. It can be seen that the spread of bearing results for the larger time delays remain constant as the distance from the source is increased.

If no further effort such as interpolation is introduced to improve the bearing resolution, the estimated bearing error will be large. However, there is a limit to what interpolation can do to increase the spatial resolution since the input signals are noise added.

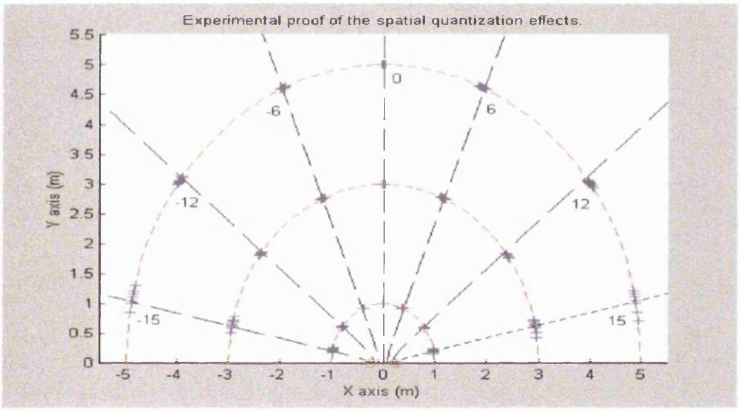

Fig. 6. 8. Effects of spatial quantisation.

A general advantage, when designing the array geometry, is to have the baselines covering as many different angles as possible. The closest example would be the Y-shaped array and has been chosen as the final design.

6.4 Array Construction

An important factor about the array design is practicality. Therefore, by considering some important facts, such as the system has to locate impulsive noise source in domestic areas or in a household, the physical dimension of the array must be kept small. And also, a small physical dimension will allow the array to be mounted on a mobile vehicle if required. Conversely, a small array dimension will restrict its ability to locate noise sources to a closer distance. With all the facts in mind, the array was built on an aluminium sheet selected from standard sizes available in a factory. The final decided dimension of the array is shown in Figure 6.9.

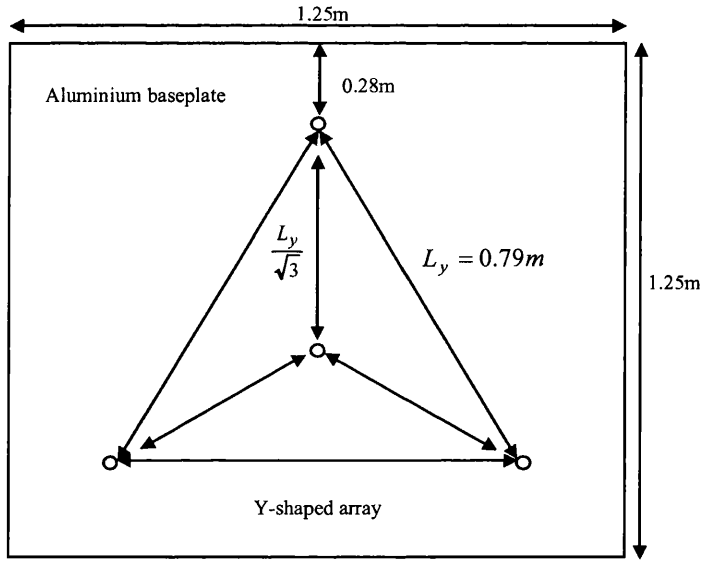

Fig. 6. 9. Y-Shaped array dimension.

The aluminium plate acts as a ground plane, which is required for the correct operation of the monopole antennas. An ideal ground plane would be infinite in dimension. In practice, it is typically recommended that the nearest edge of the plane should be at least half a wavelength of the antennas' resonant frequencies away from the antennas. For optimality, the design presented here was established

after several iterations involving moving the distance of the antennas to the edge of the plane. The choice of antenna was done with respect to its resonant frequency. The main reason is because it is easier to keep to a smaller array dimension with antennas of higher resonant frequency.

6.5 Array Calibration

A well-calibrated array should allow the locator system to locate the exact position of an impulsive noise source. Calibrating the array involves an iterative process of trail and error. A handheld spark generator, which generates wideband impulsive noise, is used to do the job – see Figure 6.10.

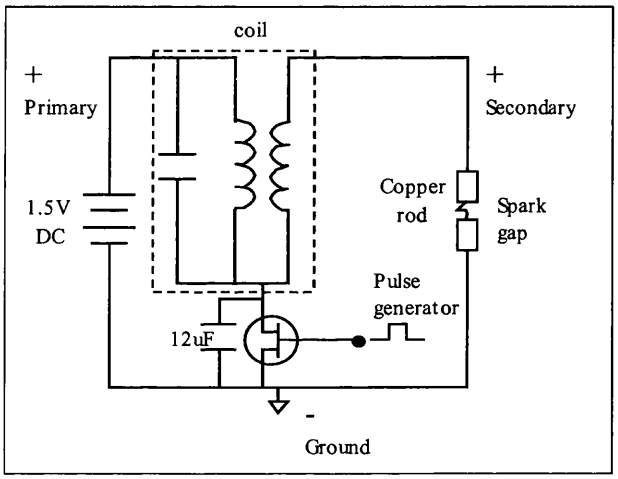

Fig. 6. 10. Handheld spark generator as calibrating source.

The spark generator employed because of its size and ability to emulate the effect of a pointed impulsive noise source. The construction is based on simple capacitor discharge principle. Pressing a trigger button can generate consistent streams of sparks. First, the primary coil is energised by a 1.5V battery as illustrated in Figure 6.10. This is followed by charging up the capacitor in parallel to the primary coil. As the pulse generator triggers and switches on the transistor,

discharges occur rapidly from the capacitor bank through the primary coil. This rapid discharge of the capacitor through the primary coil induces a very high voltage in the secondary coil and consequently forces a spark to jump across the copper rod terminals. The set-up allows a spark length of up to 0.5cm to be drawn with momentary flash of visible light accompanied by a sharp audible noise.

A set of 15 readings was taken with the generator mounted on the centre antenna position and the mean result was taken to calibrate the array. The calibration process involved making very small changes to the antenna spacing within the software in order that the calculated location of the calibrating source matched its physical location of the array. Figure 6.11 shows an example of the array calibration result. The dark cross shows the actual position of the source. The intersection of the three loci came closer than 1 cm to the cross and therefore shows the system to be well calibrated. Experience showed that no further changes to the software would improve the result better than 1cm.

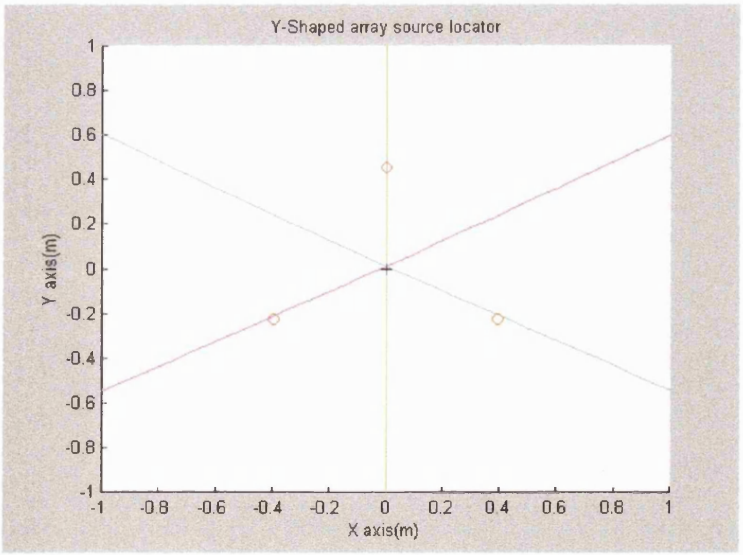

Fig. 6. 11. Calibration diagram.

6.6 References

[Ell01] Ellingson S. W., "Design and Evaluation of a Novel Antenna for Azimuthal Angle-of-Arrival Measurement," IEEE Trans. Antenna and Propagation, vol. 49, no. 6, pp. 971-979, Jun 2001.

[Hua91] Hua Y., Sarkar T. and Weiner D., "An L-shaped array for estimating 2-D directions of arrival," IEEE Trans. Antenna and Propagation, vol. 39, pp. 143-146, Feb 1991.

[Sch86] Schmidt R. O. and Franks R. E., "Multiple Source DF Signal Processing: An Experimental System," IEEE Trans. Antenna and Propagation, vol. AP-34, No. 3, pp. 281, Mar 1986.

[Sid97] Sidhu T. S., Singh G. and Sachdev M. S. "Microprocessor Based Instrument for Detecting and Locating Electric Arcs," IEEE Trans. Power Delivery, PE-331-PWRD-0-11-1997, Nov. 1997.

[Tsa96] Tsakalides P. and Nikias C. L., "The Robust Covariation-Based MUSIC (ROC-MUSIC) Algorithm for Bearing Estimation in Impulsive Noise Environments," IEEE Trans. Signal Processing, vol.44. no. 7, pp. 1623-1633, July 1996.

Chapter 7

CAPTURING AND DIGITISING IMPULSIVE NOISE

Introduction

The chapter discuss about the acquisition techniques and hardware considerations in the designing of the Wideband Impulsive Noise Location System. The fully functional proto-type impulsive noise locator is also presented in detail.

7.1 Capturing Wideband Noise

Capturing wideband noise is a problematic issue due to the broadband nature of the signal. Two techniques were considered and tested. The first technique uses an analogue wideband receiver at the front-end to receive and translate a band-limited signal down to a lower frequency for low-rate digitisation. The second technique is by sampling the signal directly at a relatively higher sampling frequency and wider bandwidth so that the true characteristics of the acquired waveform are represented accurately in the digital domain.

7.2 Frequency Translation Technique

A system based on the frequency translation technique was considered and investigations made via practical experiments. The proto-type system consists of an antenna connecting to a wideband receiver in the front-end. When an impulse occurs, the transmitted RF will be picked up by the wideband receiver via an antenna. The receiver band-limits and down-converts the signal to a lower

frequency feeding into a digitiser. If the waveform is stronger than a preset amplitude threshold, it will trigger, and be captured by, a high-speed data acquisition card which is incorporated in a desktop computer. Advance processing and analysis can then be carried out digitally. The system is illustrated in Figure 7.1.

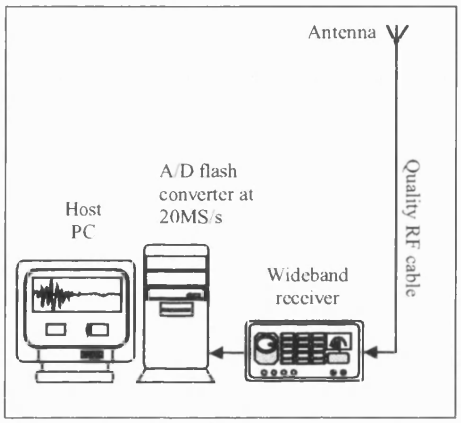

Fig. 7. 1. Impulsive noise acquisition based on frequency translation technique.

Such a system allows different reception modes including Amplitude Modulation (AM), Frequency Modulation (FM), Single Side Band (SSB) and Continuous Wave (CW), with bandwidths ranging from 3kHz to 220kHz. A 10MHz bandwidth is achievable via the use of the receiver's Intermediate Frequency (IF) output. Note that this bandwidth is not available in the demodulated outputs. If the frequency to be monitored is uncertain, the system may be set to scan for activity over a range of frequencies automatically recalled from a set of memory channels (maximum 1000). Impulsive noise generated by a faulty thermostat and one from a switching operation can be very different and may have energy concentrations at different bands. For the requirement of an accurate digital waveform representation, a wider bandwidth reception of 10MHz via the down-converted IF is preferred over demodulation techniques.

7.2.1 Superheterodyne Receiver for Frequency Down-Conversion

The wideband receiver employed, available commercially, technically belongs to the group of superheterodyne receivers. In particular, the model that was employed for measuring impulsive noise in Melksham substation, UK, was the AR5000 model shown in Figure 7.2.

Fig. 7. 2. A Superheterodyne receiver.

The process of down converting a signal, or band of signals, simply involves translating it to a lower frequency. This translation is accomplished without altering the relationship between the signals in the translated frequency band. At a lower translated frequency, the sampling requirements for the conversion into digital samples are reduced. The following equations show how down conversion is achieved mathematically.

The RF and local oscillator (LO) signals are multiplied together using a frequency multiplier, which produces a signal *S* as in equation (7.1).

$$S = \cos(\omega_{RF} t)\cos(\omega_{LO} t) = \frac{1}{2}\cos[(\omega_{RF} - \omega_{LO})t] + \frac{1}{2}\cos[(\omega_{RF} + \omega_{LO})t] \tag{7. 1}$$

where ω_{LO}, ω_{RF}, ω_{IF} are the Local Oscillator (LO) frequency, Radio Frequency (RF) and the Intermediate Frequency (IF) respectively. The high frequency term can be removed with a low pass filter leaving the lower frequency term.

$$S = \frac{1}{2}\cos[(\omega_{RF} - \omega_{LO})t] \tag{7.2}$$

Subsequently, the signal can be applied through a multiple stage filter that only accepts a bandwidth $\Delta\omega_{IF}$, so the range of accepted frequencies is $\omega_{IF} - 1/2\Delta\omega_{IF}$ to $\omega_{IF} + 1/2\Delta\omega_{IF}$. The accepted signal satisfies the equation (7.3).

$$\omega_{IF} - \frac{1}{2}\Delta\omega_{IF} < |\omega_{RF} - \omega_{LO}| < \omega_{IF} + \frac{1}{2}\Delta\omega_{IF} \tag{7.3}$$

The choice of down-conversion method generally depends on two factors. If the signal is relatively narrowband, it is possible to use a local oscillator and a mixer for frequency translation as described in equation (7.1). If the signal covers a large bandwidth, especially ones that stretches over to the image frequency of the conversion, the measurement could be corrupted. To prevent this, the signal has to be pre-filtered, or band-limited, before the mixing process to suppress the image frequency. A simplified diagram showing the components required for a minimal requirement down-conversion system is in Figure 7.3.

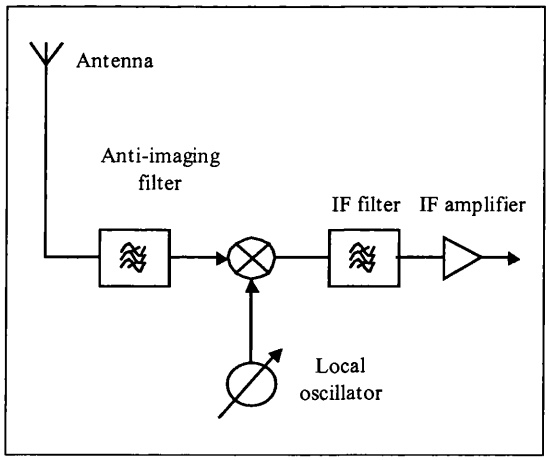

Fig. 7. 3. Radio frequency down-conversion process.

The off-the-shelf wideband receiver provides this feature in default through the receiver IF output with a 10MHz analogue bandwidth and it able to tune into receiving frequencies centre at 3kHz to 2.6GHz.

The dynamic range of the acquisition card used is large – typically from 0-5Volts. And usually the dispersed radio signals are small in amplitude. To match the dynamic range of the acquisition card, the IF output signal would require an amplifier circuit. A simple-to-built circuit configuration is shown in Figure 7.4. However, it is important to know that such direct amplification does not improve the overall Signal-to-Noise Ratio (SNR).

For a multiple antenna system needed for source location as described in chapter 3, a common oscillator is required to synchronise the down-conversion process. This is to ensure that the down-converted signals are synchronised in phase and the time delays between the signals is subject to a minimal distortion. At the same time, the dependency on the stability of the oscillator used is reduced.

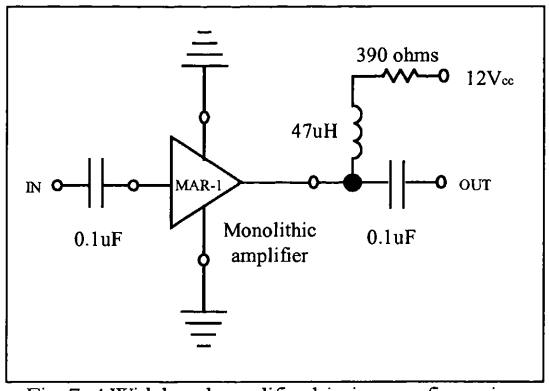

Fig. 7. 4.Wideband amplifier biasing configuration.

A small amount of gain control can be achieved via the automatic gain control (AGC) feature. Nearly every receiver has some kind of AGC to adjust the gain of the RF and/or IF amplifiers according to the strength of the input signal. Without

this feature, the receiver will overload; over-driven amplifiers can become non-linear or "clip" and the output is distorted. The AGC may be used if clipping occurs in the acquired waveform. The AR5000 receiver also provides the flexibility of switching the AGC feature off if necessary. Figure 7.5 shows an example of wideband impulsive noise captured by the system. The waveform was induced by a 132kV busbar disconnector.

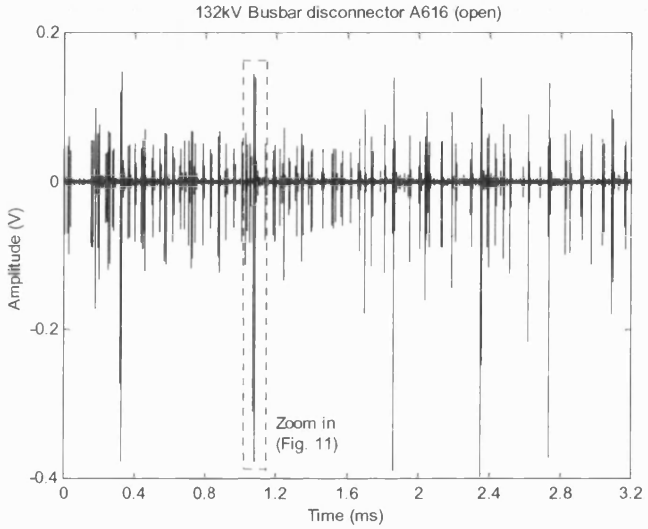

Fig. 7. 5. RF transient captured by the system.

With high sampling resolution, the data may be zoomed in for finer analysis as illustrated in Figure 7.6.

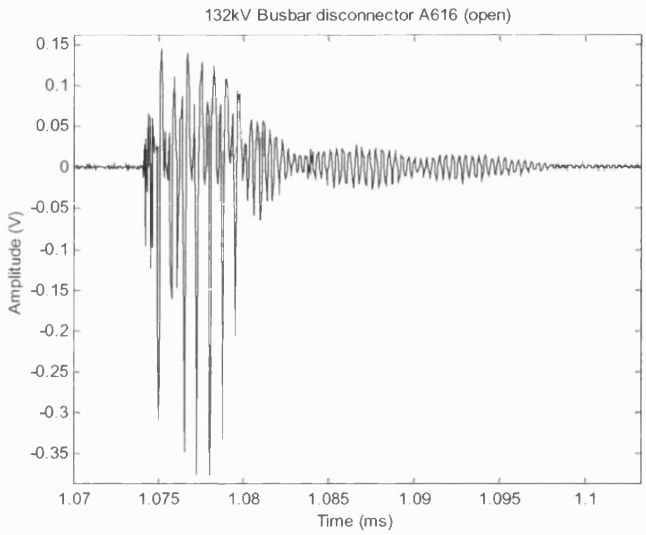

Fig. 7. 6. Expanded version of Figure 7.5.

7.2.2 Disadvantages of Frequency Translation Technique

Setbacks of the frequency translation system include the limitation of channel bandwidth, typically about 10MHz, to describe the wideband signal. The bandpass effect of the system spreads the time domain signal and at the same time reduces the received signal power. Under a lower SNR condition, the time delay correlation peak of the digitised samples, will be dampened and broadened and result in larger time delay estimation error.

Secondly, synchronizing multiple receivers with an external LO, to form a source location system, can be complicated. There are questions about its ability to work under harsh electromagnetic environment such as the substation. If the receivers are widely spaced, great length of external connection cables are exposed, and the susceptibility to the risk of electromagnetic interference is greatly increased. Consequently, it is difficult to ensure a clear transmission of the synchronised signal from the LO to the receivers required for a clean down-conversion process.

Nonetheless, such a system is very portable and requires only commercially available system components that can be bought at relatively low cost.

7.3 Direct Sampling

A more accurate way of acquiring a wideband signal is by sampling the waveform of interest directly using high-speed digitiser incorporated with flash Analogue-to-Digital (AD) converters. The current state of the art digital scope allows a signal to be sample at a rate as high as 25GS/s with a bandwidth of 1GHz. Figure 7.7 is an illustration of the system.

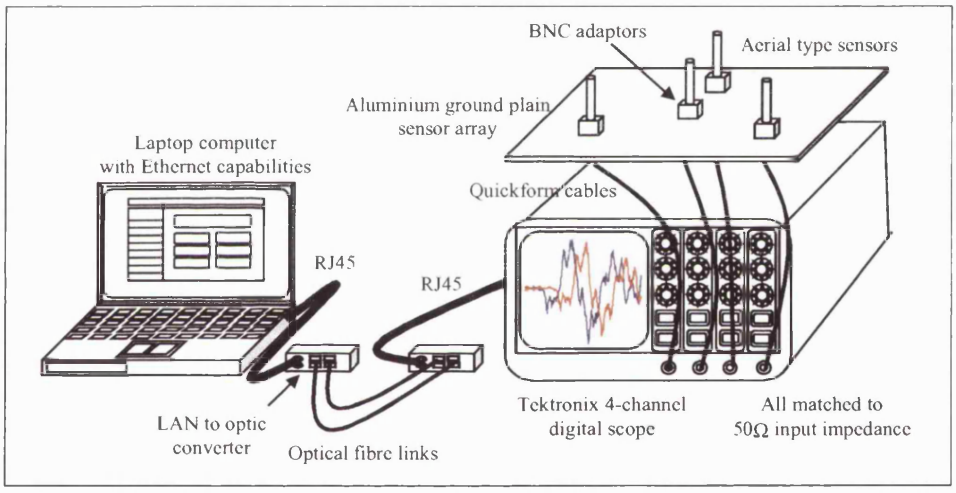

Fig. 7. 7. Impulsive noise acquisition based on direct sample technique.

The main components of the system are:

1. A Tektronix TDS7104 digital phosphor oscilloscope.
2. A sensor array.
3. Quick-form cables.
4. Optical fiber links.
5. Ethernet switches.
6. A Laptop computer and acquisition programs.

7.3.1 TDS7014 Digital Phosphor Oscilloscope

TDS7104 oscilloscope [Tek00], see Figure 7.8, is a high performance solution for verification, debug, and characterization of sophisticated electronic designs. The scope features exceptional signal acquisition performance, operational simplicity, and open connectivity to the design environment. Classic analogue-style controls, a large touch-sensitive display, and graphical menus provide intuitive control. Open access to the Windows Operating System (OS) enables unprecedented customisation and extensibility.

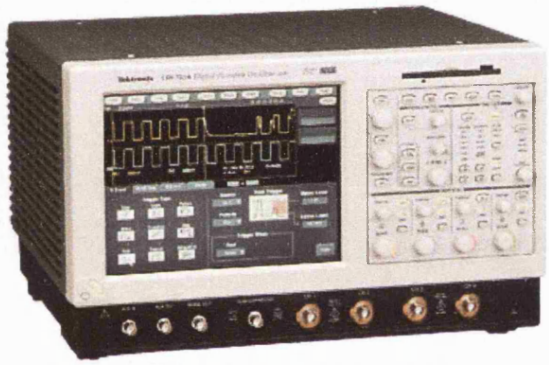

Fig. 7. 8. A TDS7014 digital phosphor oscilloscope.

The key features of the scope are:

- up to 1GHz bandwidth and 10GS/s real time sampling rate on a single input channel and 2.5GS/s on four simultaneous input channels. Features are also available to increase the sampling rate to 25GS/s for repetitive waveforms with advance signal processing techniques consisting of intelligent selection of similar waveforms and taking the average.

- signal record lengths up to 8,000,000 samples or 2,000,000 samples per channel.

- four input channels (each with 8-bit resolution).

- different acquisition modes such as sample, envelope, peak-detect and high-resolution.

- full programmability feature, with an extensive GPIB-command set and a message based interface.

- a variety of trigger modes including edge, logic, pulse and sequence at up to 1GHz bandwidth.

The oscilloscope includes a specially configured version of Windows 98 on which the user-interface application of the scope runs and provides an open desktop for the user to install other compatible applications. The TDS7104 product Software is the oscilloscope application. This software starts automatically when the oscilloscope is powered on, and provides the user interface (UI) and all other oscilloscope control functions. The GPIB programmer's option allows the scope to be controlled remotely.

7.3.2 Sensor Array.

Several array configurations were tested in shapes and with different combinations of sensors. The tested array geometries were square and Y-shaped. Extensive tests were made to decide which type of electromagnetic sensor is the most suitable one for the purpose of source location. Tests were conducted on may different sensors including a 50MHz monopole which was used in previous research to locate arcing fault and switchgear activities in a power system [Bar00]. It has appealing qualities such as good signal gain and suitability for out-door usage. However, the size of the antenna is long and it is designed to work in a

fixed position, rather than having the flexibility of moving it around because of its size.

Other sensor, such as a convenient helical antenna, which can be commonly found on a walkie-talkie set, was tested for suitability as well. Finally, it was resorted to custom designed antennas. They were a small monopole antenna and a "fondue" antenna. The performances and results of different array design are presented in chapter 8.

7.3.3 Quick-form Cables

The choice of cables is very important to minimise the coupling effects and interference via the cables. In the context of source location, such effects will constitute to unequal phase distortions in the waveforms received on different channels. At the same time, a good cable should not cause excessive radiation when channelling a signal to the required destination. It was found by conducting practical experiments that coaxial cables are very susceptible to interference.

A search for the most suitable cable was conducted and "Quickform" produced by Alcatel is deemed the best solution for the purpose. It has performance similar to a semi-rigid cable and forms into the required shape easily when required.

To achieve an accurate time delay measurement, the electrical length of a cable is a very important parameter. A uniform electrical length has to be achieved for all the cables to be used on the four channels. A very accurate way of achieving this is to make use of the HP 8510 network analyser system to make reflection and transmission measurements of the cables in time domain.

The basic ideal consists of sending a wideband pulse into a cable and the open termination of the cable at the other end reflects an inverted pulse back to the analyser. The time domain measurement shows the effect of discontinuity on the cable as a function of time (or length). Relating the measurement with the speed of the electrical pulse at $3\times10^8 m/\text{sec}$ derives the physical length of the cable.

7.3.4 Optical Fibre Links

An optical fibre link was used to connect the oscilloscope to the laptop computer running the instrument control, data logging and data analysis software. This minimized long cable runs carrying digital signals that could potentially be a source of interference to the measurement process.

7.3.5 AT-FS202 Ethernet Switches

The Ethernets switches are employed to switch the copper links, i.e. the RJ45 cables commonly used for Ethernet connections, to optical fibre links. The attractiveness of using the Ethernet is the available transfer rate of up to 100Mb/s. It also builds a platform for the possibility of implementing a remote controlled system via the Internet links.

7.3.6 Laptop Computer and Acquisition Programs

Processing software include MatLab R11 and signal processing toolbox and C complier to develop the instrument interface program via PCMCIA-GPIB. The programs are designed to control a Tektronix oscilloscope (TDS7104) via PCMCIA-GPIB interface.

It begins by configuring the scope remotely via a Laptop interface and sets the scope into the required acquisition mode. When a trigger occurs, 4 channels of waveforms are transferred from the scope to the Laptop in ASCII format. The data will be systematically stored in the hard disk as records and for further signal analysis and determination of the interference location. The whole process takes approximately a minute to complete, including the process time required to compute the time delay estimation, as described in chapter 5, and fixing the position of an interference source.

7.4 References

[Kod96] V. P. Kodali, "Engineering electromagnetic compatibility – Principles, measurements and technologies," *IEEE press*, 1996.

[Tek00] Tektronix, "User Manual for TDS7000 Series Digital Phosphor Oscilloscope," *Tektronix*, 2000.

[Tex82] Texas A & M Research Foundation, "Detection of arcing faults on distribution feeders," *Electric Power Research Institute*, Final Report EL-2757, 1982.

[Tex83] Texas A & M Research Foundation, " Measurement and Characterisation of Substation Electromagnetic Transients," Final Report EL-2982, Research Project 1359-2, *Electric Power Research Institutes*, Mar. 1983.

[Wig91] Wiggins C. M. and Wright S. E., "Switching Transient Fields in Substations," *IEEE Transactions on Power Delivery*, vol. 6, no.2, pp. 591-599, April 1991.

Chapter 8

PRACTICAL TRIALS

Introduction

Details of the trail tests for proto-type impulsive noise locator and the results are presented in this chapter. The test procedures and conditions are described and illustrated with diagrams. Results show that the system is able to locate up to about 30m with an error of about 2m. This is equivalent to a percentage error of about 7% and it is the best result so far known to the author.

8.1 The Impulsive Noise Generator

An impulsive noise generator, supplied by the Radiocommunications Agency (RA), is used to emulate the noise generated by a noisy thermostat of a gas boiler. In the generator itself, it consists of a simplified circuit of the gas boiler system installation including a genuine faulty thermostat. This technique is straightforward and ensures a realistic generation of the impulsive noise source.

The generator is built portable so that it can be easily carried around. The components and circuits are encapsulated in a metal casing with an external antenna attached to the side to assist its RF radiation. It is supplied by a mains cable at 240 volts as in a real gas boiler system. A picture of the generator on a stand is shown in Figure 8.1. The generator takes about 10 minutes to warm up before the faulty thermostat within begins to react and generate intermittent wideband impulses.

Fig. 8. 1. Wideband impulsive noise generator based on a faulty thermostat.

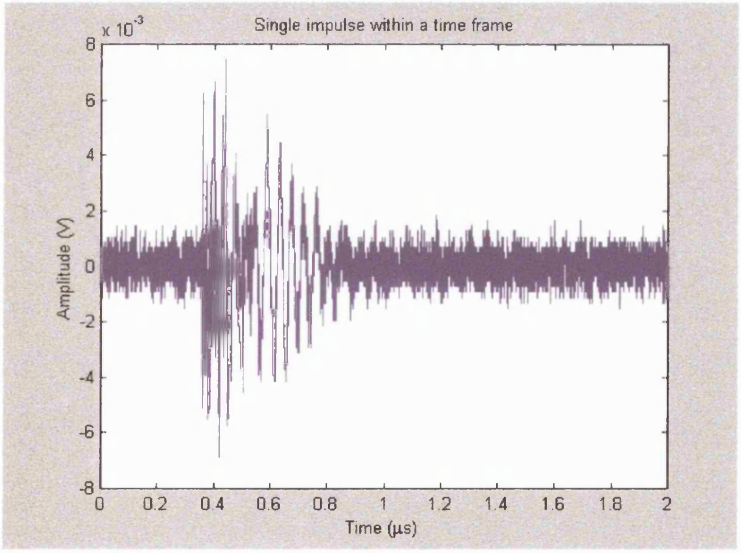

Fig. 8. 2. A waveform of a single impulse within a time frame.

Some example waveforms can be seen in Figure 8.2, 8.3 and 8.4. They have shown good mixtures of single and multiple impulses within a time frame. Other changing characteristics in the waveforms, such as amplitude and pattern, can be observed. This is mainly caused by small physical changes in the contacts of a

faulty thermostat each time it switches mechanically. Such a waveform is non-deterministic in nature and can be difficult to model via computer simulations. It became clear the progress towards locating impulses of this nature could only be made by a combination of practical experimentation and theoretical simulations.

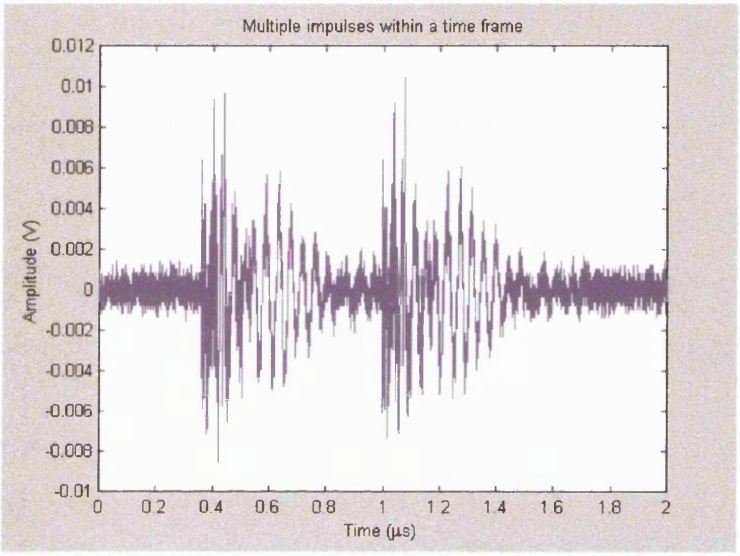

Fig. 8. 3. A waveform of multiple impulses within a time frame.

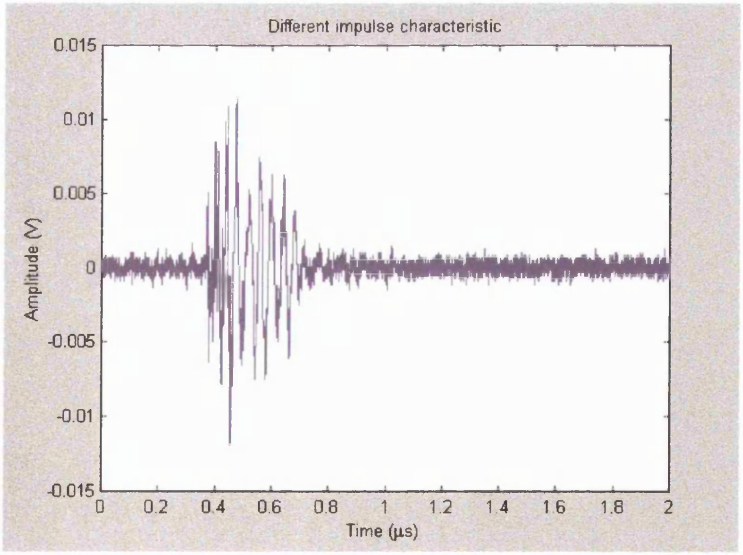

Fig. 8. 4. A different impulse characteristic from the same generator.

The waveforms in Figure 8.2 and 8.4 were captured at 2.5GS/s at 1GHz bandwidth with a Mono-conical antenna. Details of the antenna will be introduced in section 8.3. The spectrum of an impulse can be seen in Figure 8.5. It stretches up to 700MHz and dominates at about 25MHz. A range of resonant frequencies, appear at prominent spikes in the spectrum, can be easily spotted in the figure.

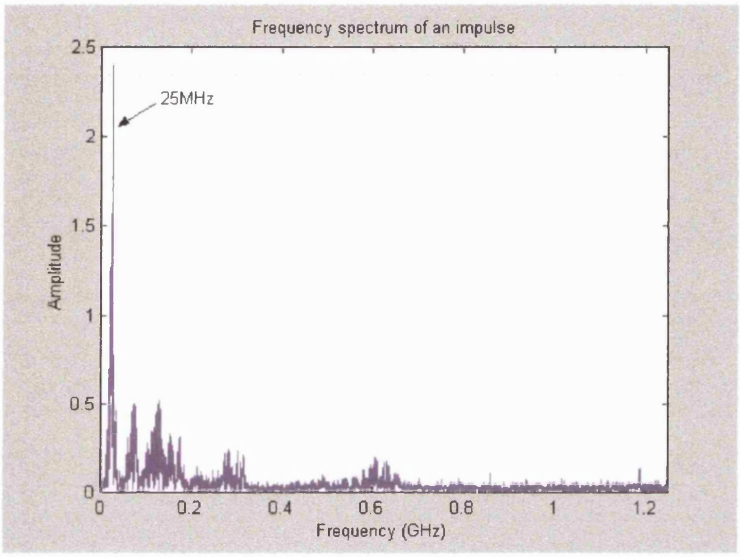

Fig. 8. 5. Frequency spectrum of an impulse.

8.2 Tests in Whyteleaves Laboratory

The first few practical attempts, to test out the proto-type locator system, were carried out in the RA's open air testing (OATS) facility located at Whyteleaves near Croydon. The OATS laboratory is built by fibreglass with minimum radio reflective objects. It is surrounded by clear grass fields stretching up to about 100 metres in radius until the next building or radio reflective object comes into obstruction. The main purpose of this laboratory is usually for EMC testing of high requirements. By using such high specification facilities, the tests were able to focus clearly on the problems of the locator system itself rather than other possible effects. This is to ensure the ease of tracing a problem if any arises.

8.2.1 Test 1 – Two Metres Square Array with Ground Plane

Test 1 uses a two metres square array with ground plane. Joining two pieces of rectangular aluminium sheets together forms it – see Figure 8.6. The antennas are pushed outward to the four corners of the plane, as shown in Figure 8.7. It was thought that, in this way, the maximum antenna spacing could be achieved to provide better location resolution.

Fig. 8. 6. A two metres square array with ground plane.

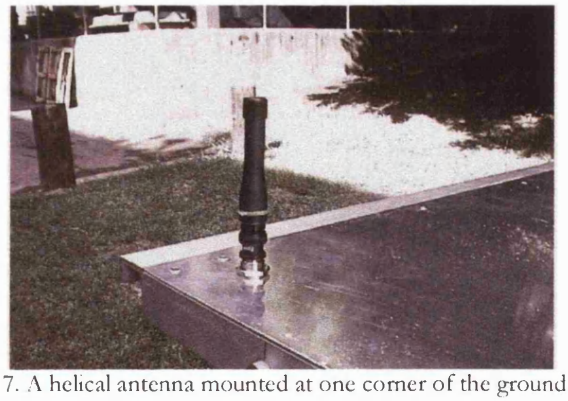

Fig. 8. 7. A helical antenna mounted at one corner of the ground plane.

Experiment findings have shown that if the generator source was within the array, the system was able to locate the source to a good accuracy. However, if the source was about 2 metres away from the array, the system starts to produce large

estimation errors and may sometimes fail to produce a common hyperbolic intersection to give a source location estimate. The unfavourable performance of the locator system has led to some clues about the effects of the ground plane. Placing the antenna close to the edge of the array causes an abrupt termination of the ground plane. However, when the source was placed within the array, this effect was not seen by the waveform propagating outwards from source sitting on the centre of the array and therefore the system was able to locate the source.

8.2.2 Test 2 – Perspex Square Array

An adverse effect may have created by having a ground plane, so a Perspex array of a smaller size of about 0.32m in length and width, to reduce construction effort, was tested in the second trail to understand the difference between having and not having a ground plane.

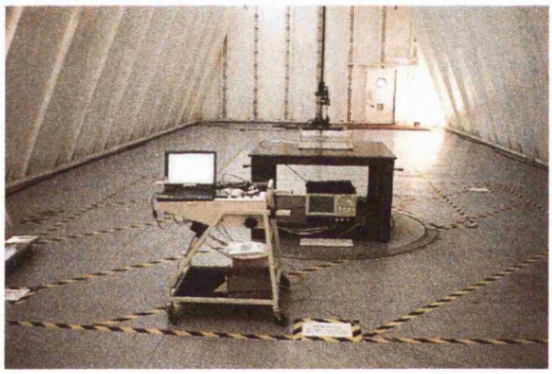

Fig. 8. 8. A Perspex based locator system under test in Whyteleaves laboratory.

The time delay estimates were considerably out from the true value and the closed-loop delay errors were large. The closed-loop delay refers to the discrepancy in the vector sum of the time delay estimates between any three antennas forming closed-loop. In ideal condition, this discrepancy is equals to zero. With a large closed-loop delay, the hyperbolas will not intersect at a

common point to indicate the position of the noise source. However, the general directions of the hyperbolic curves were pointing to the correct direction. The source was located at x=0m, y=10m as shown in the Figure 8.9, and it was an improvement over the previous array in terms of location performance and at the same time having its physical size reduced significantly.

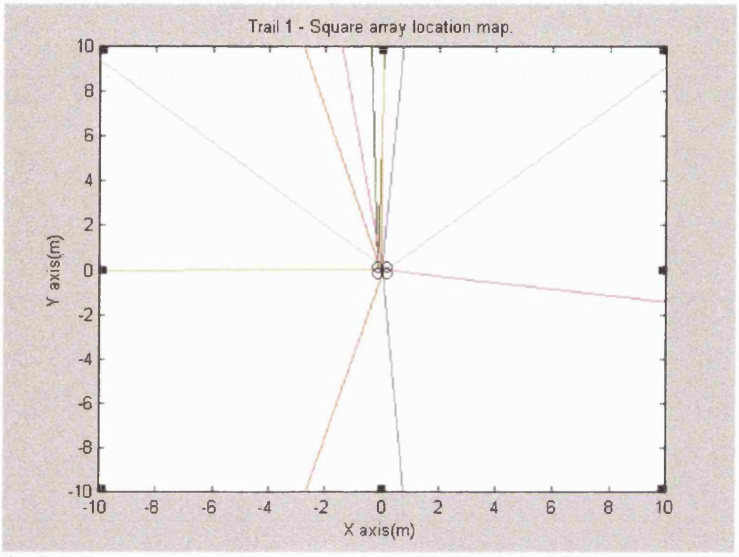

Fig. 8. 9. Square array at antenna spacing of 0.32m and with no ground plane.

In Figure 8.9, each hyperbolic curve produces a line with two ends; one pointing generally towards the true location and the other is a mirror image, along the line of symmetry, pointing to an incorrect direction. The later is an inherent mathematically correct solution. This two-fold ambiguity can be resolved if a common intersection is formed to indicate the source location. This will be clear when better results in the later sections are shown.

8.2.3 Test 3 – Y-Shaped Array with Ground Plane

The system design emphasis has been turned to focus on the ways of producing a better front-end. After much discussion, analysis and computer simulations as

presented in chapter 6, a Y-Shaped array with a ground plane was used in Test 3. At the same time the helical antennas were replaced with monopoles. These monopoles were made from BNC adaptors and copper wires of 4.8cm long. They were equally matched to be as identical as possible. The antennas were moved slowly inwards of the plane until reasonable location estimation results were obtained.

The impulsive noise position locator was set on a rotatable table 10 metres away from the noise generator. At every 10 degrees, 30 sets of records with four channels of signals were taken at 25GS/s. All the records were used without prejudices for the final results presented in section 8.2.4. The array dimension used for the tests is shown in Figure 8.10.

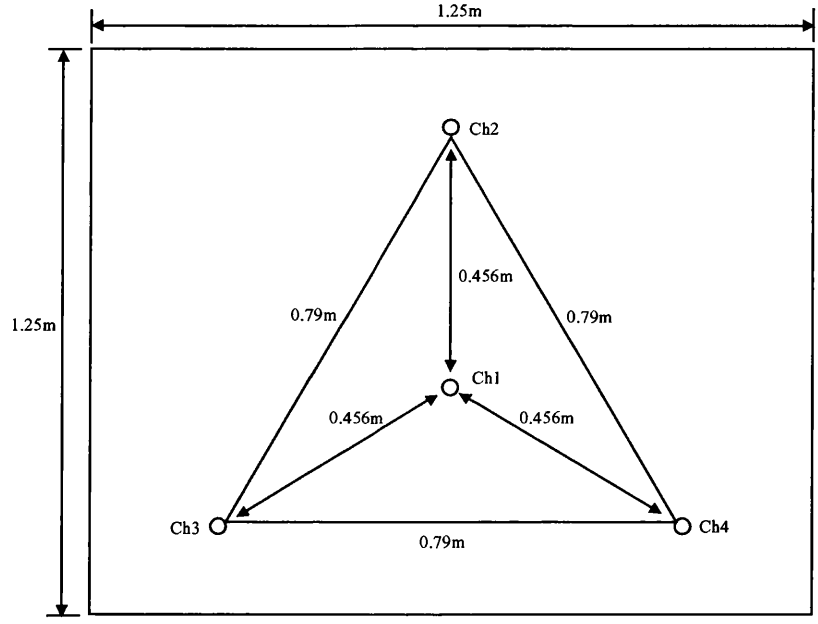

Fig. 8. 10. The dimension of a Y-Shaped array with ground plane.

To achieve a sampling rate of 25GS/s, the digital scope uses advance DSP techniques which discard the non-identical waveforms from the proportionally large group of identical repetitive waveforms and performing averaging on them

to achieve 25GS/s. This was taken as a viable approach after analysing the physical characteristics and spotting some similarities in majority of the impulses generated from the wideband noise generator. Examples of very similar impulses can be seen in Figure 8.2 and 8.3, except that there are two impulses contained in the waveform in Figure 8.3 and only one in 8.2. But, the impulses are very similar in characteristics in general, allowing averaging to be done on them when carefully selected. Figure 8.11 and 8.12 are illustrations of the tests setup.

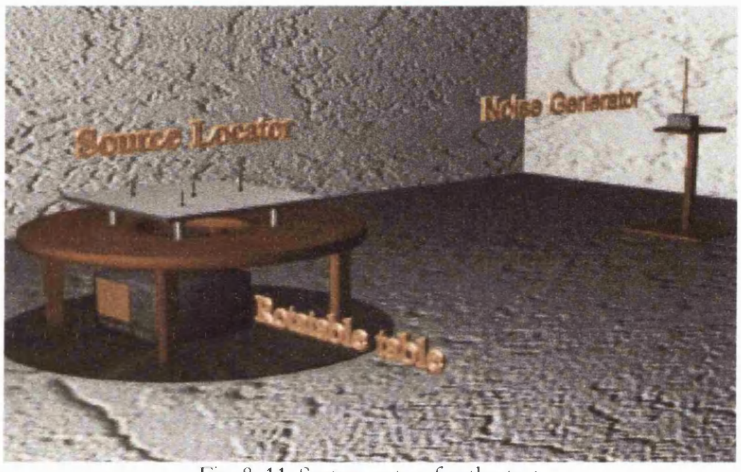

Fig. 8. 11. System setup for the test.

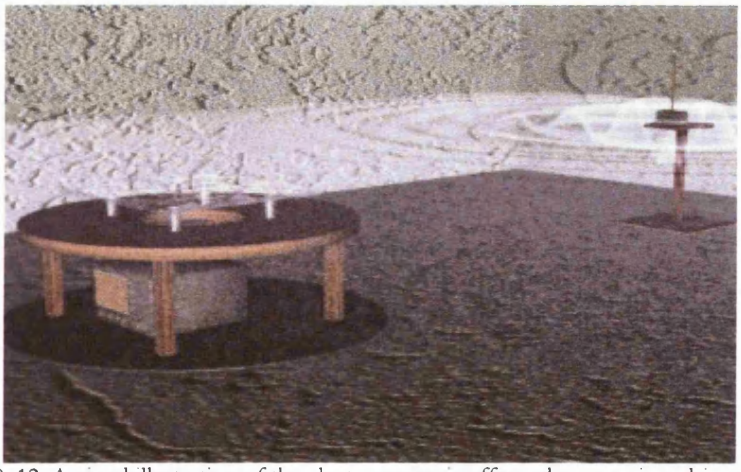

Fig. 8. 12. A visual illustration of the electromagnetic effects due to an impulsive noise.

8.2.4 Results on Y-Shaped Array with Ground Plane

With a newly developed time delay estimation algorithm, DWCC – method 2 in chapter 5, and antenna array design as described in chapter 6, the performance of the impulsive noise position locator has been improved significantly. Figure 8.13 shows an example of a location map with the source located at x=0m, y=10m. It can be observed that a common intersection can be easily determined on the three hyperbolic curves.

Figure 8.14 shows the results for 30 location estimates, each at a step of 10 degrees. It also shows that the noise locator estimate has a position variation of about 2 metres from the true value. However, the directional property of the noise locator is very consistent and accurate to about 1^0. This can be seen from the estimated positions that vary along a straight line along the direction-of-arrival (DOA). Results also show that location estimates at certain angles can be poor.

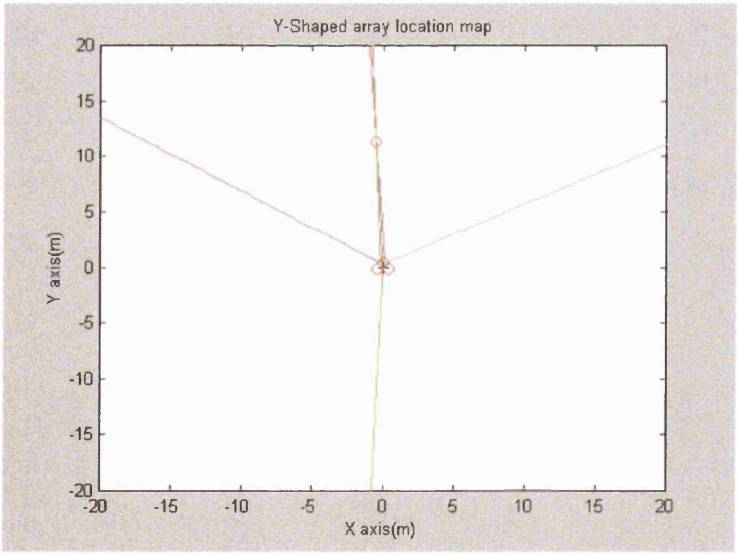

Fig. 8. 13. Improved locator with new processing algorithms and array design.

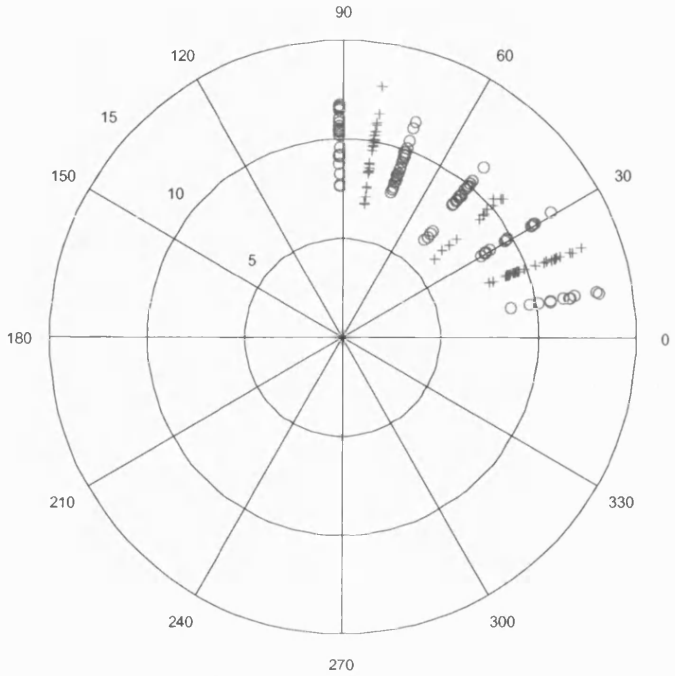

Fig. 8. 14. Results of source location.

At 60 and 0 degrees, the locator was unable to produce any estimate. This is because there will be no clear intersection point when the closed-loop delay is large and the software program is designed to produce no estimate in this condition. To find out the inherent reason behind the problem, a simulation to produce an error map is performed.

It begins by assuming the actual location of the source to be at the array centre. The theoretical or ideal time delays are calculated in reversal to a normal location process. Next, a variance of 0.5 samples is included into the time delays to emulate the effect of the system's estimation error – the variance is found by calculating the experimental time delay variance of the same system with the results presented in chapter 5. Subsequently, a new location is generated by recalculation based on the time delays with system's estimation error taken into

account. This new location is now referred to as the estimated location. Thus, the location error, when the source is at the centre of the array, is equal to:

$$Location \quad error(m) = \left| Estimated \quad location\,(m) - Actual \quad location\,(m) \right| \tag{8. 1}$$

By placing the source location at a different point, the location error at that particular point is calculated by repeating the procedure. When all the points in a defined boundary is calculated, the results are used to construct the error map, indicating the simulated performance evaluation of the locator system for sources at different positions.

Figure 8.15 shows the simulated error map. Notice that the errors are largest at 60^0, 120^0, 0^0, 180^0, 270^0 and -60^0. The simulation result concurs with the practical results explaining the possible sources of errors.

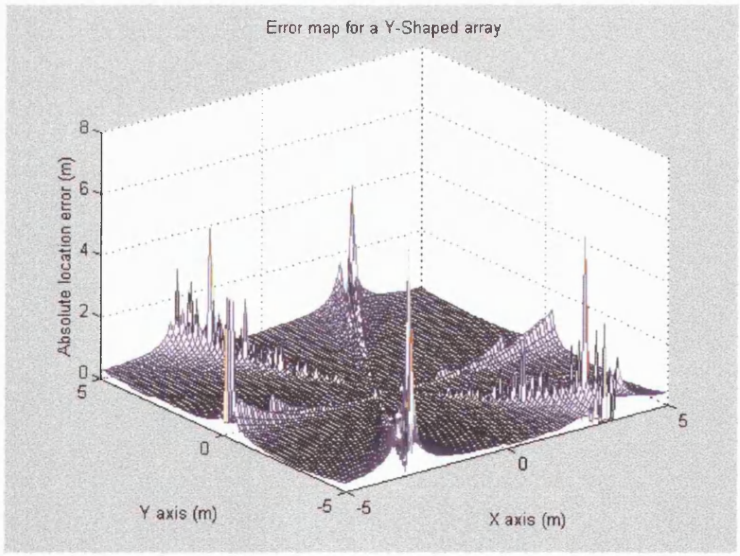

Fig. 8. 15. Error map for a Y-Shaped array due to finite sampling rate.

Figure 8.16 shows a log version of the error map to accentuate the change in the absolute error over space. The Figure shows a very clear dip at the centre of the map. Once again it indicates its estimation of a small location error when a source is bounded within the array. Noise in the signals can cause a change in location resolution over space. This effect can be minimised by using relatively larger antenna spacing or by increasing the sampling frequency of the system, or both. These findings were also indicated in the previous results presented in chapter 6.

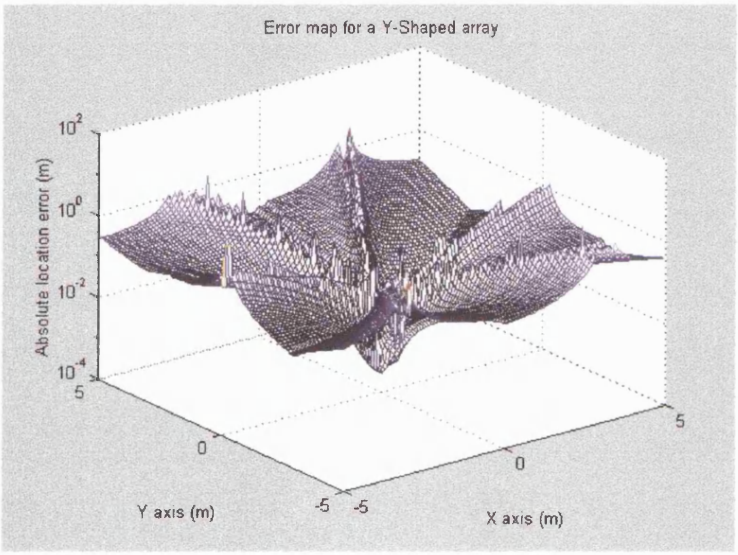

Fig. 8. 16. Log error map for Y-Shaped array due to finite sampling rate.

8.3 Tests in University of Bath Sports Hall

The final aspect of the development lies in the employment of a more advance antenna system. It was speculated that the relatively narrow-band monopoles used in the previous experiments and their antenna gains, which were limited by their small physical size, were inadequate to take the work further.

Another inherent problem of the square ground plane was that at different angle, the plane of each antenna was different. It is possible to introduce a circular

ground plane for each of the antennas so that the planes are as identical as possible to each other at all directions. Antenna experts from the Radiocommunications agency were consulted and assisted in the production of an antenna suitable for the purpose described here.

8.3.1 Employment of Advanced Antenna Design

An antenna to cope with a wider bandwidth specification and improved signal gain was produced by the Radiocommunications Agency. The conical sections of the antennas were machined from solid aluminium billet. The proto-type antenna, made from solid copper, was tested at Whyteleaves laboratory by the Radiocommunications staff. A picture of the antenna, also described as a Mono-conical, is shown in Figure 8.17 below.

Fig. 8. 17. Testing of a proto-type antenna at Whyteleaves laboratory.

Figure 8.18 shows a plot of the SWR over the designed frequency and Figure 8.19 is a Smith chart plot of the antenna's impedance.

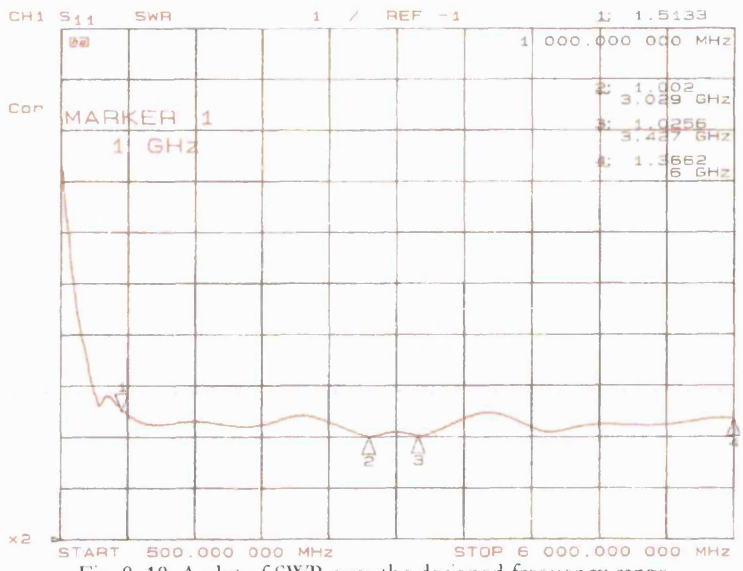

Fig. 8. 18. A plot of SWR over the designed frequency range.

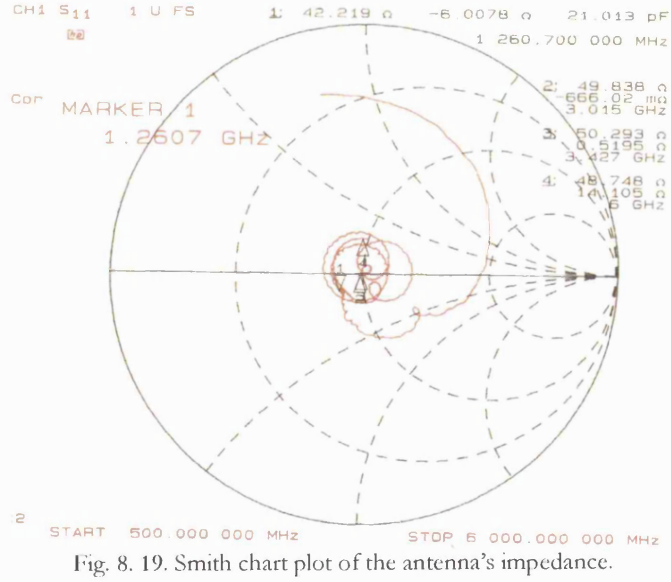

Fig. 8. 19. Smith chart plot of the antenna's impedance.

8.3.2 Tests on Mono-conical Antennas with Individual Ground Plane

The tests were specially designed to investigate the possibility of extending the location range of the system in a non-ideal environment. In section 8.2.3,

averaging techniques were used to increase the sampling rate to 25GS/s. To locate impulsive noises of dynamic and spurious characteristics, averaging may increase the possibility of introducing a greater error into the location estimate.

Furthermore, systems of such high sampling rate will be expensive and not economical to be implemented. By reducing the sampling rate of the system would mean a reduction of production cost and possibly the size requirement of such a system. The sampling rate was tuned down to 2.5GS/s. The antennas were spread out further to improve the location resolution and also to compensate for the reduction in sampling rate. The layout was adjusted close to a perfect Y shape and the measurements between the antennas were taken down for software calibration. Details of the array dimension and can be seen in Figure 8.20.

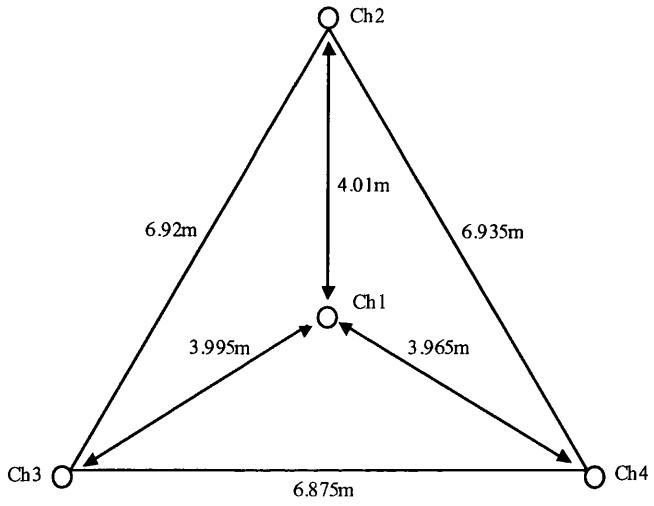

Fig. 8. 20. Antenna array dimension for tests in the University sports hall.

Figure 8.21 shows a picture of the antenna setup in the University's sports hall. Dimensions for the Mono-conical antenna can be found in the last page of the chapter in Figure 8.24.

Fig. 8. 21. Picture of the test layout in the University sports hall.

Five straight records were taken with the source place at 70 degrees and 30 metres away. The records were processed with DWCC – method 1, as presented in chapter 5, for time delay estimates and subsequently used to estimate the location of the source. An example of the location map is shown in Figure 8.22. The results for the location estimation of these five records are tabulated in table 8.1.

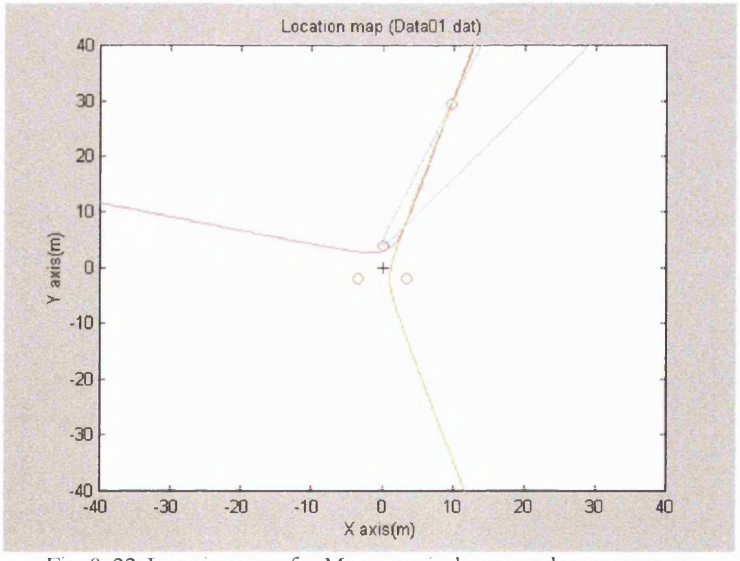

Fig. 8. 22. Location map for Mono-conical antenna locator system.

	DWCC – Method 1 Rectangular window		Location X axis	Location Y axis
Data file	**Start point**	**End point**		
Data01.dat	841	980	9.73082	29.5375
Data02.dat	801	940	10.1604	30.8619
Data03.dat	841	980	9.87238	29.3431
Data04.dat	841	980	10.2556	30.5795
Data05.dat	841	980	10.309	31.1241
Estimated Average			**10.06564**	**30.28922**
Actual Location			**10.2606**	**28.1907**
Absolute Error (m)			**0.195**	**2.0985**

Table 8. 1. Table of results of location estimation for the Mono-conical antenna locator system.

A clearer view of the results can be seen on a polar plot form in Figure 8.23.

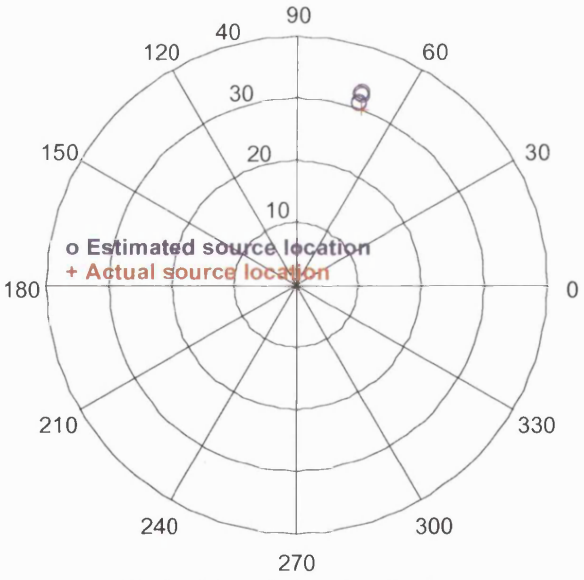

Fig. 8. 23. Results in polar plot form.

The results were able justify the source location capability of the system. The closed-loop delay for the estimation is very consistent – see Figure 8.22. Five location estimations involved fifteen time delay estimations, and they are all consistent even when the records were taken consecutively without any bias. The

system produce errors of X=0.19m and Y=2.09m for a source located at X =10.26m and Y =28.2m. The percentage error, calculated by dividing the location error over the source range, defined in (8.2),

$$\%error = \frac{\sqrt{(x - x_{est})^2 + (y - y_{est})^2}}{\sqrt{x^2 + y^2}} \times 100 \tag{8.2}$$

is ≈ 7%. x and y are the actual distances of the source measured from the centre of the array along the X and Y axis. x_{est} and y_{est} are the estimated results. This is the best result so far known to the author.

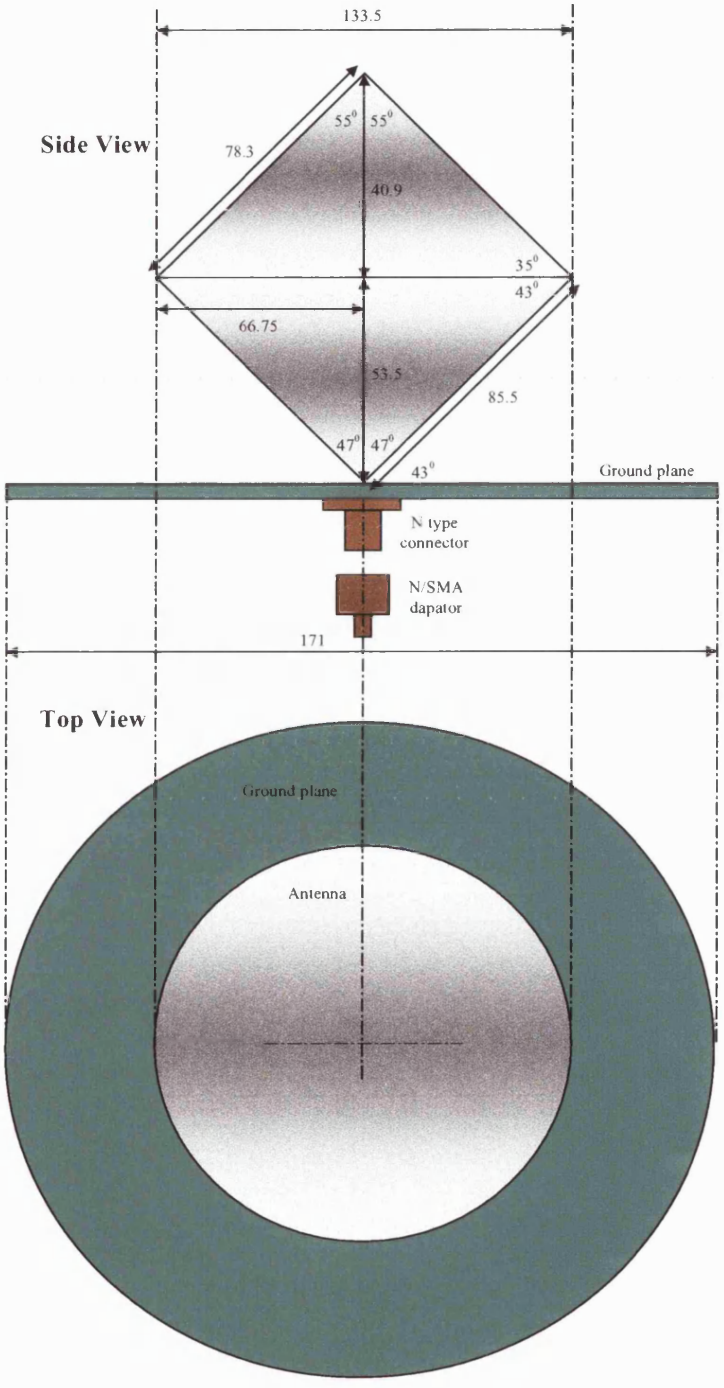

Fig. 8. 24. Dimension of a Mono-conical antenna (not to scale).

Chapter 9

APPLICATION TO SWITCHGEAR CONDITION MONITORING

Introduction

To generalise the application of the locator system, it is applied to a research for condition monitoring of the substation switchgears. The work in this chapter shows a novel technique of establishing an auxiliary measurement to the inter-pole switching time of the circuit breakers in a three-phase system. The technique does not require any contact to the circuit breakers in order to infer the inter-pole switching time measurement as required in the conventional techniques.

9.1 Switchgear Condition Monitoring

High-voltage switchgear plays an important role in transmission and distribution systems. The types commonly used in a substation include air break, air blast, SF_6, vacuum and oil, which are employed in a variety of applications including circuit breakers, isolators, transformer tap changers and earthing switches. The frequency of operation of switchgear varies, with some types operating on a daily basis to provide voltage regulation, whilst other types operate only under rarely encountered short circuit conditions.

The asset life of power-system equipment is long, typically 40-50 years for high voltage equipment and 20-30 years for protection and control equipment [Str88,Har98]. The general state of the circuit beaker's interruption medium, insulation medium and the contacts must be in optimum condition. In general, power systems are exposed to elements such as wind, rain, heat, frost, pollution

etc., and within these influences, many parts of the equipment must operate instantaneously, after long periods of quiescence. Taking these points into consideration, it can be seen to be beneficial that switchgear is frequently examined or monitored.

Switchgear maintenance periods vary with time. Failure rates for switchgears tend to follow what is termed a 'bath-tub curve', that is a high rate following installation (particularly of new designs), a levelling out of failures during the intermediate years of equipment life, and again a high rate towards the end of the operational life.

It may thus be thought that the maintenance periodicity should match this profile. However, a significant number of power system equipment failures arise from design defects and would not necessarily be prevented by maintenance. The types of failures are well categorised and statistically tabulated in the Cigré failure statistics. It shows that 54% of the major failures and 49% of the minor failures are located in the operating and other mechanical parts of a circuit breaker. They are often reflected in some of the pre-failure symptoms such as sluggish or abnormal switching duration.

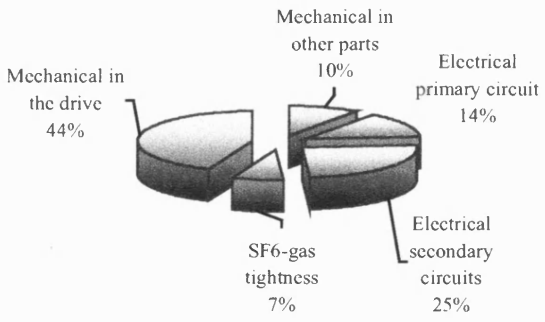

Fig. 9. 1. Origin of the major failures.

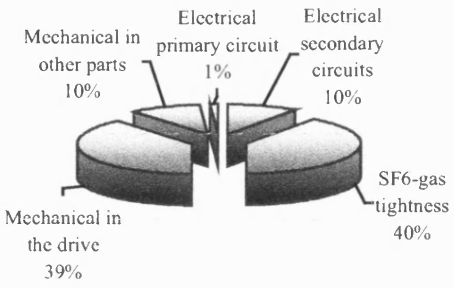

Fig. 9. 2. Origin of the minor failures.

A pre-planned maintenance strategy would not always be feasible in practice, and subject to considerable pressure from uncertain events. Generator circuit breakers, for example, must have their maintenance period aligned to generator outages, and it may be necessary for the distribution circuit breaker controlling circuits without alternative supplies to have longer maintenance periods.

Often, the maintenance activities are expensive and not fully optimised since they are a blind search over the equipments by assuming that they might be unfit for purpose over a fixed period of time. In fact, maintenance should be carried out judging by its needs rather than the time in service.

The improvement of data mining techniques over the years has lead to the development of an optimal maintenance strategy that, by continuous monitoring of equipment parameters, can predict breakdown before critical thresholds are exceeded. This kind of maintenance is commonly known as "Condition Based Maintenance (CBM)".

For efficiency, safety and economical reasons, there is continuing interest in monitoring system health and predicting imminent failures in critical power system components such as circuit breakers and isolators. The ability to identify incipient faults and make accurate predictions well in advance of system failure is the key technical challenge addressed by the research.

9.1.1 Monitoring Strategy

The strategy presented here is in the preliminary stage of relating the inter-pole switching time with the induced RF emissions from the circuit breakers in a three-phase system. This is a very important since a good synchronised timing is required when the breakers are closing or opening to the power lines. Statistics shown earlier have indicated a large proportion of the faults are related to operating and other mechanical parts of the circuit breakers and it is postulated that the inter-pole switching time may also be related to the mechanical health of the circuit breaker.

These are believed to form some of the basic information required for deriving the decisions as to when major overhauls should be performed, when major modifications and upgrading are required, when expensive diagnostic or monitoring techniques should be applied, and when the equipment should be replaced.

Conventionally, tests were done with clamp on devices and may require the disruption of the plant to carry out the work. The new concept in switchgear condition monitoring tries to achieve the same function utilising non-contact electromagnetic sensors. Non-intrusive design of the sensor is desirable so that it can be incorporated into an existing system without the need for special supporting infrastructure and easily removed when necessary. Electromagnetic

sensors can also be extended to detect arcing faults, partial discharges and possibly locating them.

The ability to incorporate changes in mission compliance, operational environment, economic rules, priority assessments, and functional requirements will be drastically increased.

9.2 Switchgear Inter-Pole Switching Time via RF Location

To infer switchgear inter-pole switching time from RF emissions is a new concept that has never been done before. It was inspired by practical waveform observations of the RF emissions induced by a circuit breaker switching. To distinguish the emissions from the three different breakers in a three-phase system, the first step is to locate the RF emissions and that has been achieved with good success.

9.2.1 High-Voltage Switching Induced Electromagnetic Waves

Arcing occurs when a circuit breaker switches. This happens to the three breakers in a three-phase system. A series of impulses is subsequently generated and can be acquired using the system described in chapter 7. An example of a wideband impulse of a 132kV three-phase capacitor bank switching in Melksham (UK) is shown in Figure 9.3. The circuit breakers use SF_6 as the interrupting medium. The hypothesis is that if the first impulse emission from each circuit breaker can be identified by location, they can then used as relative markers to infer an auxiliary measurement of the inter-pole switching time. The spatial differences of the circuit breakers make it possible for the impulses to be located and group according to their breaker. The application of wideband impulsive noise source location, described in the thesis, becomes the obvious solution.

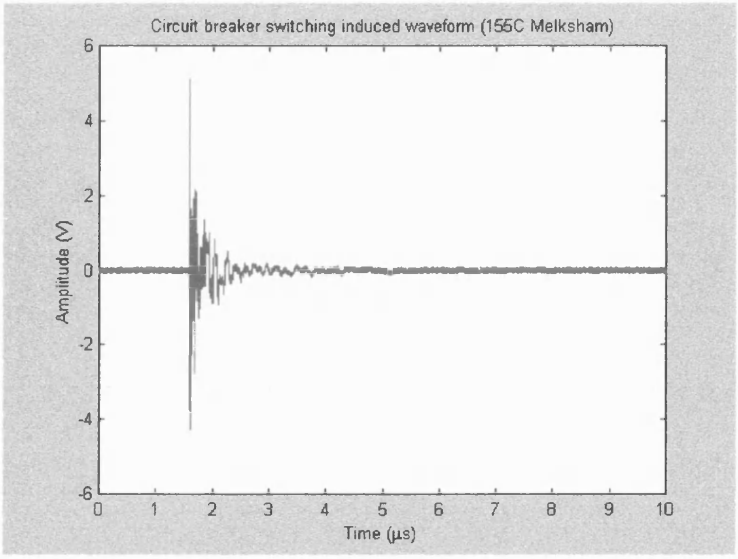

Fig. 9. 3. Circuit breaker switching induced waveform from Melksham substation.

In a closing event, three wideband impulses, similar to the one shown in Figure 9.3 were detected during a trail. There is a possibility that other weaker impulses may have escaped undetected since the scope was set to the least sensitive setting with a high amplitude trigger threshold. The scope triggered only on the three largest impulses from the three circuit breakers, each contributing to an impulse. There is a clear time space between each of the impulses allowing the deduction of what is believed to be a measurement auxiliary to the inter-pole switching time. If the impulses are locatable, the exact switching sequence and the time differences between the switching of each breaker will become apparent. The only way to find out the answer was to set up a practical test in a real substation.

9.2.2 Simplified Location Algorithm

In the switchgear condition monitoring application, the size of the antenna array is a less critical issue and therefore a relatively large array can be used. As investigated in chapter 6, the increase in antenna spacing will improve the

resolution of a locator system. Estimating the time delays required for the location algorithm is therefore simplified, since a larger margin of estimation error is allowed when the antenna spacing is large. Abiding to the principles for estimating a time delay in the DWCC technique, see chapter 5, only the direct-wave component of each of the waveforms is used. Since a larger marginal error is allowed, no further interpolation is required to enhance the location resolution and only one reference point in each of the waveforms is sufficient to determine the time delays. This is unlike the conventional methods that involve application of the cross-correlation.

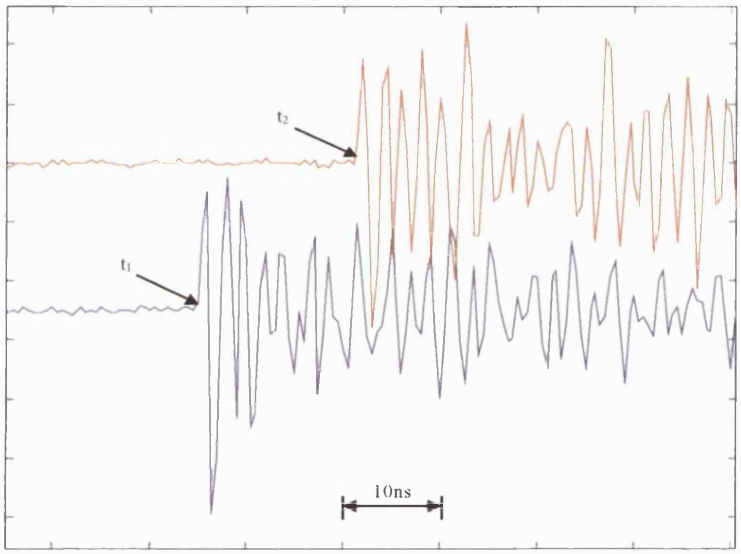

Fig. 9. 4. Estimating large time delay.

Figure 9.4 shows a pair of impulses with a large time delay between them. t_1 and t_2 set the time markers for calculating the time delay between the two signals. The markers can be easily determined by checking through the time series with a set amplitude threshold. The delay estimates are subsequently feed into the location algorithm, see chapter 3, for estimating the impulses locations.

9.3 Practical Test in Melksham Substation (UK)

In an attempt to test out the concept, the source locator system was set up in one of the largest 400 kV grid system substations located at Melksham substation in Wiltshire. The locator system was kept in a van specially designed for substation testing as shown in Figure 9.5. The locator system was set around 155C circuit breakers with all the antennas having direct line-of-sights to the circuit breakers. A drawing of the test layout is shown in Figure 9.6. Using the fast-frame feature of the TDS7104 oscilloscope, the impulses were captured at a very high speed leaving out the quiescent period in between the impulses. Each of these impulses is marked with a time stamp indicating their trigger time.

Fig. 9. 5. Equipment van for substation testing.

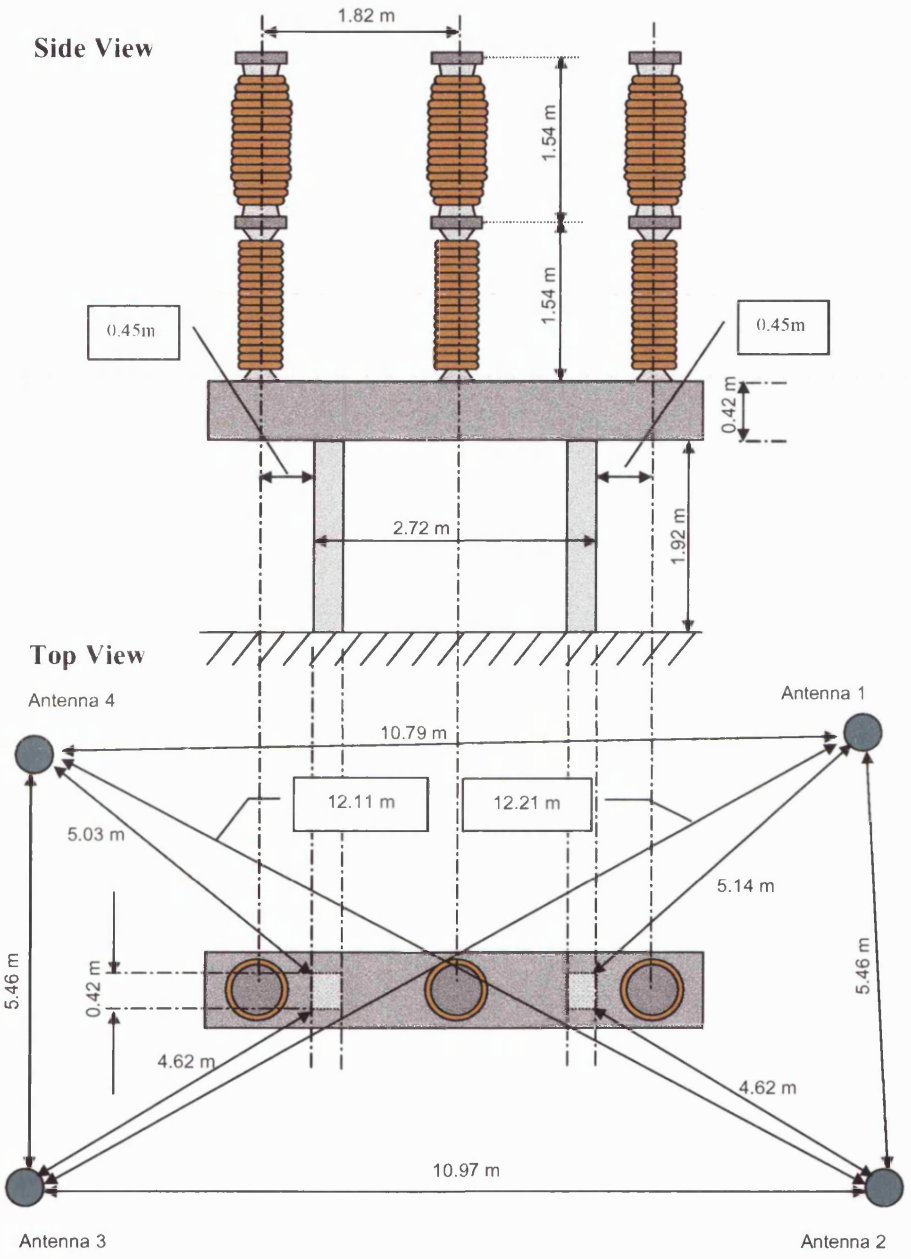

Fig. 9. 6. Dimension of the 155C circuit breaker (not to scale).

9.3.1 Results and Analysis

Figure 9.7, 9.8 and 9.9 are the location maps for the three impulses emitted from three circuit breakers in a closing event. The maps clearly show the system's ability to identify the emitter circuit breaker for each of the impulses. All the six loci are plotted on the right hand size of each figure. They are there to show the consistency of the location algorithm. To fix the location of the impulse only two loci are required and the two with the largest antenna spacing are taken. All the location estimations by the system have an absolute error of less than 0.5 metre. The switching sequence of the three circuit breakers can therefore be deduced with certainty. With this sequence and the time stamp on each of the impulses, the inter-pole switching time is deduced and tabulated in table 9.1.

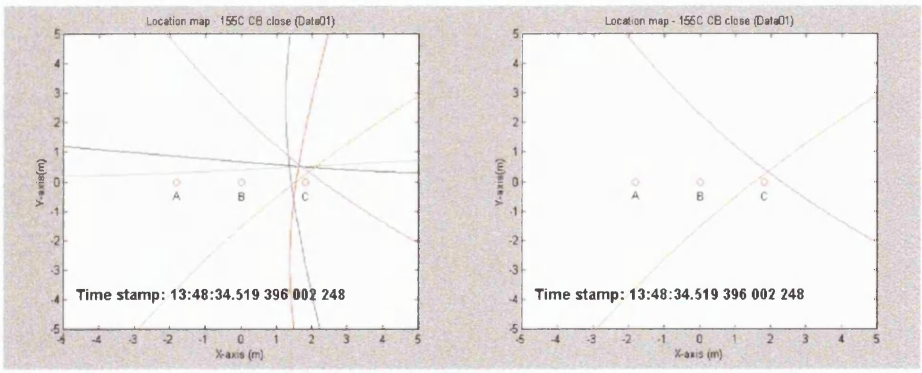

Fig. 9. 7. Location of first impulse at C-phase.

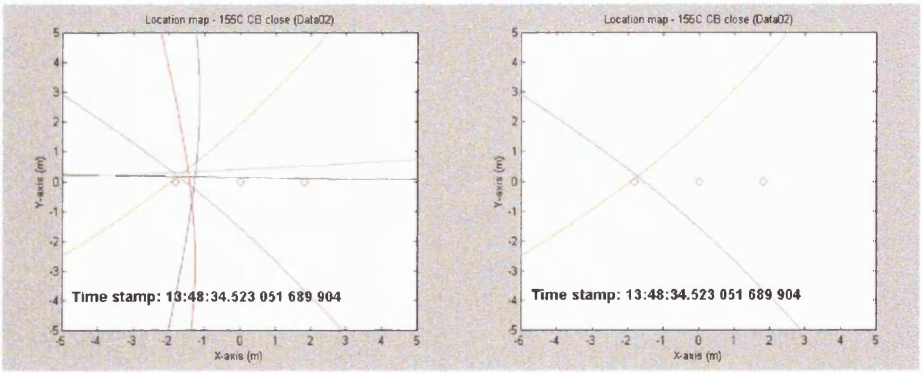

Fig. 9. 8. Location of second impulse at A-phase.

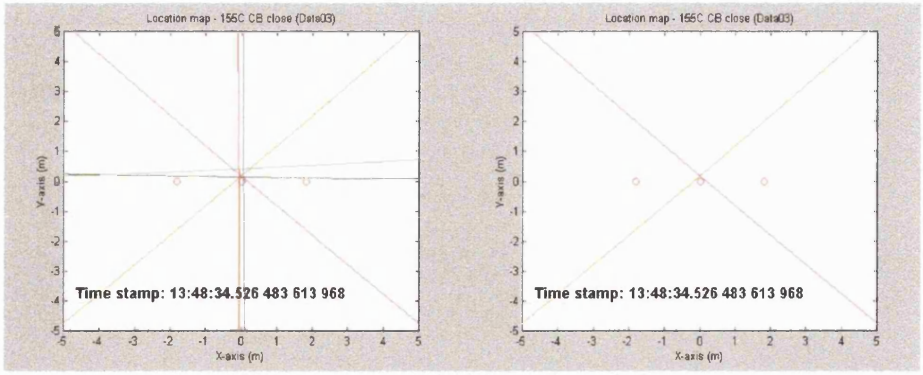

Fig. 9. 9. Location of third impulse at B-phase.

Sequence	Time stamp	Inter-pole switching time
C	Data01: 15 Jan 2002 13:48:34.519 396 002 248	0*ms*
A	Data02: 15 Jan 2002 13:48:34.523 051 689 904	3.66*ms*
B	Data03: 15 Jan 2002 13:48:34.526 483 613 968	7.09*ms*

Table 9. 1. Time stamps and inter-pole switching time.

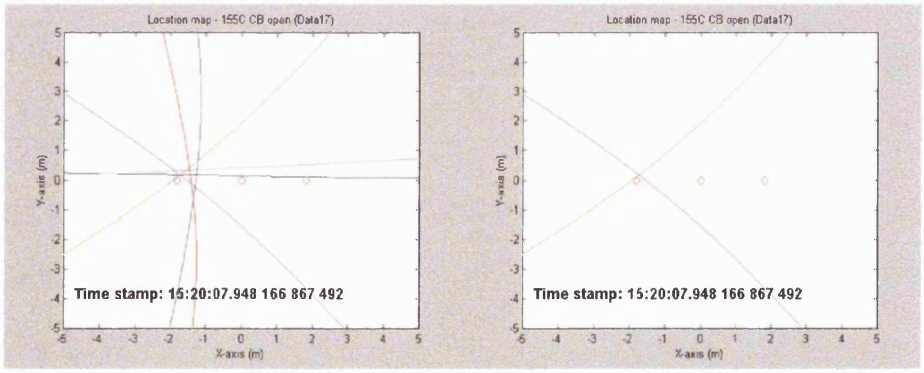

Fig. 9. 10. Location of impulse at A-phase for opening event.

When closing the three-phase lines onto the capacitor bank via the circuit breakers, the control mechanism tries to synchronise the contact timings with the current zeros of the power lines. In this way, the potential across the contacts, with uncharged capacitors trying to draw current at one side, will be minimised

and the arcing across the circuit breakers' contacts will be reduced. This condition is less severe in an opening event. In the case of an inductive load, the effect is the opposite way round.

All these information are deemed useful in the development of a switchgear monitoring system. Development of a proper monitoring system, however, requires more work to be done. Nevertheless, this can be considered as good research advancement from the perspective of a monitoring system utilising only non-contact electromagnetic sensors.

9.4 References

[Str88] Strokes A. D., Timbs L., "Circuit breaker Diagnostics," in proceedings of the 1988 CIGRE meeting in Paris.

[Har98] Harker K., "Power system commissioning and maintenance practice," *IEE power series*, vol. 24, 1998.

[Wig91] Wiggins C. M., Wright S. E., "Switching Transient Fields in Substations," *IEEE Trans. on Power Delivery*, vol. 6, no. 2, April 1991.

[Tex82] Texas A & M Research Foundation, "Detection of arcing faults on distribution feeders," Electric Power Research Institute, Final Report EL-2757, 1982.

[Gli98] Glinkowski M. T., Schmidt L., Ververka E. F., "Bibliography of switchgear literature IEEE committee report," *IEEE Trans. on Power Delivery*, vol. 13, no. 1, Jan. 1998.

[McD88] McDougall T., "132kV SF_6 switchgear – an inside story," *Power engineering journal*, Jan. 1988.

Conclusions

Currently, experts in the field of noise location are using a hand held radio set and years of experience to hunt down the interference sources and their locations. The ability to translate the knowledge and interpretation of the experts into logical processes, for machine handling, is very valuable but difficult to achieve. The project has solved the problem by completing a fully functional proto-type system designed to locate wideband impulsive noise source.

Both theoretical research and practical experiments were vital in making the right decisions in the development stage. Feasibility studies of building an impulsive noise locator system were conducted by substitution with a direction finding system and estimating the Direction-Of-Arrival (DOA) of impulsive noise emulated by a handheld spark generator. An accuracy of 20 degrees was attained in the bearing estimation by incorporating advance Digital Signal Processing (DSP) techniques and hardware. This achievement was very encouraging and the key factors were found in the Hannon and Thomson (HT) processor in the DSP, and most importantly the use of high sampling rate of 1GS/s for data acquisition. Although the attained accuracy was inadequate for any location purpose, it became an important cornerstone to the work and instilled confidence to carry the work further.

Reviewing the different types of location techniques has drawn to the conclusion of using Hyperbolic Position Location (PL) technique to fix the position of an impulsive noise. Solving simultaneous hyperbolic equations is never a straightforward problem. The conventional approaches for fixing the position of two or more hyperbolic intersection are indirectly achieved by iterative techniques

such as Newton Raphson's. Such an approach is only an approximation and can be computationally intensive. An initial condition will typically be required at the beginning of the iterative process, and if it is too far off from the actual answer, the process can become slow and the estimate can be ambiguous. The problem has been alleviated by cross-disciplinary research and the application of advance mathematical algorithm adopted from navigation science. These algorithms are able to give an exact solution and process more efficiently.

Further proves and validations were done by simulations to establish the locator's methodology. In the process, better understanding in the difficulties of position location, rather than just estimating the general Direction-Of-Arrival (DOA) of an impulsive noise source, was gained. Other problems such as inherent mathematically ambiguous solutions that contradict with the only practical solution were carefully considered.

To achieve an accurate position location of a noise source, one of the most critical processes was found in the estimation of the Time-Difference-Of-Arrival (TDOA) required in the hyperbolic equations. This can be achieved through the use of correlation techniques in which the received waveform at one sensor is correlated with the received waveform at another sensor. Four existing time delay estimation algorithms, well known in the realm of sonar research, were implemented and investigated, namely the Cross-Correlation (CC), Smoothed Coherence Transform (SCOT), Hannan and Thomson (HT) processor and Adaptive Time Delay estimation based on Cumulants (ATDC). The cumulants based approach, ATDC, has the ability to suppress correlative noise peak, which may obscure the true peak indicating the required time delay. The four techniques were applied to synthesized signals and signals recorded from practical experiment. Results on the synthesized signals showed that the ATDC is the most superior in suppressing correlative noise peak.

Unfortunately, they were all unsuitable in the impulsive noise location application. The estimation errors were too large to make any sensible location estimate. As a result, it was resorted to the development of a new time delay estimation algorithm to take the problem further.

Through visual analysis of practical signal trends and collective experience from conducting experiments, a new time delay estimation technique called the Direct-Wave Cross-Correlation (DWCC) has been developed to overcome the accuracy problem for physically small arrays. Step-by-step mathematical proves were also established. In principle, the algorithm selects the direct-wave segments of the signals for processing and thus the effects of mulitpath are minimised. This would not have been achieved without a very high sampling rate.

The performance of the DWCC was compared with some of the well-known techniques and was found to be the most superior for this particular application. When applied to estimating impulsive noise time delay between spatially separated antennas at a spacing of 0.79m, it performed with an accuracy of 40×10^{-12} *s*. This is equivalent to a bearing accuracy of 0.9 degree.

Apart from just suitable digital signal processing techniques in the system development, a proper receiving array is also vital towards the contribution in the overall performance of the noise locator system. Simulations on the locator's performance on different array geometries were carried out, under the aspect of finite sampling rate imposed by the digital acquisition system, using a newly developed technique called the Resolution Map (RM) assessment. It has been concluded that, for a given baseline, a Y-Shaped array provides the best location resolution compared to a uniformly spaced linear array and a square array. Relationship between the antenna array baseline and location resolution were also established.

A prototype system was built after much consideration such as practicality, choice of hardware and the constraints of the available project fund. The system uses components with good screening from electromagnetic interference. It uses optical fibre links for data transmission between the remote controller, which is a laptop, and the digital oscilloscope. Employing the most recent digital oscilloscope made by Tektronix, with advance digital signal processing techniques, allows waveforms to be digitised accurately at 25GS/s with 1GHz bandwidth on four simultaneous channels. This was achieved by applying a feature offered by the scope, allowing repetitive waveforms to be averaged to improve the sampling resolution.

Practical trials were conducted using an impulsive noise generator source and open air testing (OATS) facility provided by the Radiocommunications Agency. The locator system was tested with location accuracy of about 2m and directional accuracy of about 1 degree for a source, which was placed about 10m away.

Further developments were instigated by using a more advanced antenna system. This time the sampling rate was decreased to 2.5GS/s real time sampling on four simultaneous channels. This alleviated the reliance on repetitive nature of the signal, so that only one impulse acquisition is required to locate the source. Tests in non-ideal condition, in the University's Sports Hall, were able to attain an accuracy of about 2m for a source place 30m away.

Generalisation of the impulsive noise locator system has been proven by the locating impulses generated from circuit breakers in a three-phase system. It is used to infer an auxiliary measurement to the inter-pole switching time in a novel switchgear condition monitoring concept utilising only non-contact electromagnetic sensors. The preliminary studies of the application were achieved

with good success, showing the ability to locate the impulses within 0.5 metre from the breakers.

These conclude the potential of building a more accurate and generalised impulsive noise locator, which will extend to a further distance with further research and development. The work has shown an enormous inherent potential in itself as well as in other applications that are waiting to be discovered. Emphasis of future works should now be on the bases of developing the four fundamental aspects of the system. In order of priority, the four aspects are: 1. antenna and array design. 2. digital signal processing algorithm. 3. graphical user interface. 4. data logging and statistics.

Summary of Research Contributions

A concise summary of novel research contributions, presented in the thesis, are listed as follows:

- Established the possibility of locating the source of an impulsive noise.

- Developed a new *ad-hoc* Time Delay Estimation technique called the Direct-Wave Cross-Correlation (DWCC), which excels over other existing algorithms when estimating the time delay of wideband impulsive noise source.

- Developed a new assessment technique, called the Resolution Map, for configuring the optimal array geometry for the locator system under the aspect of finite sampling rate.

- Realised a new working proto-type system, software and hardware, for locating wideband impulsive noise source and established its performance and limitations.

- Realised an antenna design suitable for impulsive noise location systems. (Sean and Bob of the Radiocommunications Agency contributed the main efforts in designing and constructing the antennas).

- Generalized the locator system to locate other sources of impulsive noise.

- Application of the locator system to infer an auxiliary measurement to inter-pole switching time of the circuit breakers in a three-phase system; a novel application to the condition monitoring of substation switching equipment using non-contact electromagnetic sensors.

Future Work

Application to Switchgear Condition Monitoring

A basis is formed in the possibility of using non-contact electromagnetic sensors for switchgear condition monitoring. Results have shown the potential of inferring an auxiliary measurement from the radiated RF of a circuit breaker. However, there are many more aspects to be covered before commissioning a working proto-type system. The possible future works are list as follows:

- Inferring the magnitude of the arcing current, in a circuit breaker, via the analysis of the radiated RF. It is possible to obtain more understand by using a clamp-on current transformer, at the low-voltage side of the circuit breaker, for comparison at the investigation stage.

- Deducing the arcing duration via the radiated RF. In the tests presented in chapter 9, only one impulse was detected from each of the three circuit breakers in the three-phase system when the scope was set to the least sensitive setting during the acquisition to prevent the waveforms from clipping. It is possible to capture a complete set of impulses by increase the dynamic input range of the front-end with an input scalar of logarithmic nature. In this way, the impulses of relatively smaller amplitude will not be missed out and thus a more accurate arcing duration may be deduced.

- Establishing a remote control system via the use of Internet. Internet has become a very common aspect in many people's life due to the advantages it offers and the infrastructure supporting it. Establishing an Internet link

allows the flexibility of having an off-site operator and thus a possible reduction in the operating cost.

- Increasing the user friendliness of the system. This aspect would need large amount of programming effort to construct a Graphical User Interface (GUI) to control and use the system all by the click of mouse on the virtual buttons on the computer screen.

Application to Partial Discharge (PD) Detection and Location

Partial discharge (PD) measuring techniques has been used to detect defects in insulation materials of HV equipment in a power system. Existing international standards require PD measurements on all types of power cables. The discharges emit electromagnetic waves, which may interfere with communication systems. The broadband nature of the emission can be easily received by a television set and visualize as "snow flakes" on the screen and at the same time producing sharp cracking noise. Similarly, the interference can be easily picked up by a radio set.

Due to various different types of cable constructions, insulating materials, insulation wall thickness, background noise levels, etc., it is difficult to identified a PD source through analysis of signal trends received through a conventional PD detector. If PD levels exceed acceptable standards, it is necessary to employ modern, advance techniques to accurately locate the position of the partial discharge so that remedies can be carried out.

Partial Discharge Detection

In order for system to detect and locate PD, it must be designed to handle the different bandwidth requirements of the electromagnetic waves induced by a PD. This requires a good front-end reception by employing broadband PD sensors. Similarly, real time digitisation system with fast sampling rate and broadband width will be prerequisites for capturing such waveforms.

Roaming System to Track Location of PD

The physical characteristics of the electromagnetic emission generated by PD can be categorised as wideband impulsive interference. Thus, the principle position location and signal processing techniques, described in the thesis about locating wideband impulsive noise source, may be employed to determine the position of the PD.

The location range of the proposed system in the thesis is fairly short – tested to about 30m. However, its directional accuracy is good and consistent. The coverage of the system may be increased indirectly by mounting the antenna array on a mobile vehicle so that the array position can be shifted to different positions. With the aid of a Global-Positioning-System (GPS), which tells the grid of the array positions, the interference source may be estimated by seeking the bearing intersections at different array positions. This requires specialised software for detecting, acquiring and computing the position estimation of the interference source and maybe used as bases for the future work.

A DIRECTION FINDING TECHNIQUE FOR WIDEBAND IMPULSIVE NOISE SOURCE

C. H. Peck and P. J. Moore, *Senior Member, IEEE.*

Abstract--A direction finding technique for wideband impulsive electromagnetic interference is presented. An experimental investigation was performed using a spark generator as the impulsive noise source. The signals were captured using a 2 antenna array directly sampled at 1 GS/s. A digital signal processing based correlation technique allowed assessment of the time delay between the antennas. Results in a non-ideal radio propagation environment show the bearing can be estimated to an accuracy of 20°.

Index Terms-- Direction finding (DF), Impulsive noise, Electromagnetic Interference (EMI), Time delay estimation.

I. INTRODUCTION

Impulsive, manmade noise is responsible for wideband disturbances to communications systems and is the subject of considerable research [e.g. 1,2]. Due to the increasing utilisation of the broadcast radio spectrum, caused in part by the growth of mobile communications and wideband digital services, the EMC requirements for impulsive noise sources must be continually reviewed. An allied aspect to this process is the requirement to be able to *locate* impulsive noise sources in order that remedial action may be taken. Interested parties to the location of impulsive noise sources include managers of radio spectra, electricity supply operators and EMC specialists. The objective of this work was to evaluate, through realistic experimental investigation, a direction finding technique to aid the location of an impulsive noise source.

Impulsive noise is caused mainly by electrical discharges which may be either complete or partial in nature. Common sources of impulsive disturbances include electrical switchgear of all voltage levels, from 765 kV circuit breakers to domestic thermostats; power system fault arcs, caused predominantly by atmospheric disturbances to overhead lines; corona discharges on high voltage plant; discharge tubes, particularly fluorescent lighting; and automotive vehicle ignition systems.

Direction finding (DF) of the impulsive sources relies upon the estimation of time delay of signals received from two spatially separated antennas. The bearing of the source can then be calculated from the time delay and the antenna positions. DF is fundamental to locating impulsive noise sources, since time delay estimates from multiple antenna pairs can be processed to reveal the impulsive origin. Recent work describing the location of partial discharges from defective insulation [3] utilised a 4 antenna array and conventional delay estimation calculations. The delay estimation error reported is almost an order of magnitude greater than results described here - an improvement made possible by more efficient signal processing techniques.

The finite time duration of impulsive transients and the wideband nature of their frequency components make them difficult to DF, if not expensive for such a system to be realized. Electromagnetic transients generated by high voltage switching is about 20μs [4] and spark discharge can be as short as 1μs – refer to figure 4. Generally a high sampling rate and multiple observations are required to achieve a statistically significant estimation of the pulse characteristics.

II. DIRECTION FINDING ALGORITHMS

Radio frequency direction finding (DF) is very well established in many areas including mobile communication [5,6] and sonar and radar systems [7-10]. DF signal processing utilises the records of multiple sensors to locate one or more sources of coherent energy. It is usually assumed that the signal wave-front is plain and emitted from a point source. The major difficulty in DF of signals generated by impulse transients is the prior knowledge of the source to be located in a known frequency band. Impulse transients are wideband and, due to their electrical discharge origins, often occur non-deterministically. In addition, the characteristics of the impulse transients vary more with the electrical source circuit and local conditions of the discharge, rather than the nature of the discharge itself. For these reasons, DF of impulsive noise can be problematic, with unknown variation from one situation to another, and little literature is available in this area.

To DF the source of impulsive noise, a non-intrusive interference location technique based on electromagnetic wave propagation is robust and attractive if only its accuracy is within a reasonable tolerance. The accuracy of such technique is therefore directly proportional to the variance of the DF technique and the projection method employed. A simple triangulation or a more complicated

C. H. Peck and P. J. Moore are currently with the Power and Energy Systems Group (PESG) – Department of Electronics and Electrical Engineering of the University of Bath, BA2 7AY, UK.

parabolic projection may be used to locate the source depending on the shape of the wave-front.

The next few sections will explain the DF algorithms for non-coherent electromagnetic transients generated by spark discharge.

III. Direction Finding of Impulsive Noise

A. Signal Model

Direction finding relies upon reception of a target signal, $s(t)$, at two spatially separated receivers. If the source of the target signal is nearer to one receiver than the other, then a time delay, D, between the reception of $s(t)$ at the two receivers will be apparent. The time delay, being a function of receiver separation and the velocity of propagation of $s(t)$, can be used to calculate the bearing of target source from the receivers. In this context the target is the radiated component of an impulsive noise source that is received by two antennas, as shown in figure 1. Assuming that the antennas are not responsive to static fields, all antenna signals may be considered to be zero mean.

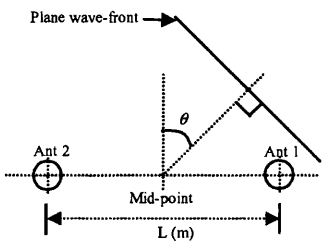

Fig. 1. Determine bearing from time-delay.

The bearing θ of the noise source from the antenna baseline can be calculated from an estimation of D by:

$$\theta = \sin^{-1}\left(\frac{D}{D_{\max}}\right), \quad D_{\max} = \frac{L}{c} \tag{1}$$

where D_{max} is the maximum possible time delay between the two antennas spatially separated by L meters and c is the speed of light assumed to be constant at $3\text{x}10^8$ m/s. The antenna signals, $x_1(t)$ and $x_2(t)$ can be modeled as:

$$x_1(t) = s(t) + n_1(t) \tag{2}$$

$$x_2(t) = \alpha s(t+D) + n_2(t) \tag{3}$$

where α is an amplitude factor, and $n_1(t)$ and $n_2(t)$ are wide sense stationary, Gaussian and mutually uncorrelated noise components. The target impulsive noise signal, $s(t)$, is also uncorrelated with $n_1(t)$ and $n_2(t)$ and, being of finite duration, may be treated deterministically. This signal model pair is commonly used in the field of time-delay estimation, especially in sonar and radar detection [9,11]. This representation assumes no prior knowledge of the signal's characteristics and is thus suited for this application.

B. Direct Cross-Correlation (DCC)

Estimation of D is conventionally achieved using the cross-correlation function. This is a measure of the similarity of two functions x_i and x_j, as one is displaced through time τ relative to the other, and is expressed as:

$$C_{x_i x_j}(\tau) = E\left[x_i(t)x_j(t+\tau)\right] \text{ i = 1,2 \& j = 1,2} \tag{4}$$

The frequency spectrums of the signal and noise components are therefore,

$$X(f) = \mathsf{F}\ \{x_i(t)\} \tag{5}$$

$$S(f) = \mathsf{F}\ \{s(t)\} \tag{6}$$

$$N(f) = \mathsf{F}\ \{n_i(t)\} \tag{7}$$

Section D describes how consistent frequency domain estimates of stationary signals can be obtained.

The power spectral density can be expressed as:

$$P_{x_i x_j}(f) = \mathsf{F}\ \{C_{x_i x_j}(\tau)\} \tag{8}$$

which, according to the Wiener-Khinchine theorem, is also equivalent to:

$$P_{x_i x_j}(f) = X_i(f)X_j^*(f) \tag{9}$$

Making substitutions from equations (2) to (7) into (9):

$$P_{x_1 x_2}(f) = [S(f) + N_1(f)][\alpha S(f)e^{-j\omega D} + N_2(f)]^* \tag{10}$$

Assuming that the signal and noise are not correlated the cross-spectral density works out to be:

$$P_{x_1 x_2}(f) = \alpha P_{ss}(f)e^{-j\omega D} + P_{n_1 n_2}(f) \tag{11}$$

Since $n_1(t)$ and $n_2(t)$ are zero mean, Gaussian and spatially uncorrelated, $P_{n_1 n_2}(f)$ is negligible. Equation (11) is reduced to:

$$P_{x_1 x_2}(f) = \alpha P_{ss}(f)e^{-j\omega D} \tag{12}$$

which can be expressed in time domain as:

$$C_{x_1 x_2}(\tau) = \alpha C_{ss}(\tau) * \delta(\tau - D) \tag{13}$$

* *denotes convolution*

Equation (13) shows that the correlation peak of $C_{ss}(\tau)$ is displaced through the required time delay of D seconds

which may be readily estimated. Given the foregoing assumptions, $C_{ss}(\tau)$ is effectively the autocorrelation of the target signal $s(t)$. Note that $C_{x1x2}(\tau)$ can be estimated from a finite number of observations of the antenna signals $x_1(t)$ and $x_2(t)$.

C. Hannan and Thomson (HT) processor

In practice, the non-ideal signal propagation environment can make estimation of D problematic.

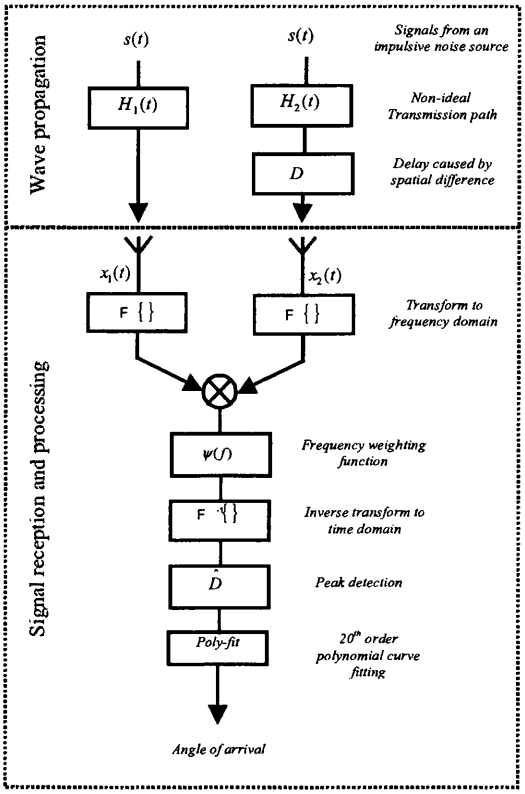

Fig. 2. Model of impulsive noise propagation and bearing calculation signal processing.

This can be modelled by modification of equation 13 in the frequency domain:

$$C_{x_1x_2}(\tau) = \int \psi(f) P_{x_1x_2}(f) \exp(j2\pi f\tau) df \qquad (14)$$

where $\psi(f)$ is frequency weighting function given by $H_1(f)H^*_2(f)$. $H_1(f)$ and $H_2(f)$ are the frequency responses of the transmission paths between the impulsive noise source and the receiving antennas as shown in figure 2. Note that in the direct cross correlation calculation there is no weighting function introduced to compensate for the effects of $H_1(f)$ and $H_2(f)$ i.e. $\psi(f) = 1$. Consequently, the correlation will be poor when the Signal-to-Noise Ratio (SNR) is low.

To improve the situation, the weighting function can be estimated and many approaches have been developed including the Roth processor [12]. Detailed assessment of the major techniques available [13] has concluded that the Hannan and Thomson (HT) processor [14] provides the optimum likelihood weighting function, defined as:

$$\psi_{HT} = \frac{1}{\left|P_{x_1x_2}(f)\right|} \cdot \frac{\left|\gamma_{x_1x_2}(f)\right|^2}{\left[1-\left|\gamma_{x_1x_2}(f)\right|^2\right]} \qquad (15)$$

The first right hand term is used to achieve good resolution and the second term adjusts itself to weight according to the phase coherence of the two signals. Derivation of the equation is based on the assumption that the phase is differentiable and has a smooth derivative. In estimating spectra and cross spectra for a pair of stationary signals, the estimation of the phase may be replaced by an estimation of the group delay.

To evaluate the second right hand term of equation 15, it is necessary to find values for the complex coherence function. This function measures the smoothness of the phase and, for two zero-mean stationary random processes $x_1(t)$ and $x_2(t)$, is defined (16) as the normalized cross-spectral density:

$$\gamma_{x_1x_2}(f) = \frac{P_{x_1x_2}(f)}{\sqrt{P_{x_1x_1}(f)P_{x_2x_2}(f)}} \qquad (16)$$

By squaring the coherence function, a measure called the Magnitude-Squared Coherence (MSC) function is defined by (17). The terms in the equation may be unknowns and need to be estimated.

$$\left|\gamma_{x_1x_2}(f)\right|^2 = \frac{\left|P_{x_1x_2}(f)\right|^2}{P_{x_1x_1}(f)P_{x_2x_2}(f)} \qquad (17)$$

where $0 \le \left|\gamma_{x_1x_2}(f)\right|^2 \le 1, \quad \forall f$

D. Spectral estimation

To evaluate equation 14, consistent estimates of $\left|\gamma_{x_1x_2}(f)\right|^2$ and $\left|P_{x_1x_2}(f)\right|$ are required. This can be achieved using the 50% overlapping strategy suggested in [15], which is essentially similar to the more familiar Welch's averaging modified periodograms technique used here. The long sequences of data processing, for the purpose of spectral analysis, is conventionally performed by dividing the data into L short sections of M size. Frequencies that are not integer multiples of the frequency resolution (ΔF) will leak out throughout the entire frequency axis. To improve the situation, the samples of each section are multiplied by a window function. The window function is applied to the data section to control leakage, which otherwise causes a bias in the estimate.

The Fourier transform of the L-modified sequences are then obtained using the Fast Fourier Transform (FFT) algorithm as follows:

$$W_i(f_k) = \frac{1}{M}\sum_{n=0}^{M-1} x_i(n)a(n)\exp(-j2\pi nk/M) \qquad (18)$$

where i is the section (time) index and k is the frequency index. The data window $a(n)$ is selected to achieve desired specification requirements, and $W_i(f_k)$ is the frequency spectrum of the modified input sequences. The L-modified periodograms are:

$$J_i(f_k) = \frac{M}{U}\left|W_i(f_k)\right|^2 \qquad (19)$$

where

$$U = \frac{1}{M}\sum_{n=0}^{M-1} a^2(n) \qquad (20)$$

and the FFT bin frequencies are:

$$f_k = k\frac{F_s}{M} = k\Delta F \qquad (21)$$

where F_s is the sampling frequency. The spectral estimate is finally obtained by averaging these modified periodograms:

$$P_{xx}(f_k) = \frac{1}{L}\sum_{i=1}^{K} J_i(f_k) \qquad (22)$$

The Hanning window was chosen for the investigation. This function has side-lobe levels more than 70dB down, and a main-lobe with single-sided bandwidths of approximately four FFT bins. To keep the required FFT bin width alias free, it is necessary to increase the sampling frequency by a minimum factor of approximately four.

IV. Experiment Setup

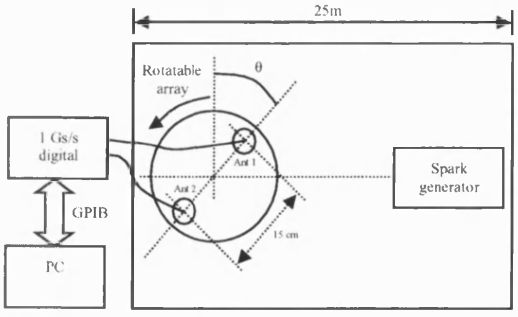

Fig. 3. Impulsive noise generator and acquisition system.

The source of the impulsive noise was generated using a simple spark gap. Constant streams of discharges were generated at intervals regulated by a pulse generator. This form of noise is representative of vehicle ignition systems, or the momentary breakdown of a power system insulation gap before, and sometimes during, the establishment of a stable conducting arc [17]. The experimental spark generator, figure 3, is based on the well known automotive inductive discharge principle. The equipment allows a discharge length of up to 1cm to be drawn with momentary flash of visible light accompanied by a sharp audible noise.

To capture the radiated electromagnetic transient, a two-channel digital real-time Tektronix oscilloscope, having a sampling resolution of 1GS/s, was placed 25 meters from the spark generator. The oscilloscope was connected to two helically-wound receiving antennas, spatially separated by 15cm. The antenna array was rotatable between 0°, where the antennas were equidistant from the spark generator, through to 90°, where one antenna was 15 cm nearer the generator than the other; this latter position gave the maximum time lag between the antenna signals (see figure 3). The scope was amplitude triggered and recorded 2,500 data points which were transferred to hard disk. During the experimental procedure, the antenna array was rotated between 0° and 90° at 10° intervals; at every array position, 5 separate data recordings were made. The tests were made in a University building that was deliberately chosen to provide a realistic environment for the objectives of the work. Therefore, the tests benefited from neither a screened, nor anechoic, environment.

The maximum time delay, corresponding to the two antennas and the spark generator being co-linear (i.e. θ = 90° in figure 3), is 0.5ns assuming that the signal propagates at $3\text{x}10^8$m/s. Since the sampling interval is 1 ns, it is necessary to interpolate between sampling points to find the cross-correlation peak.

V. Results

The one-shot event of a discharge can be observed in figure 4.

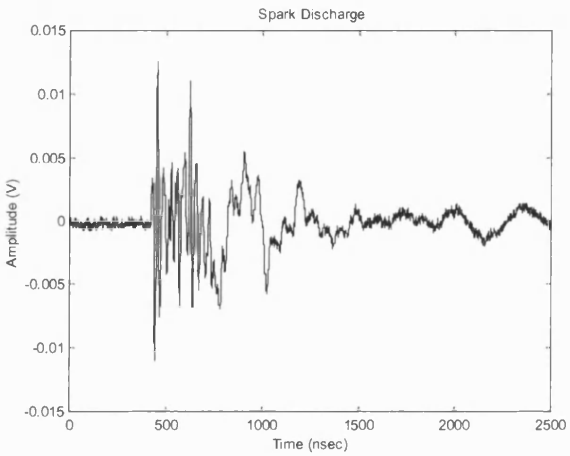

Fig. 4. Time domain waveform of impulsive noise.

The event exhibits an excursion of a typical transient with characteristics of damped sine waves decaying exponentially with time. Two dominant frequency components are apparent in figure 4. The spectrum of the discharge, measured independently using a 2.5 GHz spectrum analyser, showed that the majority of the signal power occurred in the region 0 – 500 MHz. Although the antenna signals were sampled at 1 GS/s, the oscilloscope inputs are bandlimited to 100MHz; the antenna signals are effectively 5x oversampled. An FFT plot of figure 4 is shown in figure 5.

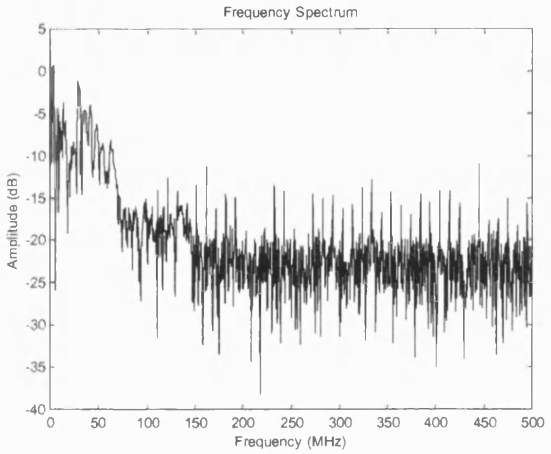

Fig. 5. Filtered frequency spectrum.

An example of the magnitude squared coherence function (MSC) is shown in figure 6. The MSC is bounded within the range of 0 and 1 as described in equation (17). Ideally, the desirable characteristic for the MSC would be unity for all frequencies. However, in view of the 100MHz bandwidth of the oscilloscope, the MSC demonstrates a high level of coherence within this spectral region.

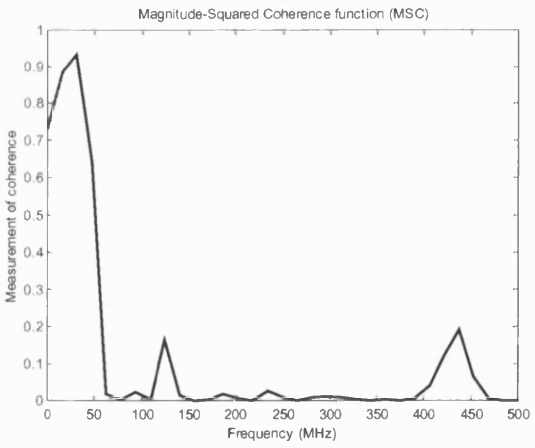

Fig. 6. Magnitude-Squared Coherence.

From the MSC and the cross spectrum, the weighting function of equation 15 is found and applied, in the frequency domain, to the modified cross-correlation expression, equation 14, which is evaluated using the Inverse Fast Fourier Transform (IFFT). An example of the cross-correlation estimation is shown in figure 7.

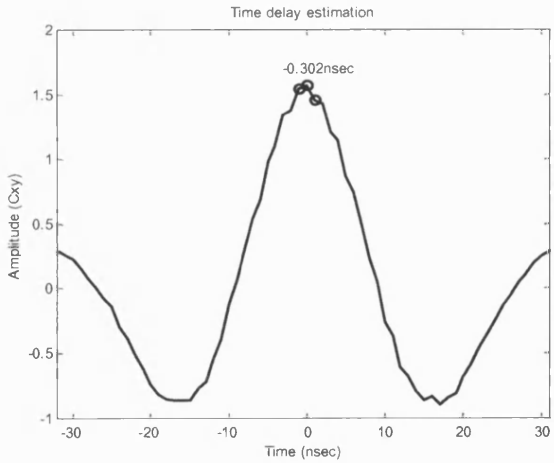

Fig. 7. Time delay estimation.

In principle, the delay is estimated from figure 7 by measuring from the peak of the main lobe to the time axis origin. In practice this measurement is complicated by the required delay (0.5 ns maximum) being less than the chosen sampling interval (Ts = 1 ns). To overcome this difficulty, a 20th order polynomial was fitted to the curve of the cross-correlation function which, due the periodogram based spectral estimation method, consists of 32 points. The position of the peak was found by differentiating the polynomial and searching for the zero crossing using a time-step of 1 ps. Polynomial curve fitting gave significantly improved results compared to a simple linear interpolation technique used initially.

The results for DCC and HT estimators are presented in figure 8 and 9 respectively. The delay estimates for each data recording are shown discretely together with the mean of the estimates for each array angle. Also shown on the figures is the ideal delay curve calculated assuming plane wave propagation between the spark source and the antenna array. Since the spark generator was constructed compactly, it can be assumed to act as a point source in which case the wave propagates, more correctly, with a spherical wavefront. However, calculations show, for the experimental set up used, that the path length difference between plane or spherical wavefront propagation is negligible.

VI. Discussion of Results

Considering the mean of the individual estimates, it is clear that the HT estimator, having a maximum bearing error of 20°, provides greater accuracy than the DCC approach, having a maximum error of 57°. It is interesting to note that both the DCC and HT mean curves deviate from the ideal characteristic at similar positions, e.g. overestimating the delay at 10°and underestimating at 60°. It is likely that the general shape of the curves is due to multipath effects since the room used for the tests is part of a steel framed building and reflections from unknown metallic structures buried in the walls could not be prevented. The existence of multipath effects is further highlighted by the shape of the example time delay estimation curve of figure 5. Although this

curve has a clearly defined peak, it is not smooth, implying that it represents the aggregate of several local maxima.

Considering the individual estimates, rather than the mean, it is clear that the HT yields a lower variance of estimates compared to the DCC approach using the 5 measurements taken for each angle.

VII. Conclusions

A direction finding technique applicable to wide band impulsive noise sources has been investigated using digital sampling equipment connected to two spatially separated antennas recording signals generated by a spark gap noise source. A digital signal processing technique based on the Hannan-Thomson delay estimation processor has shown to give a direction bearing accuracy of 20° using an average of 5 estimates. This technique has shown a significant increase in accuracy compared to the direct cross-correlation approach.

The results for this work were taken in a realistic working environment that was free from neither external noise nor multipath effects.

Although the bandwidth of the receiving equipment is 100 MHz, and uses time samples that are large in comparison to the antenna spacing, the reported delay accuracy was estimated by a combination of 5 times oversampling and polynomial curve fitting of the correlation peak.

Acknowledgements

The authors would like to thank the University of Bath, UK, and Omicron Electronics GmbH, Austria, for supporting this project.

References

[1] M. Sarmadi, "Radio and television interference caused by corona discharges from high-voltage transmission lines: fast changing parameters influencing RN generation," *Proceedings of the American Power Conference 58th Annual Meeting*, vol.2, pp.1601-6, 1996.

[2] M. G. Sanchez, L. de Haro, M. C. Ramon, A. Mansilla, C. M. Ortega and D. Oliver, "Impulsive noise measurements and characterization in a UHF digital TV channel," *IEEE Trans. Electromagn. Compat.*, vol. 41, no. 2, May 1999.

[3] A. Tungkanawanich, J. Abe, Z-I. Kawasaki and K. Matsuura, "Location of partial discharge source on distribution line by measuring emitted pulse-train electromagnetic waves", *Proceedings of IEEE Power Engineering Society Winter Meeting 2000*, IEEE catalog 00CH37077C, CDROM 0-7803-5938-0.

[4] C. H. Peck and P. J. Moore, "Source identification and analysis of wideband electromagnetic interference generated by switchgears in a high voltage substation," *Proceedings of the EMC York 2000 Conference*, Jul. 2000.

[5] W. Featherstone, H. J. Strangeways, "Mobile transmitter AOA estimation under multipath conditions using an MLE based superresolution algorithm and comparison with weighted spectrum methods," *IEE Colloquium Novel Methods of Location and Tracking of Cellular Mobiles and their System Application*, pp.4/1-5. May 1999.

[6] M. Ali, "The system applications of novel methods of location and tracking of cellular mobiles," *IEE Colloquium Novel Methods of Location and Tracking of Cellular Mobiles and their System Application*, pp.6/1-4, May 1999.

[7] R. O. Schmit, "Multiple emitter location and signal parameter estimation," *IEEE Trans. Antennas and Propagation*, vol. AP-34, no. 3, pp. 276-280, Mar. 1986.

[8] A. Nehorai and E. Paldi, "Vector-Sensor array processing for electromagnetic source localization," *IEEE Trans. Signal Processing*, vol. 42, no. 2, pp. 376-398, Feb. 1994.

[9] G. C. Carter, "Time delay estimation for passive sonar signal processing," *IEEE Trans. Acoust, Speech, Signal Processing*, vol. ASSP-29, no. 3, Jun. 1981.

[10] B. V. Hamon and E. J. Hannan, "Spectral estimation of time delay for dispersive and non-dispersive systems," *Appl. Statist.*, vol. 23, no. 2, pp. 134-142, 1974.

[11] D. R. Brillinger, P. R. Krishnaiah, "Handbook of statistics 3 – Time series in the frequency Domain," Elsevier Science Publishers B. V., pp. 111-123, 1983.

[12] P. R. Roth, "Effective measurements using digital signal analysis," *IEEE Spectrum*, vol. 8, pp. 62-70, Apr. 1971.

[13] C. H. Knapp and G. C. Carter, "The generalized correlation method for estimation of time delay," *IEEE Trans. Acoust., Speech, Signal Processing*, vol. ASSP-24, pp. 320-327, Aug. 1976.

[14] E. J. Hannan and P. J. Thomson, "Estimating group delay," *Biometrika*, vol. 60, pp. 241-253, Feb. 1973.

[15] G. C. Carter, C. H. Knapp and A. H. Nuttall, "Estimation of the magnitude-squared coherence function via overlapped fast Fourier transform processing," *IEEE Trans. Audio Electroacoustics*, vol. AU-21, no. 4, pp. 337-344, Aug. 1973.

[16] G. C. Carter, A. H. Nuttall and P. G. Cable, "*The smoothed coherence transform*," *Proc. IEEE (Letter)*, vol. 61m, pp. 1497-1498, Oct. 1973.

[17] Texas A & M Research Foundation, "Detection of arcing faults on distribution feeders", Electric Power Research Institute, Final Report EL-2757, 1982.

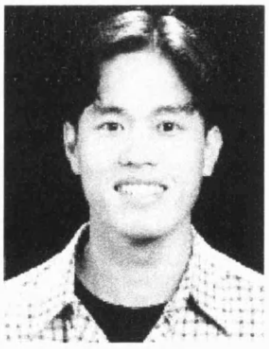

Chye Huat Peck was born in Singapore. He graduated with a 1st class honors in Electrical and Electronic Engineering (B.Eng.) from the University of Bath in July 1999. He is currently a research student in the university and his research interests include digital signal processing and electrical substation switchgear condition monitoring based on radiometric analysis of the radio frequency interference generated by the switching.

Philip Moore was born in England. He received his BEng in Electrical Engineering from Imperial College London in 1984 and his PhD in Power System Protection from City University London in 1989. From 1984 to 1987 he was a Development Engineer at GEC Alsthom Protection and Control, Stafford, UK. From 1987 to 1991 he was a lecturer in Electrical Engineering at City University. He joined the University of Bath in 1991 where he is presently a Senior Lecturer. Dr Moore is currently an investigator on a number of major research grants funded by government and industry sources. Dr Moore has published over 100 conference and journal papers in the fields of power system protection, measurements and EMC. Dr Moore's research interests include digital signal processing applied to power engineering, high voltage discharges, power system simulation, fault location and switchgear condition monitoring.

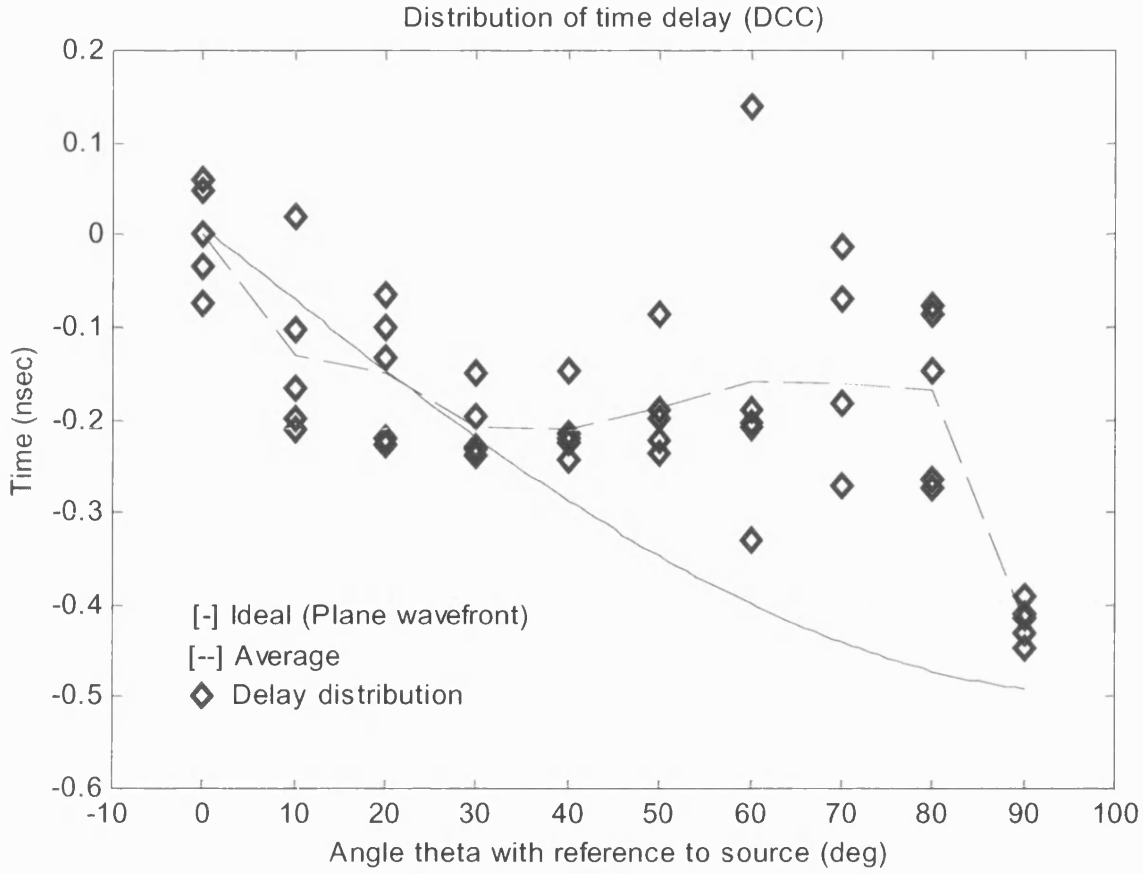

Fig. 8. The direct cross-correlation estimator

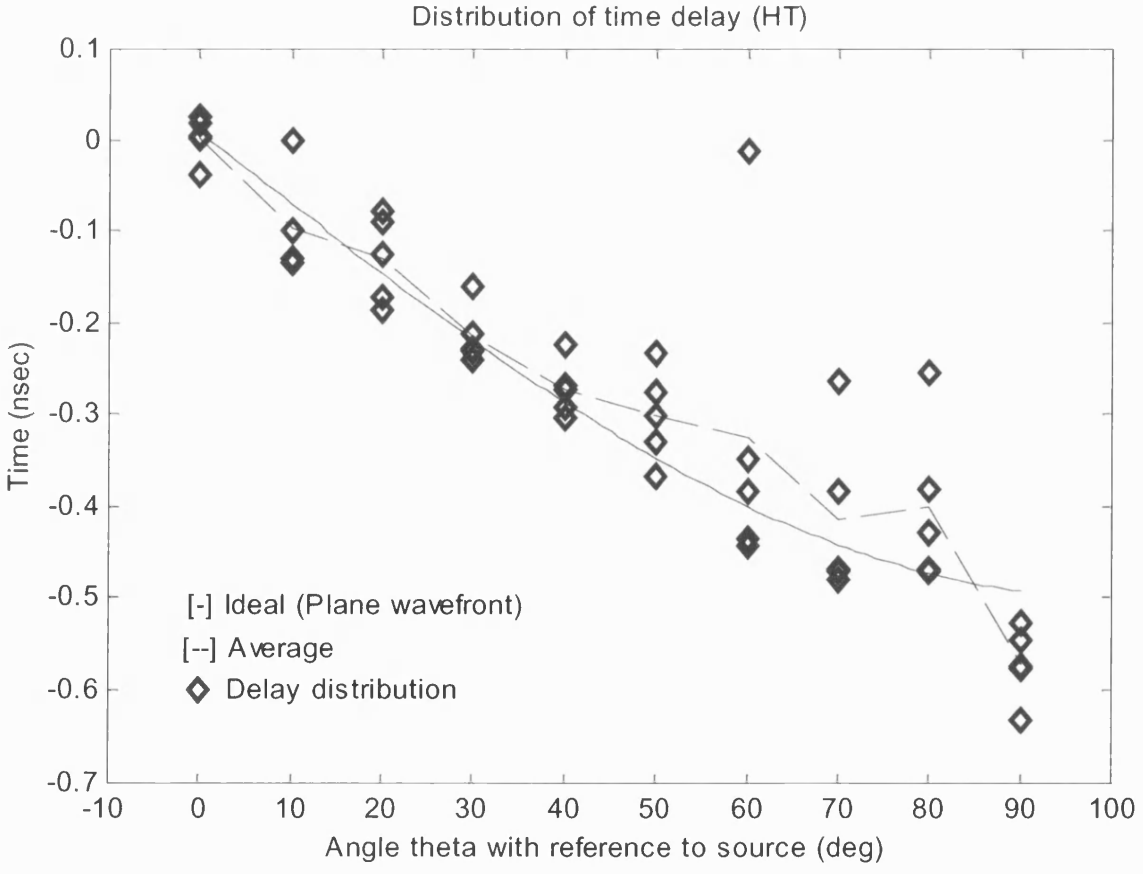

Fig. 9. The HT based estimator

Appendix B

ANSI/IEEE STANDARDS

ANSI C63.2-1987, American National Standard for Electromagnetic Noise and Field Strength, 10kHz to 40GHz Specifications.

ANSI C63.4-1991, American National Standard for Methods for Measurement of Radio Noise Emissions from Low-Voltage Electrical and Electronic Equipment in the Range of 9KHz to 40GHz.

ANSI C63.4-1992, American National Standard for Methods for Measurement of Radio Noise Emissions from Low-Voltage Electrical and Electronic Equipment in the Range of 9KHz to 40GHz.

ANSI C63.5-1988, American National Standard for Calibrating of Antennas Used for Radiated Emission Measurements in Electromagnetic Interference (EMI) Control.

ANSI C63.6-1988, American National Standard Guide for Construction of Open Area Test Sites for Performing Radiated Emission Measurements.

IEEE Std. 140-1990, Recommended Practice for Minimization of Interference from Radio Frequency Heating Equipment (ANSI).

IEEE Std. 187-1990, Standard on Radio Receivers: Open Field Method of Measurement of Spurious Radiation from FM and Television Broadcast Receivers (ANSI).

IEEE Std. 430-1986, Standard Procedures for the Measurement of Radio Noise from Overhead Power Lines and Substations (ANSI).

IEEE Std. 518-1982 (Reaff 1990), Guide for the Installation of Electric Equipment to Minimise Noise Input to Controllers from External Sources (ANSI).

IEEE Std. 644-1987, Standard Procedures for Measurement of Power Frequency Electric and Magnetic Fields from AC Power Lines (ANSI).

IEEE C62.45-1987 Guide on Surge Testing for Equipment Connected to Low-Voltage AC Power Circuits (ANSI)

IEEE C62.47-1992 (draft), Guide on Electrostatic Discharge: Characterization of the ESD Environment.

BSI PUBLICATIONS

BS 613, Specification for Components and Filter Units for Electromagnetic Interference Suppression, 1977/1980.

BS 800, Specification for Limits and Methods of Measurement of Radio Interference Characteristics of Household Appliances, Portable Tools, and Other Electrical Equipment Causing Similar Types of Interference, 1990.

BS 5406, Disturbances in Supply Systems Caused by Household Appliances and Similar Electrical Equipment, 1988.

PD 6582, Eelctromagnetic Compatibility (EMC). Guide to Generic EMC Standards, 1993.

CISPR/IEC PUBILCIATIONS

CISPR 9, Limits of Radio Interference and the Leakage Currents, 1978.

CISPR 12, Limits and Methods of Measurement of Radio Interference Characteristics of Vehicles, Motor Boats, and Spark Ignited Engine Driven Devices, 1978/1986.

CISPR 13, Limits and Methods of Measurement of Radio Interference Characteristics of Sound and Television Receivers, 1975/1983.

CISPR 14, Limits and Methods of Measurement of Radio Interference Characteristics of Household Electrical Appliances, Portable Tools and Similar Electrical Apparatus, 1985.

CISPR 17, Methods of Measurement of the Suppression Characteristics of Passive Interference Filters and Suppression Components, 1981.

CISPR 18, Radio Interference Characteristics of Overhead Power Lines and High Voltage Equipment, 1982/1986.

CISPR 21, Interference to Mobile Radio Communications in the Presence of Impulsive Noise – Methods of Judging Degradation and Measures to Improve Performance, 1985.

IEC 801-2, Electromagnetic Compatibility for Industrial Process Measurement and Control Equipment: Part 2 – Electrostatic Discharge Requirements, 1991.

IEC 801-4, Electromagnetic Compatibility for Industrial Process Measurement and Control Equipment: Part 4 – Electrical Fast Transient/Burst Requirements, 1988.

EURO NORMS

EN 50065-1, Signalling on Low-Voltage Electrical Installations in the Frequency Range 3 to 148.5kHz, 1990/1992 (Part 1: General Requirements, Frequency Bands and Electromagnetic Disturbances).

EN 55014, Limits and Methods of Measurement of Radio Interference Characteristics of Household Electrical Appliances, Portable Tools and Similar Electrical Apparatus, 1993.

EN 55015, Limits and Methods of Measurement of Radio Interference Characteristics of Fluorescent Lamps and Luminaries, 1987/1993.

EN 61000-2-2, Compatibility Levels for Low-Frequency Conducted Disturbances and Signalling in Public Low-Voltage Power Supply Systems, 1993.

EN 61000-4-7, General Guide on Harmonics and Inter-harmonics Measurements and Instrumentation, for Power Supply Systems and Equipment Connected Thereto, 1993.